Sodium channel diversity in the vestibular ganglion: evidence for $Na_V1.5$-like and $Na_V1.8$-like currents

by

Xiao-Ping Liu

B.A. Applied Math in Neuroscience
Harvard University, 2004

SUBMITTED TO THE DEPARTMENT OF HEALTH SCIENCES AND TECHNOLOGY IN PARTIAL FULFILLMENT OF THE REQUIREMENTS FOR THE DEGREE OF

DOCTOR OF PHILOSOPHY IN HEALTH SCIENCES AND TECHNOLOGY
AT THE
MASSACHUSETTS INSTITUTE OF TECHNOLOGY

SEPTEMBER 2012

Signature of Author: _____
Department of Health Sciences and Technology
July 13, 2012

Certified by: _____
Ruth Anne Eatock, PhD
Associate Professor of Otology and Laryngology and Associate Professor of Neurobiology
Harvard Medical School and Eaton-Peabody Laboratories, Massachusetts Eye and Ear Infirmary
Thesis Supervisor

Accepted by: _____
Arup Chakraborty, PhD
Director, Institute for Medical Engineering and Sciences and the Harvard-MIT Program in Health Sciences and Technology
Robert T. Haslam Professor of Chemical Engineering, Chemistry and Biological Engineering

Sodium channel diversity in the vestibular ganglion: evidence for $Na_V1.5$-like and $Na_V1.8$-like currents

by
Xiao-Ping Liu

Submitted to the Department of Health Sciences and Technology
on July 13th, 2012 in Partial Fulfillment of the
Requirements for the Degree of Doctor of Philosophy in
Health Sciences and Technology

ABSTRACT

Voltage-gated sodium (Na_V) channels are diverse, comprising nine known mammalian subunits, which are classified pharmacologically into tetrodotoxin-sensitive (TTX-S) and tetrodotoxin-insensitive (TTX-I) categories. The pattern of Na_V channel expression shapes response properties of neurons, while changes in these expression patterns are related to many pathological conditions. Previous RT-PCR results indicated the expression of a variety of Na_V channel subunits in the vestibular ganglion, the sensory ganglion that conveys information about motion and orientation. The expressed subunits included several TTX-I subunits with unique biophysical properties that have been extensively characterized in somatosensory neurons and the heart, but never reported in published electrophysiological studies of the vestibular ganglion. Using whole-cell patch clamp, we show the presence of two types of TTX-I Na_V currents in acutely dissociated rat vestibular ganglion neurons (VGNs) from the first postnatal week: a fast and negatively-inactivating current (midpoint of inactivation: ~−100 mV) that resembled current previously described for the $Na_V1.5$ subunit, and a slower current with a depolarized voltage range of inactivation (midpoint ~−30 mV) which had properties consistent with $Na_V1.8$ channels. All neurons also expressed TTX-S Na_V currents with similar properties to those previously described in VGN (midpoint of inactivation: ~−75 mV). The $Na_V1.5$-like current contributed about 10% of the total Na_V current, was expressed in most VGNs on the first postnatal day (P1), and gradually decreased in prevalence throughout the first week. The $Na_V1.8$-like current was present in ~25% of cells and was correlated with broader action potentials, higher voltage thresholds, and minimal spike height accommodation. We confirmed the expression of $Na_V1.8$ using a reporter mouse in which fluorescence is restricted to $Na_V1.8$-expressing cells; intense fluorescent signal was seen in many VGN cell bodies and peripheral processes. These results suggest that $Na_V1.8$ may be expressed in non-somatosensory peripheral neurons. Na_V channel expression in immature VGNs may contribute to development, while differential expression in adulthood may underlie diversity of mature response properties.

Thesis Supervisors:

Ruth Anne Eatock, PhD, Associate Professor of Otology and Laryngology and Neurobiology, Harvard Medical School

M. Charles Liberman, PhD, Professor of Otology and Laryngology, Harvard Medical School

ACKNOWLEDGMENTS

I would like to express my gratitude to Dr. Eatock for showing me the diversity of ion channels, the specificity with which they are expressed, and the impact they have on sensory processing. Thank you also for teaching me principles of experimentation and analysis, for working with me with such detail and consistency to improve my communication skills, and for sharing enthusiasm and insight towards the life and career of research. In summary, thanks for being such a devoted mentor!

I am grateful for the opportunity to learn from my co-advisor Dr. Liberman, both in classes and in lab meetings, and for his input on this project. Your interests in themes of sensory processing, such as parallel streams of encoding, dynamic range, phase-locking, efferent feedback, adaptation, and pathological changes, have infected and informed my thinking.

Our collaborators Dr. Anna Lysakowski, Steven Price, and Sophie Gaboyard-Niay worked hard work to get beautiful reporter mouse and immunohistochemistry data. The critical $Na_V1.8$ reporter mouse was provided by Qiufu Ma and Fu-chia Yang, who despite her busy schedule offered us mice that she was using in her own research. A special thanks goes to Jane Maunsell for her dedication in scoring the morphological data.

My thesis committee provided a wide range of input from helping me prioritize experiments, to pointing out technical issues, to improving the clarity of my writing. Thank you John Guinan, Bill Sewell, and Chinfei Chen for your expertise, your critical questioning, and your desire to make this study as strong as possible. Bruce Bean and Chris Shera also provided valuable input.

I must also thank my fellow EPLer's and labmates for such a supportive and helpful lab environment, in particular Michaela Meyer, Radha Kalluri, Jocelyn Songer, and Albena Kantardzhieza. You are true friends and mentors. Many others also offered assistance, amusement, thoughtful conversations, or emotional support (and chocolate!). I could not have asked for a more supportive community.

My deepest gratitude goes to my parents for bringing me to the U.S. so that I could have a better education. Your hard work and perseverance showed that if there is a will there is a way.

Greg, thank you for your emotional and practical support during the "final push", help with clarifying and strengthening my writing and talks, and your kind but honest second perspective.

This research was made possible by support from NIH training grant T32 DC000038 and NIH grant RO1 DC002290.

TABLE OF CONTENTS

LIST OF TABLES

Page

LIST OF FIGURES

Page

INTRODUCTION

The five vestibular end organs of the inner ear sense orientation and motion to drive powerful ocular, autonomic, and postural reflexes as well as providing us with a sense of our relationship to space. The three semicircular canal organs sense rotational acceleration, while the two otolithic organs (utricle and saccule) sense static orientation as well as linear acceleration. Together with vision and proprioception, these sensory organs allow us to balance and see steady visual images during simple acts such as walking, and to learn to perform complex acts such as riding bicycles, dancing, or even performing acrobatics. This often overlooked sense (in fact the inner ear was thought to house only the sense of hearing until the late nineteenth century), becomes impossible to ignore when it creates debilitating symptoms like nausea and vertigo, or is disrupted in outer space or by life-altering medical disorders.

Anatomy of the vestibular epithelium

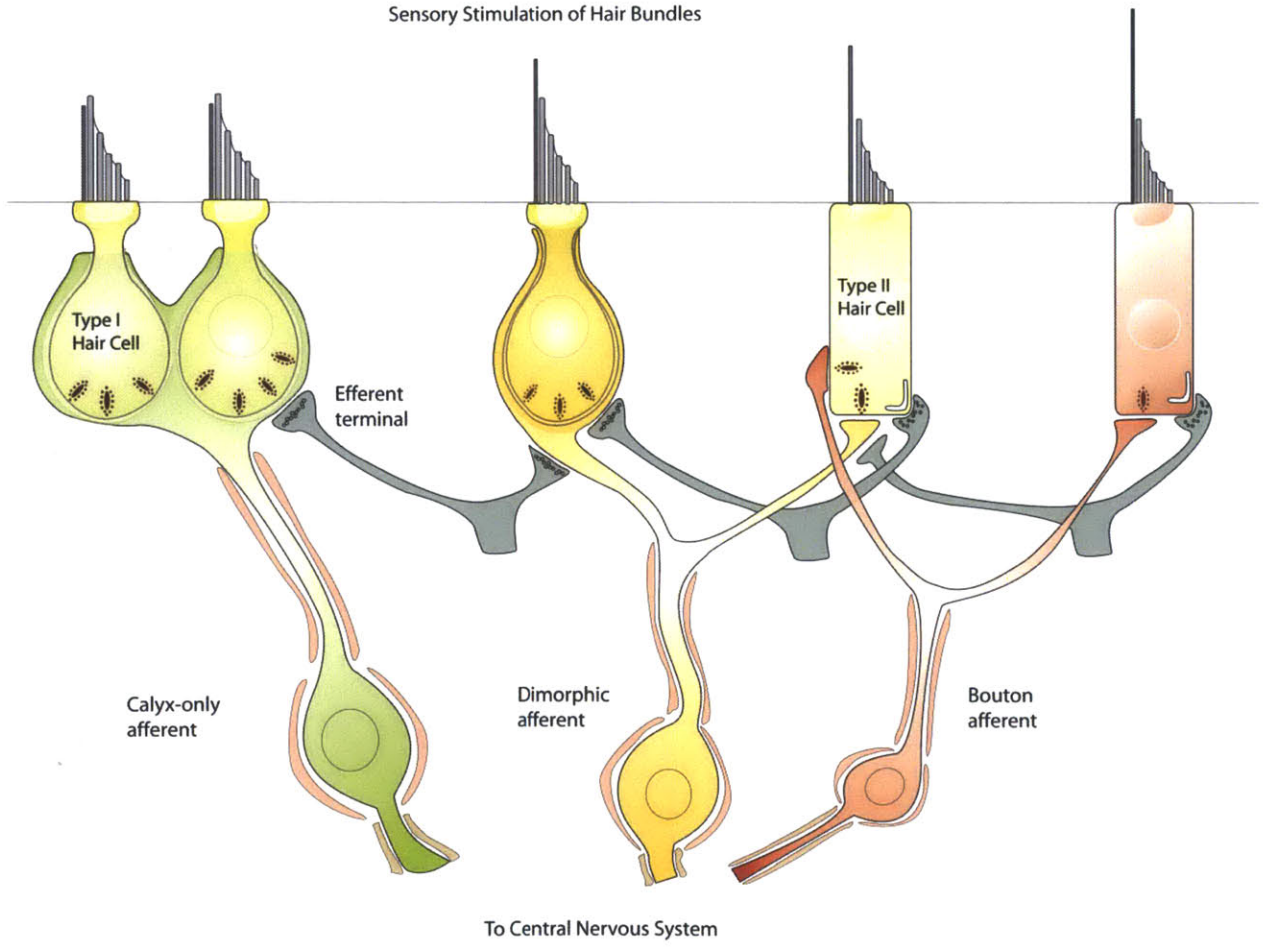

Intro Figure 1. Anatomy of the vestibular epithelium and ganglion.

The vestibular sensory epithelium (Intro Fig. 1) is populated by two types of sensory cells (*type I* and *type II hair cells*), organized anatomically into a *central* or *striolar* zone and *peripheral* or *extrastriolar* zones. Studies of hair cells have revealed systematic differences in cell morphology both between zones and hair cell types (Lysakowski and Goldberg, 1997; Li et al., 2008). The type I and type II hair cells synapse onto calyceal and bouton types of afferent endings, respectively. The afferent neurons of the vestibular ganglion can be classified into 1) those that only form calyces and therefore only receive input from type I hair cells (*calyx-only*, prevalent in the central zone), 2) those that only form bouton synapses and receive input from type II hair cells (*bouton-only*, prevalent in the peripheral zone), and 3) those that form both types of endings (*dimorphic*, present throughout). Vestibular ganglion neurons (VGNs) are diverse in their physiology as well, for example varying greatly in the regularity of the interspike interval of action potential discharge (Baird et al., 1988). Calyx-only afferents have the most irregular firing patterns and phasic responses to head motions; central dimorphic afferents are also irregular and phasic; and peripheral dimorphic afferents and bouton-only afferents are regular and tonic (reviewed in Goldberg, 1991). Co-labeling with antibodies against only three markers (two calcium binding proteins and the intermediate filament peripherin), distinguishes at least four types of VGNs, which appear to correspond to calyx-only afferents, central dimorphic afferents, peripheral bouton afferents, and peripheral dimorphic afferents (Kevetter and Leonard, 2002). VGNs project to various vestibular brainstem nuclei and parts of the cerebellum in patterns that depend on the end organ and epithelial zone of origin (Carpenter et al., 1972; Carleton and Carpenter, 1984; Maklad et al., 2010).

Ion channels in vestibular hair cells and neurons

In the sensory epithelium, hair cell ion channel expression varies in a complex and systematic way with hair cell type, age, and zone (e.g.,Rusch et al., 1998; Wooltorton et al., 2007) and must shape responses to stimuli. Given the diversity of the neuronal population, we wondered whether vestibular ganglion neurons also have diverse ion channels and whether such diversity could underlie firing regularity or other response properties. Indeed, differential expression of low-voltage activated K^+ channels (K_{LV}) between terminals in different zones has been suggested to contribute to differences in firing regularity, action potential shape, firing threshold, and frequency filtering (Kalluri et al., 2010; Lysakowski et al., 2011).

As part of a previous project examining sodium current expression in hair cells, RT-PCR was performed on the vestibular ganglion as well as the sensory epithelia (Wooltorton et al., 2007). The results revealed expression of a broad range of sodium channel subunits in the vestibular ganglion, including several unexpected α subunits.

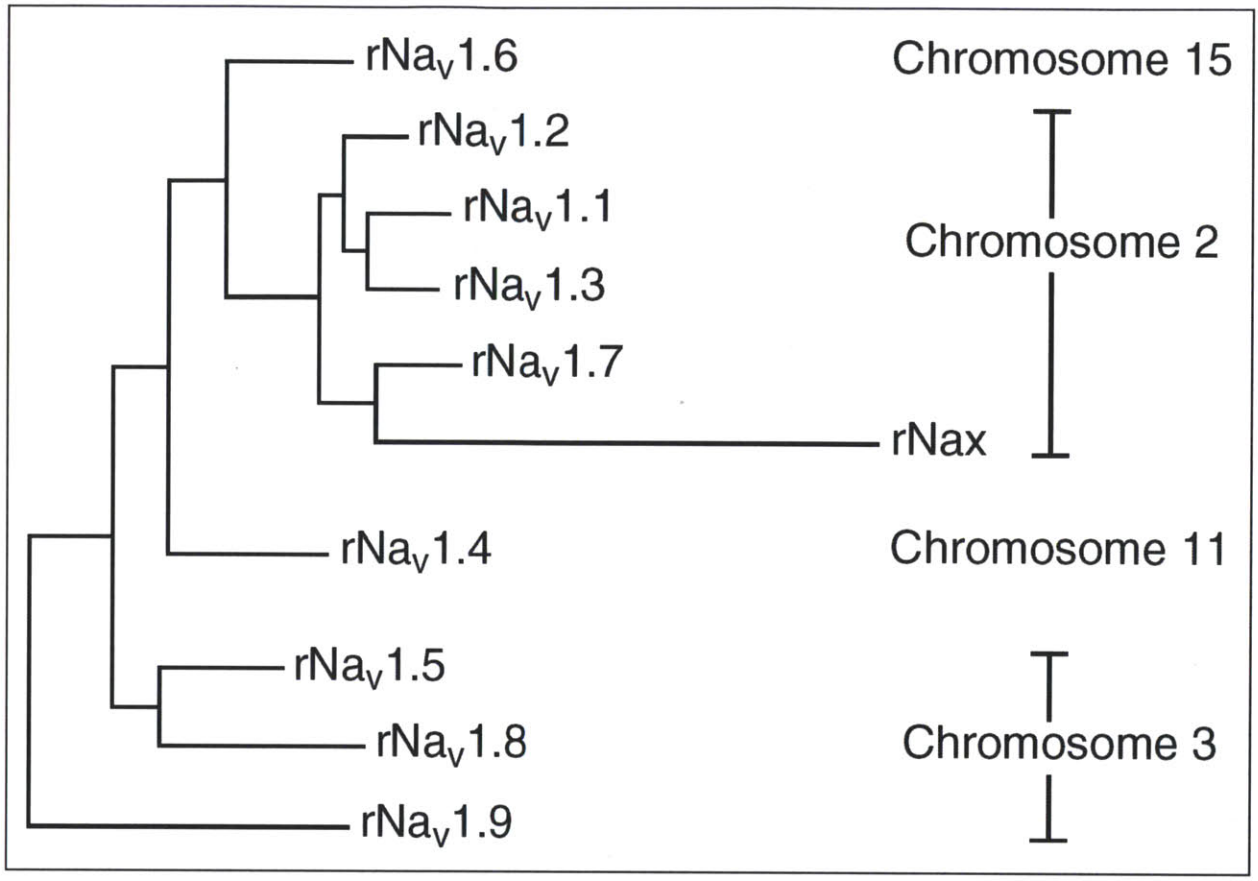

Intro Figure 2. Evolutionary relationship of sodium channel α subunits based on rat sequence alignment (using ClustalW and PAUP), and human chromosomal locations. Nax is likely not voltage-gated but relates to sodium homeostasis or sensing. Reproduced from Yu and Catterall (2003).

Na_V channels are best known for their role in generating the upstroke of the all-or-none action potential which allows signals to propagate along neurons without decaying in amplitude with distance. However, the textbook action potential ignores for simplicity the considerable diversity and modulatability of voltage-gated ion channels and firing patterns. Each sodium channel consists of one pore-forming α subunit (with four repeating domains) and potentially associated accessory β subunits. There are nine characterized α subunits of mammalian Na_V channels which are categorized based on their sensitivity to the drug tetrodotoxin (TTX) into three groups: TTX-sensitive, moderately TTX-insensitive, and highly TTX-insensitive (also referred to as TTX-resistant). We refer to the TTX-sensitive channels as TTX-S, and both TTX-insensitive categories as TTX-I. The TTX-I subunits ($Na_V1.5$, $Na_V1.8$, and $Na_V1.9$) were first reported outside of the central nervous system and have very different biophysical properties from the TTX-S subunits ($Na_V1.1$, $Na_V1.2$, $Na_V1.3$, $Na_V1.4$, $Na_V1.6$, and $Na_V1.7$). $Na_V1.5$ is most highly expressed in ventricular myocytes of the heart, where it is the primary isoform, and has a substantially more negative voltage dependence of inactivation than all other subunits (Rogart et al., 1989; Cribbs et al., 1990; Zeng et al., 1996). It has since also been reported in the adult

brain (Hartmann et al., 1999; Wu et al., 2002), and developmentally in skeletal muscle (Kallen et al., 1990) and dorsal root ganglion (DRG) neurons (Renganathan et al., 2002). The negative voltage dependence of inactivation does not pose a problem for sodium channel availability since resting potential is ~−85 mV in ventricular myocytes, whereas pacemakers of the sinoatrial node typically have a minimum potential of ~−50 mV and exhibit spontaneous pacemaking activity; the difference is thought to be due to comparatively high expression in ventricular myocytes of inwardly-rectifying potassium channels open at rest (Schram et al., 2002). $Na_V1.8$ has only been reported in peripheral sensory ganglia, is preferentially expressed in small-diameter nociceptive neurons, and has slower kinetics and a positively-shifted voltage range of activation and inactivation relative to TTX-S channels (Akopian et al., 1996; Sangameswaran et al., 1996; Akopian et al., 1999). The most slowly inactivating subunit, $Na_V1.9$, was first noticed as a TTX-I current that remained in small DRG neurons of $Na_V1.8$-null mice (Cummins et al., 1999). In the DRG, $Na_V1.9$ has been localized to a subset of nociceptive neurons that bind isolectin-B4 (IB4+) and have receptors for glial cell line-derived neurotrophic factor (GDNF) (Fjell et al., 1999; Fang et al., 2006).

RT-PCR data from our lab (Wooltorton et al., 2007 and unpublished results) indicated that many α-subunits, including all three TTX-I subunits, and all four β subunits are transcribed in the vestibular ganglion. $Na_V1.8$ and $Na_V1.9$ are transcribed in the ganglion but not the epithelium, and $Na_V1.5$ is transcribed in both the ganglion and the epithelium, in agreement with the observation of $Na_V1.5$-like current, but not $Na_V1.8$ or $Na_V1.9$-like current, in hair cells (Wooltorton et al., 2007). We were particularly intrigued by the expression of both $Na_V1.8$ and $Na_V1.9$ in RT-PCR of the vestibular ganglion, which is not known to contain nociceptors, as well as by the strong calyx staining and zonal patterning of $Na_V1.5$ when visualized by immunohistochemistry (Wooltorton et al., 2007; Lysakowski et al., 2011). However, previous electrophysiological studies on the vestibular ganglion have only reported TTX-S sodium currents (Chabbert et al., 1997; Risner and Holt, 2006). We decided to revisit the issue of sodium channel diversity with the particular intent of looking for TTX-I currents.

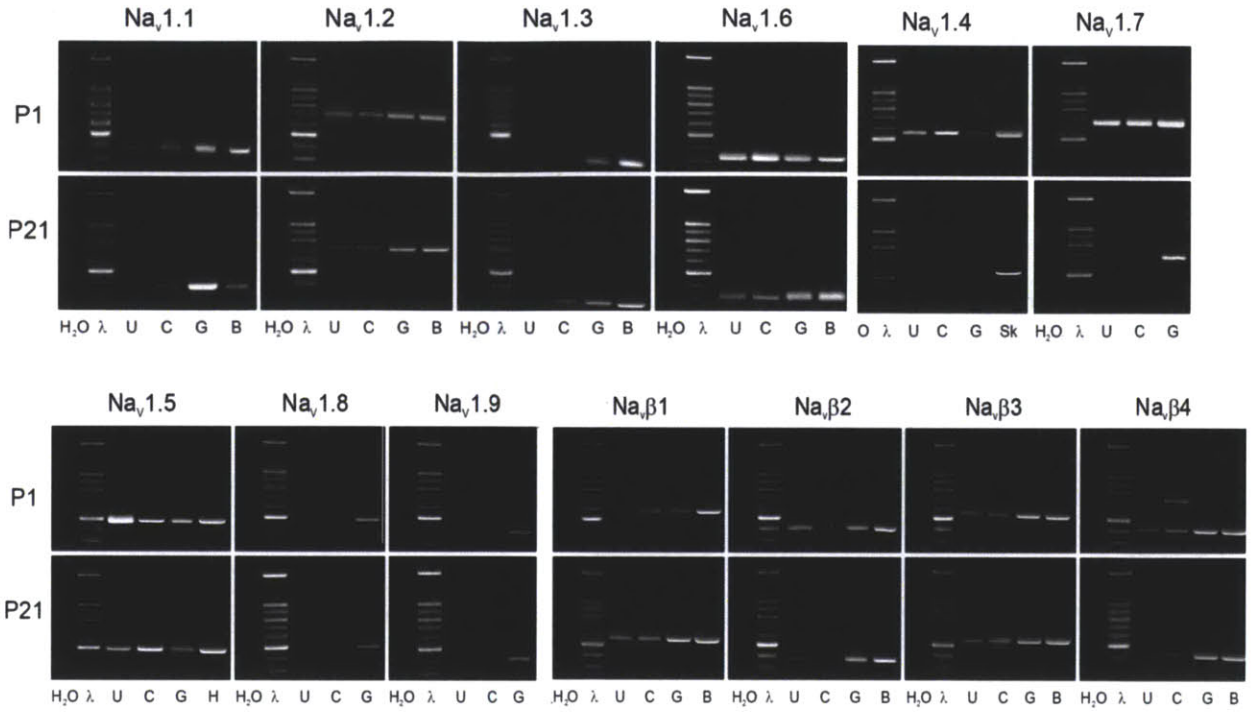

Intro Figure 3. Whole tissue RT-PCR of the superior vestibular ganglion shows expression of many Na_V channel subunits. U = Utricle, C = Crista, G = Superior vestibular ganglion, B = Brain, Sk = Skeletal muscle, H = Heart

We take inspiration from studies in the DRG, the best-studied peripheral ganglion in terms of ion channel expression. DRG studies have illustrated the importance of sodium channel diversity in setting firing properties in different subtypes of ganglionic neurons. In nociceptors, the prominent expression of $Na_V1.8$, which recovers rapidly from fast inactivation and inactivates at more positive voltages, supports sustained firing that is relatively insensitive to depolarization of the resting membrane potential (Renganathan et al., 2001; Choi and Waxman, 2011). In addition to the expression of TTX-I channels being restricted to particular neuronal types, the biophysical properties of TTX-I and TTX-S channels differ between cell types. For instance, the TTX-S current has slow recovery from inactivation (repriming) in small DRG neurons (which also have TTX-I currents) but fast repriming in large DRG neurons (Cummins and Waxman, 1997; Everill et al., 2001), which may be due to subunit differences, modifications of the channel, or regulatory proteins that associate with the channel. In another example, slow inactivation of $Na_V1.8$ develops more rapidly and recovers more slowly in IB4+ cells as compared with IB4− neurons, which project to parallel central pathways (Braz et al., 2005; Choi et al., 2007).

Studies in the DRG also implicate changes in Na_V channels in pathological conditions and modulations of excitability (reviewed in Rush et al., 2007). The diversity of channel types may also create opportunities for targeted therapeutics given a sufficient understanding of normal and pathological expression patterns. Changes in both TTX-S and TTX-I channels can be seen in

a variety of DRG-based pain models. Treatments that induce inflammatory pain increase TTX-I currents and selectively upregulate $Na_V1.3$ and $Na_V1.7$ but not other TTX-S subunits (Black et al., 2004). Furthermore, $Na_V1.3$ and $Na_V1.7$ subunits both have relatively large ramp currents (sodium currents generated during slow depolarization of the membrane around resting potential) due to slow entry into inactivation from the closed state (Cummins et al., 1998; Cummins et al., 2001); such currents could amplify subthreshold events and more easily bring the cell to firing threshold, resulting in sensitization of nociceptors (which normally have high mechanical thresholds) during inflammation. TTX-I currents are also increased in inflammatory pain, with upregulation of $Na_V1.8$ but not $Na_V1.9$ (Tanaka et al., 1998; Black et al., 2004). Inflammatory signaling molecules such as prostaglandin E2, adenosine, and serotonin also acutely potentiate TTX-I currents by shifting the voltage-dependence of activation in the hyperpolarizing direction (thus reducing activation threshold) and speeding up kinetics, resulting in an increase in excitability (England et al., 1996; Gold et al., 1996; Cardenas et al., 1997).

In contrast, axotomy of the peripheral processes of small DRG neurons downregulates $Na_V1.8$ and decreases TTX-I current (as well as changing the type of TTX-S current expressed), possibly due to deprivation from peripherally-released growth factors (Dib-Hajj et al., 1996; Cummins and Waxman, 1997; Sleeper et al., 2000). Application of exogenous nerve growth factor (NGF) increased $Na_V1.8$ but not $Na_V1.9$ transcript levels, while GDNF increased transcripts for both, consistent with the restriction of $Na_V1.9$ to IB4+ GDNF-responsive neurons, but expression of $Na_V1.8$ in both IB4+ and IB4– (NGF-responsive) neurons (Fjell et al., 1999). Both TTX-I currents decrease by 7 days in dissociated culture, a condition somewhat analogous to axotomy, and both currents are dramatically increased by addition of GDNF to cultured neurons, suggesting the possibility of rescuing some axotomy-related changes with GDNF exposure (Cummins et al., 2000).

Recently, the compound A803467 has emerged from an iterative screen as a potent and selective blocker of $Na_V1.8$ that is an effective analgesic in several pain models (Jarvis et al., 2007). The existence of such subunit-selective drugs (and perhaps even better ones in the future) provides an important therapeutic opportunity. If $Na_V1.8$ is expressed in the vestibular ganglion, such drugs may prove to be of clinical significance for vestibular disorders. At the same time, if such drugs are used against pain, they should be thoroughly assessed to ensure that they do not significantly interfere with the function of non-nociceptive neurons (such as VGN).

In general, dysregulation of ion channels could be involved in vestibular disorders, requiring that we better examine ion channel expression under normal and pathological conditions. Ménière's disease, a devastating but poorly understood multifactorial disease that seems to be

related to trauma, allergies, viral infection, or autoimmunity and relieved by glucocorticoids like dexamethasone, may therefore be linked to inflammation (Greco et al.; Berlinger, 2011; Banks et al., 2012). Since membrane rupture from endolymphatic hydrops is no longer considered the certain cause of sensory symptoms in Ménière's disease (vertigo, tinnitus, and hearing loss), non-mechanical mechanisms, including but certainly not limited to changes in ion channel expression of hair cells or neurons, should be considered. Indeed, it has been noted that Ménière's disease has many of the hallmarks of a channelopathy (Gates, 2005). For instance, a low sodium diet is often effective in alleviating the symptoms of Ménière's disease, as are diuretic drugs that affect ion pumps and electrolytic balance. Another parallel to the DRG may be found in pathologies such as ototoxicity or excitotoxicity, the aftermath of which may share some similarities with axotomy.

The goals of this project were to look for evidence of the various TTX-I Na_V channels using whole-cell patch clamp of dissociated vestibular ganglion cells; to determine whether expression differed substantially from cell to cell (suggesting the possibility of subpopulations with different ion channel expression); and to explore the contributions of TTX-I channels to neuronal discharge. In the following chapters, I outline the evidence for $Na_V1.5$-like and $Na_V1.8$-like current in the ganglion, the firing patterns of cells expressing each type of current, and possible morphological differences between the cells. I also present data from a reporter mouse supporting transcriptional expression of $Na_V1.8$ in many cells in the vestibular ganglion. Finally, I speculate on the possible significance of this expression and suggest future experiments.

METHODS

Cell preparation

Superior vestibular ganglia (innervating the utricle, lateral and anterior semicircular canals, and parts of the saccule) were dissected out from Long-Evans rat pups in chilled and oxygenated Leibovitz-15 medium (L-15, Sigma-Aldrich, St. Louis) supplemented with 10 mM HEPES (pH 7.4, ~325 mmol/kg). The excised tissue was then incubated in 0.25% trypsin and 0.05% collagenase (Sigma-Aldrich) for 30 minutes at 37°C. The ganglia were dissociated by gentle trituration onto glass-bottomed culture dishes (MatTek, Ashland, MA). Animals were handled in accordance with the *National Institutes of Health Guide for the Care and Use of Laboratory Animals* and all procedures were approved by the animal care committee at the Massachusetts Eye and Ear Infirmary. Chemicals were obtained from Sigma-Aldrich (St. Louis, MO) unless otherwise specified.

For acute dissociations, somata were isolated from postnatal day 1-8 rats (P0 as day of birth), allowed to settle at room temperature on uncoated glass, and recorded from at times between 1 and 7 hours post-trituration. For overnight-cultured dissociations, somata were isolated from P1-P11 rats, triturated onto poly-d-lysine coated glass, then incubated in serum-free MEM+Glutamax (Invitrogen, Carlsbad, CA) supplemented with 10 mM HEPES and 1% penicillin/streptomycin (Invitrogen). Cultured cells were maintained in 5% CO_2/ 95% air at 37°C for ~20 hours to reduce satellite cells and improve access to the neurons. In a few experiments (where specified), the medium was supplemented with 5 ng/mL BDNF (PeproTech, Rocky Hill, NJ).

Solutions

During recording sessions, cells were held in a bath of pre-oxygenated L-15 medium. The recorded cell was locally superfused with an external solution designed to minimize ionic currents other than sodium currents by including the K channel blocker tetraethylammonium (TEA; 50 to 75 mM), substituting Cs^+ for K^+, and substituting Mg^{2+} for Ca^{2+}. Solutions used are listed in Table 1. External solution was adjusted to a pH of ~7.4 with NaOH (except for $NMDG^+$ solutions which were titrated with HCl); internal solutions were adjusted to pH 7.3-7.35 with CsOH or KOH for Cs^+ and K^+-based solutions respectively. "Early" external solutions (from the early phase of this project) had osmolality of ~300 mmol/kg, while the "standard external solutions", developed later, had osmolalities of ~325 mmol/kg to match L-15 medium. The standard internal solution had an osmolarity of ~315 mmol/kg. Internal solutions had 0 or 0.8 mM Ca^{2+} and 5 or 10 mM EGTA; with 0.8 mM Ca^{2+}, the calculated free internal Ca^{2+} concentrations was between 10 and 20 nM (MaxChelator WEBMAXC, Chris Patton).

Ruptured patch whole-cell recordings

Cells were visualized by Nomarski optics at 600X with an inverted microscope (Olympus IMT-2; Olympus, Lake Success, NY). We targeted neurons by picking cells with diameters >10 μm

and sometimes partially covered by remnants of their enveloping satellite cell. In the vast majority of cases, these cells had large sodium currents, suggesting that they were neurons.

Data were acquired with a Multiclamp 700B amplifier, Digidata 1440A digitizer, and pClamp 10 software (Axon Instruments, Molecular Devices, Sunnyvale, CA) with 10 kHz low-pass Bessel filtering and at 100 kHz sampling rate. Recordings were made at room temperature (20-25°C) in whole-cell ruptured patch mode with 1–4 MΩ electrodes and 80–90% series resistance compensation (except in cases of very small currents). Electrodes were pulled on a horizontal puller from borosilicate glass (Sutter Instruments, Novato, CA) and coated with a silicone elastomer (Sylgard 184; Dow Corning, Midland, MI) to reduce electrode capacitance. Cells analyzed for voltage-dependent properties were recorded with seal resistances > 1 GΩ and series resistances (R_s) ranging from 4 to 14 MΩ.

For voltage clamp recordings in ruptured patch mode, the average residual series resistance after compensation was 1.7 ± 0.15 MΩ (n = 126, this includes recordings of small TTX-I currents where less compensation was used in order to minimize the transient artifact; for recordings that were analyzed for total Na_V current, R_{resid} was typically ≤ 1 MΩ). The mean clamp rise time ($R_s \times C_m \times$ (1-%prediction), where "prediction" was set on the amplifier) was 54 ± 4 μs (n = 80) for cells without $Na_V1.8$. Because cells with $Na_V1.8$ had more capacitance, the mean clamp rise time for those cells was 77 ± 7 μs (n = 36), which was not problematic since $Na_V1.8$ has slower overall kinetics. Activation curves were computed from recordings with < 5 mV error from series resistance at peak voltage (typically much less for the TTX-I currents due to their smaller size), good clamp time constants, and evidence of good clamp from the recorded traces. Recordings were corrected for a 5–6 mV liquid junction potential as calculated with JPCalc (Barry, 1994). Some recordings (where indicated) were performed at 37°C with a heated platform and temperature controller (TC-344B; Warner Instruments, Hamden, CT). For the purpose of identification of the type of Nav current that a cell had, moderately leaky recordings were accepted if they were unambiguous, e.g., showed the slow kinetics and positive half-inactivation values characteristic of $Na_V1.8$. Cells were held at –70 mV. To study voltage-dependent activation and inactivation, we used a 25 to 50 ms prestep to –120, –125, or –130 mV followed by an iterated series of steps from –125 to +30 mV, and terminating in a step to –15, –20, or –30 mV. Activation and inactivation were obtained from the same protocol, although in one case, separate activation and inactivation protocols were used and we obtained the same basic result. To study use-dependence, I held the cell at –90 to –100 mV and stepped by +100 mV (to 0 – 10 mV) for 7 ms at a repetition rate of twice per second.

Firing patterns were recorded using current clamp at 23-25°C (temperature controlled with heating platform if necessary to reduce variability in ambient temperature) in L-15 medium with a K^+-based internal that had a slightly higher Na^+ concentration than the Cs^+ internal (giving a predicted E_{Na} of ~+50 mV in L-15). Kalluri et al., (2010) showed that firing pattern categories ("transient" versus "sustained") were fairly robust to temperature changes. Other properties, in particular kinetics, would be expected to be different at body temperature.

Perforated patch recordings

Perforated patch recordings were achieved by adding amphotericin B at 200 μg/mL to the internal solution. Amphotericin B pores allow the passage of small monovalent ions but not divalent ions or other molecules (Horn and Marty, 1988). The internal solution for perforated patch recordings used K_2SO_4 (see Table 1) to reduce the Cl^- concentration to be closer to the intracellular concentration. This was to minimize Donnan potentials which can be generated by Cl^- diffusing freely while larger intracellular anions are unable to pass through the pores (Horn and Marty, 1988). Solutions were made fresh and discarded after 1 hour.

Pharmacology

TTX was dissolved in water to make 2 mM or 200 μM stocks which were then frozen. The appropriate amount was added to 10 mL of external solution on the day of the experiment to the working concentration. Drugs were applied via local perfusion using a Valvelink 8 perfusion controller (AutoMate Scientific, Berkeley, CA). Multiple drug lines were merged at a manifold that flowed into a single tip of 250 μM diameter and about 1 inch length. This dead volume created a useful temporal separation between any transient mechanical artifacts from line switching and onset of drug. To reduce artifacts due to the static mechanical effect of perfusion, I collected control recordings under constant perfusion of control solution. In order to visualize flow, 2 μL of latex beads (0.46 μm mean particle size, Sigma) was added to the control and drug external solutions. Cells were confirmed to be in the path of bead movement, and the flow was adjusted to a gentle but steady rate. Wash-in and wash-out of the drug was tracked by a protocol that applied a single repeated voltage step at 10-s intervals. Series resistance was noted both in control and drug solutions, and only recordings from cells with stable R_s were compared. In most cases when the cell was held for long enough to apply wash-out control solution, a satisfactory reversal was obtained (see Results).

Analysis

Analysis was performed in Matlab (The MathWorks, Natick, MA) and Clampfit (Axon Instruments, Molecular Devices, Sunnyvale, CA). Figures were prepared using Origin 8 (OriginLabs, Northampton, MA). Data are given as mean ± standard error of the mean, SE. Activation curves were generated by first plotting the peak current against step voltage, fitting the linear upper region of this curve (typically from 0 to +30 mV) to find the reversal potential (E_{rev}, which approaches E_{Na}), then dividing the peak currents by the driving force ($V-E_{rev}$). The activation curves were fit by a single Boltzmann sigmoid:

$$g\ V\ = \frac{g_{max}}{1+e^{(V_{1/2,act}-V)/s}} \qquad \text{(Eq. 1)}$$

where g_{max} is the maximum conductance, $V_{1/2}$ the voltage of half-maximal activation, and s the slope factor.

Inactivation curves were generated by plotting the peak current against the voltage of the preceding prepulses and fitting with a Boltzmann function:

$$I\ V\ = \frac{I_{max}}{1+e^{(V-V_{1/2,Inact})/s}} \qquad \text{(Eq. 2)}$$

In some cases with large artifacts and small currents and where the artifact changed smoothly and linearly with level, transient capacitive artifacts were corrected offline using a customized version of P/N subtraction: We examined the voltage traces where the sodium current had already inactivated (or had not yet activated). The largest such "pure artifact" traces were averaged to obtain an artifact waveform, whose amplitude was fit linearly across the entire range of "pure artifact" and extrapolated into the range of sodium current activity. The extrapolated artifact was then subtracted from the traces. To test the validity of this method, I compared the results with those obtained by subtracting data collected at 5 or 10 μM TTX from 300 nM TTX data (canceling out the artifact, leak, and any remnant non-Na^+ currents), and those results were found to be similar to the artifact-corrected and leak-subtracted results.

Assuming simple single-site block with an excess of drug relative to sodium channels and no conductance in the blocked state, we can apply the Langmuir equation to fitting drug dose-response curves:

$$y = \frac{1}{\frac{K_d}{drug}+1} \qquad \text{(Eq. 3)}$$

where *y* is the percent blocked (or bound) by drug.

Rearranging the Langmuir equation allows us to calculate the dissociation constant (K_d) from the amount of block at a single drug dose:

$$K_d = drug \times \frac{(1-y)}{y} \qquad \text{(Eq. 4)}$$

For determining whether cells had a component of Nav1.5 or not, only cells with total sodium current > 4 nA in vehicle solution without TTX were counted. In cells with small amounts of total current, a 7% remaining current in 300 nM TTX might be too noisy to be confidently analyzed for voltage dependence.

For calculating the relative size of $I_{TTX\text{-}I,slow}$ and $I_{TTX\text{-}S}$, we sometimes used the biophysical properties of the two currents to separate them. The TTX-S and slow TTX-I currents have almost non-overlapping inactivation ranges and different kinetics (see Fig. 9*C*), allowing for separation of the two components by inspection within the inactivation region of the total I_{Nav}. A correction must be applied since inactivation was obtained at −15 mV, and TTX-S current peaks at around −15 mV while $I_{TTX\text{-}I,slow}$ peaks around −5 mV because of its more positive activation

range. $I_{TTX\text{-}I,slow}$ was 76 ± 3.6% of peak at −15 mV (n = 13) and therefore the current size at −15 mV needed to be divided by this percentage to obtain the peak current. Using VGNs for which we had data in both vehicle and TTX conditions, we confirmed that applying a correction to current sizes obtained by visual segregation of the total I_{Nav} inactivation curves produces TTX-S : TTX-I current ratios that are in good agreement with those obtained by pharmacological separation. We applied a correction factor of 76% to cells with only TTX-free recordings to obtain approximate estimates of $I_{TTX\text{-}S}$ and $I_{TTX\text{-}I,slow}$ size.

Transgenic reporter mouse

The reporter mouse was provided by Fu-Chia Yang and Qiufu Ma at the Harvard Neurobiology department. The reporter mouse was generated by crossing an SNS-cre line (Agarwal et al., 2004) with a reporter line from Jackson Laboratory in which a *loxP*-flanked STOP cassette prevented transcription of a CAG promoter-driven red fluorescent protein variant (tdTomato) (Madisen et al., 2009). Tissue was dissected in L-15, then transferred to a 4% paraformaldehyde solution for 3 hours. The vestibular ganglion and epithelium was sectioned, counterstained, and visualized with a confocal microscope. The live epithelium was also examined under differential interference contrast (DIC) and epifluorescence microscopy.

	NaCl	Na_2 CrPhos	KCl	CsCl	$MgCl_2$	TEA-Cl	4-AP	ATP	EGTA	$CaCl_2$
Standard External Solution (Cs^+)	80			5.4	2.5	75				
Standard Internal Solution (Cs^+)		3.5		148				3.5 (Mg)	5 or 10	0.8
Standard External Solution (K^+) (for Na_V isolation)	100		5.4		2.5	50	10			
Drug-free External (L-15) (for current-clamp)	138[1]		5.33		1.8 ($MgCl_2$ and $MgSo_4$)					1.26
Standard Internal Solution (K^+)	5	5	135					3.5 (Mg)	5	0.8
Perforated patch internal			75 K_2SO_4; 25 KCl		5				5	0.1
Early Cs^+ External	65			5.4	2.5	75				
Early External 2	130			5.4	1.2		0 or 5		1	
Early Cs^+ Internal		3.5 to 5		130	0 or 3.5			3 to 5 (Mg or Na_2)	0.2 to 10	0 or 0.8

TABLE 1. Solutions. Concentrations given in mM. All internal solutions contained 0.1 mM Li_2GTP, 0.1 mM Na-cAMP, and 5 mM HEPES. All external solutions contained 10 mM HEPES buffer, and 5 or 10 mM D-Glucose, depending on osmolarity. "Early" solutions were used in the early exploratory stages of this study. A few cells were recorded with variants of the above solutions where an equivalent molarity of TEA-Cl was substituted for NaCl in order to increase or decrease the overall size of Na currents. For NMDG substitution experiments, a matching solution was made in which all NaCl was replaced by NMDG-Cl. External solutions were pH'ed with approximately 4 mM NaOH.

[1] L-15 also contained 1.34 mM Na_2HPO_4 and 5 mM Na-pyruvate. The full formulation for L-15 can be found at http://www.invitrogen.com/site/us/en/home/support/Product-Technical-Resources/media_formulation.80.html

RESULTS

Whole-cell current and/or voltage recordings were taken from 234 somata of neurons (VGNs) isolated from the superior vestibular ganglion of rats, aged P1-P8. In all VGNs, fast inactivating inward currents that were consistent with voltage-gated sodium current (I_{NaV}) could be evoked by depolarizing voltage steps following a hyperpolarizing prepulse. Voltage-clamp recordings aimed at characterizing the inward currents were generally made with a CsCl-based external solution ("standard external solution, SES_{Cs}", Table I) designed to minimize K^+ currents (I_K) and Ca^{2+} currents (I_{Ca}), and to which various additional blockers were added. For studies correlating current clamp behavior with sodium current expression, the external ("SES_K") and internal ("SIS_K") solutions contained KCl instead of CsCl and were designed to have a more physiological sodium equilibrium potential (E_{Na}) in blocker-free external solution.

To test for TTX-insensitive (TTX-I) currents, we initially applied TTX at 300 nM, a dose chosen to almost fully block TTX-sensitive (TTX-S) currents, but expected to block TTX-I currents by at most 50%.

In some cells (69/111, 62%), the TTX-I current had a fast time course and other properties that resembled $Na_V1.5$ current, while in other cells (47/178, 26%), it was slower and resembled $Na_V1.8$ current. The remaining cells (32/109 or 29%) had neither current. In no case did we detect both currents in a single cell, although the small number of cells for which this could be unambiguously demonstrated (4), does not rule out the possibility of overlap. (Denominators differ because the data available for some cells allowed for identification of one TTX-I component but not the other, and many cells provided current-clamp data only and could not be analyzed for TTX-I currents; cultured cells were not included in the counts reported in this paragraph for reasons decribed later). We will refer to these two TTX-I components as $I_{TTX\text{-}I,fast}$ and $I_{TTX\text{-}I,slow}$ and to total Na_V current as I_{Nav}. Evidence for each TTX-I component is provided in sequence in the following sections.

Previous reports of Na_V currents in young rodent VGNs characterized a single, TTX-S, type of current (Chabbert et al., 1997; Risner and Holt, 2006). Our data suggest why TTX-I currents were not previously detected. Most of our sample (about 75%) either had only TTX-S current (Fig. 1; Table 2) or had an additional $I_{TTX\text{-}I,fast}$ that was too small to affect the gross voltage dependence of the total Na_V current (see next section).

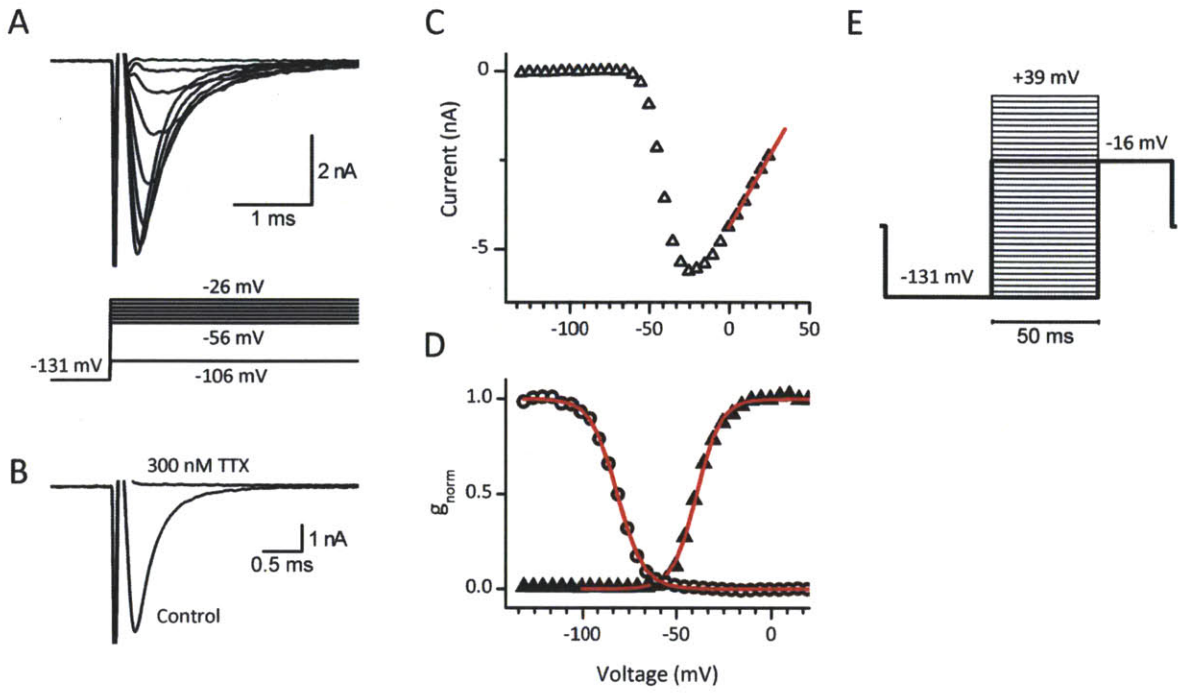

FIGURE 1. Some VGN expressed only TTX-sensitive currents with fast kinetics and moderately-negative voltage dependence. Examples are shown for a cell from postnatal day 3. *A*: Activation was assessed after a 50 ms prestep to ~−130 mV. The capacitive artifact has been truncated. *B*: No fast inward current remained in 300 nM TTX (step to −20.6 mV). *C*: The I-V curve peaks at ~−25 mV; a line fit to the inactivation region (*red*) reverses at +55 mV. *D*: Activation was fit by a Boltzmann sigmoid with: $V_{1/2act}$ = −39.4 mV, s = 6.3 mV, g_{max} = 82 nS. Inactivation was fit with: $V_{1/2inact}$ = −81 mV , s = −7.0 mV, I_{max} = −5631 pA (*red curves*). *E*: A single protocol was used to obtain activation and inactivation voltage dependence. A de-inactivating step to ~−130 mV was followed by a series of 50 ms (or in some cases, 80 ms) long steps in 5 mV increments. Typically, inactivation voltage-dependence was obtained from an activating step to ~−15 mV. Junction potential is included in these values. Activation from the first sweep differed from the 24th sweep (*thick lines*) only by the duration of the pre-step and the order of delivery (referred to in a later section).

Some vestibular ganglion neurons express a fast TTX-insensitive I_{Na} that resembles $Na_v1.5$ current

PROPERTIES OF $I_{TTX\text{-}I,FAST}$. Many isolated VGN had a small but significant component resembling current carried by $Na_V1.5$ channels, as revealed in 300 nM TTX. TTX-S currents are blocked by TTX with K_d values in the 1-10 nM range, while $Na_v1.5$ current has ~100-fold lower sensitivity (Cribbs et al., 1990). Thus, 300 nM TTX would be expected to block most TTX-S current while sparing more than half of $Na_V1.5$ current. The total Na_V current (I_{Nav}) in these cells had typical TTX-S voltage dependence (Table 2) and was blocked by ~93% in 300 nM TTX. The small current that remained in 300 nM TTX, however, had very different voltage dependence (Fig. 2). As compared to the total sodium current, the current isolated in 300 nM TTX ($I_{TTX\text{-}I,fast}$) had similar

time course of inactivation at 0 mV of between 200 and 300 µs (Table 2), but was slightly slower in its activation (t_{peak} = 330 ± 30 µs, n = 8 for I_{Nav}; 470 ± 30 µs, n = 9 for $I_{TTX\text{-}I,fast}$). Close inspection revealed, however, that $I_{TTX\text{-}I,fast}$ had substantially more negative voltage dependence than I_{Nav} (Fig. 2, Table 2). The midpoint of inactivation of $I_{TTX\text{-}I,fast}$ ($V_{1/2inact}$ = −102.8 ± 1.47 mV, s = 9.9 ± 0.64 mV, n = 18) was ~25 mV more negative than total current and the activation midpoint ($V_{1/2act}$ = −48 ± 1.3 mV, s = 8.2 ± 0.41 mV, n = 11) was ~8 mV more negative. The rapid activation and inactivation time courses strongly differentiate both $I_{TTX\text{-}S}$ and $I_{TTX,I\text{-}fast}$ from the $Na_V1.8$-like current ($I_{TTX\text{-}I,slow}$) described in a later section. The voltage dependence of activation and inactivation are substantially more negative for $I_{TTX\text{-}I,fast}$ than for both $I_{TTX\text{-}S}$ and $I_{TTX\text{-}I,slow}$. Thus, the $V_{1/2inact}$ of $I_{TTX\text{-}I,fast}$ is consistent with $Na_V1.5$ subunits and no others (see Discussion and Table 3.).

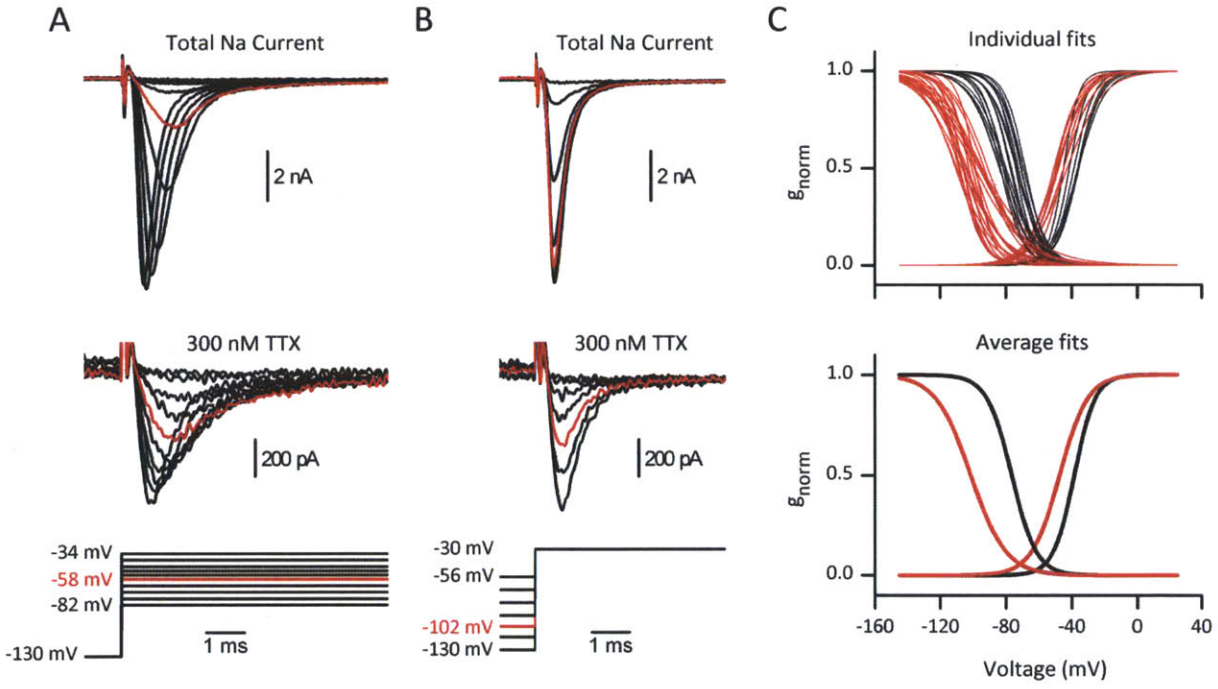

FIGURE 2. Some VGN expressed a small Na^+ current component with moderate TTX insensitivity, fast kinetics,and negative voltage dependence, consistent with the $Na_V1.5$ subunit. Responses in 5 µM TTX were subtracted from both the total current and the current in 300 nM TTX. This method underestimates the size of the $Na_V1.5$-like component, but provides a cleaner isolation of sodium currents. *A*: Most of the current was eliminated by 300 nM TTX (see scale bar), but the current that remained activated at slightly more negative voltages than the total Na^+ current (which was dominated by TTX-S current). *B*: Current remaining in 300 nM TTX inactivated at much more negative voltages, as is characteristic of $Na_V1.5$ current. *C*: Activation and inactivation properties of total Na^+ current (black) and current in 300 nM TTX in cases where a significant fast-inactivating current remained (red). (Black curves were taken from all cells for which TTX-S current data were available, including cells with exclusively TTX-S currents.)

In cells with $I_{TTX\text{-}I,fast}$, TTX-S current ($I_{TTX\text{-}S}$) made up the majority of I_{Nav}. It is not surprising therefore that previous studies on VGNs concluded that all Na_V current is TTX-sensitive. $I_{TTX\text{-}S}$ could be obtained by subtraction of records in 300 nM TTX (or lower doses of TTX) from control records and had similar voltage dependence and time course to I_{Nav} (Table 2.). Despite the very different voltage-dependence properties of $I_{TTX\text{-}I,fast}$, its small size meant that I_{Nav} generally resembled $I_{TTX\text{-}S}$ in its properties. The mean within-cell difference in $V_{1/2inact}$ value between $I_{TTX\text{-}S}$ and I_{Nav} was 0.48 ± 0.24 mV (n = 9) which is less than the standard error of the mean for measurements averaged across cells, and the within-cell difference in time course was always ≤ 40 µs and typically ≤ 20 µs (8 cells, 2 to 4 pairs of measurements of t_{peak} or τ_{inact} per cell). Although $I_{TTX\text{-}I,fast}$ might be expected to be add a second component to the voltage dependence curves, in practice, we found deviations from a single Boltzmann fit to be minimal. This is consistent with a simulation where $I_{TTX\text{-}I,fast}$ contributes 10% of the total Na_V current (Fig. 4*B*).

Current	VGN	Inactivation		Activation			Time course		
	population	$V_{1/2}$ (mV)	S (mV)	$V_{1/2}$ (mV)	S (mV)	nS/pF	t_{peak} at 0 mV (ms)	t_{peak} at −15 mV (ms)	τ_{inact} at 0 mV (ms)
Na_V (total)	VGN with $I_{TTX\text{-}I,fast}$	−76.9 ± 1.5 (13)	7.5 ± 0.4	−40.1 ± 2.0 (6)	6.0 ± 0.5	7.4 ± 1.4	0.33 ± 0.03 (8)	0.42 ± 0.03 (10)	0.26 ± 0.02 (10)
	VGN without $I_{TTX\text{-}I,fast}$ or $I_{TTX\text{-}I,slow}$	−79.5 ± 1.3 (3)	6.6 ± 0.2	−38.6 (1)	6.2	7.24	0.25 ± 0.003 (3)	0.31 ± 0.01 (5)	0.21 ± 0.01 (4)
	cultured VGN (no BDNF)	−76.3 ± 0.2 (12)	7.6 ± 0.1	−37.4 ± 0.7 (8)	5.2 ± 0.1	9.8 ± 0.4			
	cultured VGN (+BDNF)	−69.5 0.7 (3)	6.1 ± 0.3	−31.8 (2)	7.4	5.7			
TTX-S	VGN with $I_{TTX\text{-}I,fast}$	−74.3 ± 1.7 (9)	6.3 ± 0.4	−39.8 ± 2.5 (6)	5.7 ± 0.8	6.1 ± 0.4	0.32 ± 0.03 (7)	0.40 ± 0.04 (8)	0.25 ± 0.02 (7)
	VGN with $I_{TTX\text{-}I,slow}$	−66.9 ± 1.8 (9)	11.5 ± 1.12	−32.3 ± 0.7 (6)	5.9 ± 0.5	3.1 ± 0.34 (5)			
TTX-I, fast	all	−102.8 ± 1.47 (18)	9.9 ± 0.6	−48 ± 1.3 (11)	8.2 ± 0.4	1.0 ± 0.2 (9)	0.47 ± 0.03 (9)	0.53 ± 0.03 (11)	0.27 ± 0.03 (8)
TTX-I, slow	all	−31.4 ± 0.6 (23)	5.2 ± 0.2	−16.5 ± 0.6 (8)	4.5 ± 0.2	1.5 ± 0.3 (7)	1.4 ± 0.1 (6)	3.1 ± 0.2 (6)	2.4 ± 0.1 (11)

TABLE 2. Electrophysiological properties of Na_V currents in vestibular ganglion neurons. Values are means ± standard error of the mean, with n in parentheses. $I_{TTX\text{-}S}$ was computed by subtracting currents in 300 nM TTX (or a lower dose of TTX that would mostly block TTX-S current) from I_{Nav}. Recording quality requirements are higher for activation analysis, hence the smaller samples for activation than inactivation. Time course measurements were made on data in which inward current exceeded outward current by ≥15-fold, indicating a low level of contamination, or , in the case of $I_{TTX\text{-}I,fast}$, after subtraction of recordings made in a higher concentration of TTX or in +200 µM Cd^{2+}.

Current type	TTX K_d	$V_{1/2inact}$ (mV)	$V_{1/2act}$ (mV)	K_d for block by Cd^{2+}	τ_{inact} (ms)
Na_V TTX-S	1 to 25 nM[1]	−35 to −78[1]	−8 to −40[1]	4.5 to 5.5 mM[1]	0.3 to 1.3[1]
$Na_V1.5$	150 nM to 2 μM[2]	−82 to −106[2]	−47.8 to −56[2]	50 to 250 μM[2]	0.6 to 1[2]
$Na_V1.8$	60 to >100 μM[3]	−53 to −29[3]	−21 to −9[3]	300 μM[3]	2.6 to 13.5[3]
$Na_V1.9$	39 to 200 μM[4]	−99 to −32[4]	−36.3 to −31.8[4] (Cl^- internally)	233 μM or resistant up to 1 mM[4]	3 to 101[4]
Ca_V T-type					
$Ca_V3.1$	n/a	−84 to −62[5]	−63 to −45[5]	128 μM[5]	11 to 62[5]
$Ca_V3.2$	n/a	−86 to −47[5]	−60 to −39[5]	65 μM[5]	13 to 120[5]
$Ca_V3.3$	n/a	−73 to −69[5]	−56 to −37[5]	157 μM[5]	6 to 273[5]

TABLE 3. Reported properties of inactivating inward currents.

[1] Smith and Goldin (1998), Noda et al. (1986), Chen et al. (2000), Moran (2003), Dietrich et al., (1998), and Sangameswaran et al., (1997).

[2] DiFrancesco et al. (1985), Frelin et al. (1986), Sheets and Hanck (1992), Yamamoto et al. (1993), Kuo et al. (2002), O'Leary (1998), Cummins et al. (1998), and Sheets and Hanck (1999).

[3] Roy and Narahashi (1992), Elliott and Elliott (1993), Akopian et al. (1996), Sangameswaran et al. (1996), Cummins and Waxman (1997), Scholz et al., (1998), Renganathan et al. (2002), Zhou et al. (2002), Cummins et al. (2002), Leffler et al. (2005), Ho and O'Leary (2011).

[4] Cummins et al. (1999), Rugiero et al. (2003), Maruyama et al. (2004), Coste et al. (2004), Renganathan (2002); inactivation voltage dependence depends on protocol and internal anion.

[5] IUPHAR Ion Channel Database (Catterall et al.), Dìaz et al. (2005); voltage dependence is unaffected by being carried by Na^+ (Fukushima and Hagiwara, 1985).

Given the small size of the $I_{TTX\text{-}I,fast}$ component, we sought additional evidence that it did not simply consist of a small fraction of the TTX-S current not blocked by 300 nM TTX. Another property of $Na_V1.5$ current that distinguishes it from TTX-S current is its sensitivity to block by divalent cations, such as cadmium and zinc, which are typically thought of as calcium channel blockers (Backx et al., 1992; Chen et al., 1992; Heinemann et al., 1992; Satin et al., 1992b). The reported half-blocking concentrations (IC_{50}) for Cd^{2+} against $Na_V1.5$ current range from 50 to 250 μM (DiFrancesco et al., 1985; Scornik et al., 2006; Wooltorton et al., 2007) in contrast to 5 mM for TTX-S currents (Frelin et al., 1986; Roy and Narahashi, 1992). The sensitivity of $Na_V1.5$ channels to Cd^{2+} is thought to reside in the same pore loop residue (cysteine 374) that confers TTX insensitivity, although that residue does not seem to determine the Cd^{2+} sensitivity for $Na_V1.8$ and $Na_V1.9$ (Backx et al., 1992; Satin et al., 1992b; Leffler et al., 2005).

We hypothesized that if $I_{TTX\text{-}I,fast}$ were primarily composed of $Na_V1.5$ subunits, it would be significantly blocked by 200 μM Cd^{2+}, a dose that should have only a small effect on $I_{TTX\text{-}S}$. Recordings were started in SES_{Cs}-300 nM TTX and were switched into SES_{Cs} containing 300 nM TTX plus 200 μM $CdCl_2$. Voltage pulses were delivered every 10 seconds from a de-inactivating pre-step at −130 mV to a test step at −20 mV, chosen to activate nearly maximal I_{Nav}. Indeed, 200 μM Cd^{2+} reversibly blocked $I_{TTX\text{-}I,fast}$ by 52.7 ± 4.4% (*n* = 13) (Fig. 3*A-B*). Assuming that the block is of a single current, and applying the Langmuir equation (Eq. 4, Methods), we estimate the K_d to be about 179 μM. If any TTX-S current remained in 300 nM TTX, it should not have been blocked by Cd^{2+}, and the actual fractional block of $Na_V1.5$ would have been underestimated. In that case, the actual K_d of the TTX-I component would have been even lower than we estimated. Since divalent ions, and especially Cd^{2+} and Zn^{2+}, compete for a common binding site with guanidinium toxins such as TTX, Cd^{2+} IC_{50} values estimated in the presence of TTX, as we have done, may be at the upper end of the range (Doyle et al., 1993; Renganathan et al., 2002).

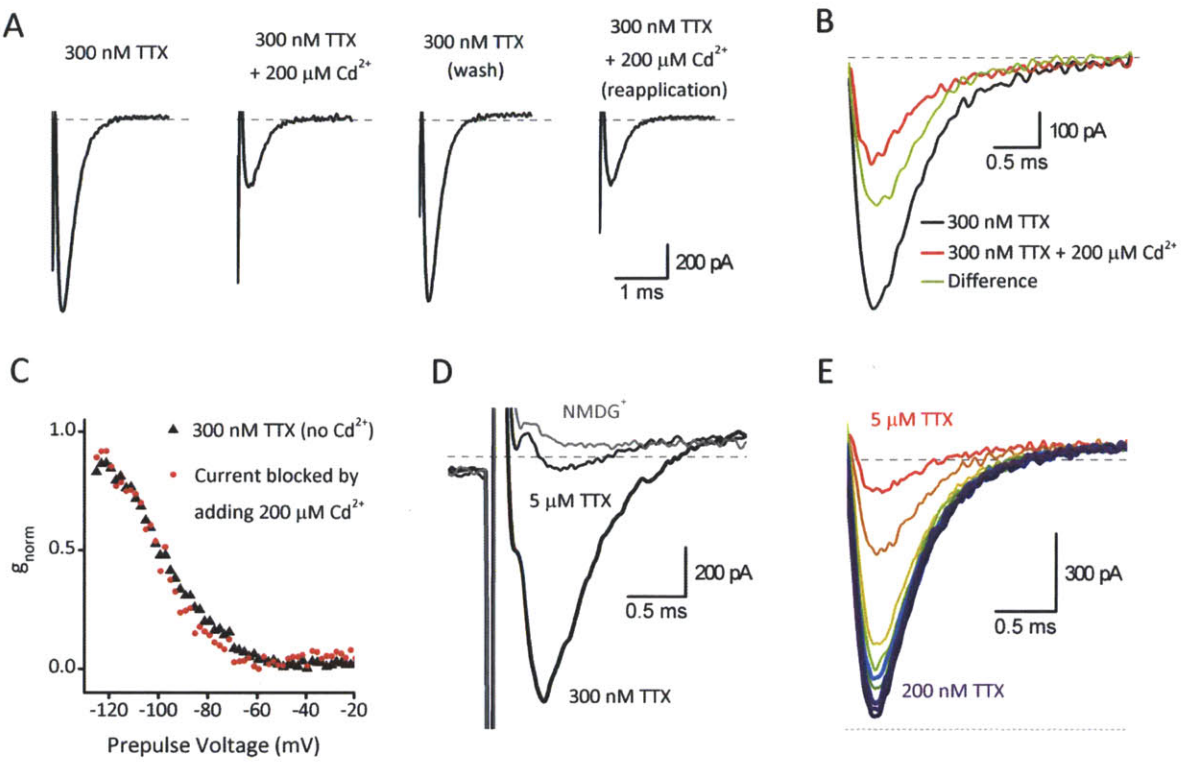

FIGURE 3. Further evidence that $I_{TTX\text{-}I,fast}$ is carried by $Na_V1.5$-like channels: it was partly blocked by 200 µM Cd^{2+}, mostly blocked by 5 µM TTX, and was eliminated by $NMDG^+$ substitution for Na^+. *Dashed gray line* indicates 0 pA; in some cases, a small amount of late outward current (likely carried by Cs^+ or K^+) remained in our standard solutions. *A:* The current isolated by 300 nM TTX was highly sensitive to external Cd^{2+} and could be blocked repeatedly and reversibly (*A*). The current that was blocked by Cd^{2+} (likely exclusively $Na_V1.5$ current) had time course (*B*) and inactivation properties (*C*) similar to the total current remaining in 300 nM TTX. *D*: A P7 neuron with $I_{TTX\text{-}I,fast}$ that was mostly blocked by 5 µM TTX and eliminated by $NMDG^+$ substitution (no TTX). This cell was lost after the current had recovered to 64% of its original size in 300 nM TTX (not shown). *E*: Drug washout from 5 µM to 200 nM TTX in a P2 neuron showed almost complete recovery (dotted line indicates peak amplitude in 200 nM TTX before 5 µM TTX was applied).

The current blocked by 200 µM Cd^{2+} resembled the total $I_{TTX\text{-}I,fast}$ in its inactivation voltage-dependence (Fig. 3C) and kinetics (Fig. 3B), supporting the interpretation that a single Cd^{2+}-sensitive, negatively-inactivating current dominated at 300 nM TTX. At 200 µM, Cd^{2+} is not expected to affect t_{peak} or voltage dependence of inactivation, but has been reported to shift activation (Hanck and Sheets, 1992). We did not observe an obvious Cd^{2+}-induced shift in activation. The lack of a major shift in voltage-dependent properties validates the use of a single large voltage step to assess approximate extent of block. As a negative control, we confirmed that the total sodium current in the absence of TTX, which is dominated by TTX-S current, was not significantly blocked by 200 µM Cd^{2+} (block of 0.6 ± 4.7%, n = 3). Although the

$Na_V1.5$-like component in the total current should be half-blocked in 200 μM Cd^{2+}, our recording stability did not always permit us to detect a 50% block of a 10% component, and $Na_V1.5$-like current was absent in one of these cells and unconfirmed in the other two.

Given that $I_{TTX\text{-}I,fast}$ was partly blocked by 200 μM Cd^{2+} (Fig. 3), can we rule out the possibility that it is a Ca^{2+} current? First, $I_{TTX\text{-}I,fast}$ could be mostly blocked by a high dose of TTX (5 μM or more) with no change to the outward current (~90% block in going from 200 nM to 5 μM TTX, n = 2; from 300 nM to 5 or 10 μM TTX, n = 4; from 1 μM to 10 μM TTX, n = 1). In two of these cells, we tested for reversibility and in both cases the additional block could be applied and reversed multiple times. The difference current obtained by subtracting current in 5 or 10 μM TTX from current in 300 nM TTX had similar biophysical properties to $I_{TTX\text{-}I,fast}$, consistent with $I_{TTX\text{-}I,fast}$ being primarily a single, TTX-blockable (and therefore Na_V), current. The elimination of outward currents in the subtraction made the characterization more reliable and such a subtraction method was applied to the raw traces shown in Fig. 2*A* and 2*B*. Secondly, the current was eliminated by replacement of external Na^+ with the impermeant $NMDG^+$ (Fig. 3*D*). Secondly, inactivation of $I_{TTX\text{-}I,fast}$ was too fast and too negative in its voltage range for a T-type Ca^{2+} current; reported voltage ranges of Na_V currents and T-type currents are compared in Table 3. Lastly, our external solutions for recording Na_V currents had no added Ca^{2+}; trace amounts were not measured but were unlikely to be > 10 μM. Calcium channels become somewhat permeable to Na^+ at concentrations of Ca^{2+} below 10^{-5} or 10^{-6} M (Almers and McCleskey, 1984; Hess and Tsien, 1984). These extremely low concentrations are usually achieved with chelators since trace calcium levels are about 10^{-5} M, e.g., Levi and DeFelice, 1986) but at 10 μM external Ca^{2+} they should be prevented from becoming Na^+ permeable (e.g., used in Elliott and Elliott, 1993). Our external solution had no Ca^{2+} chelating agents and did include 2.5 mM Mg^{2+}, which would have greatly diminished currents through Ca_V channels (Fukushima and Hagiwara, 1985; Kurejová et al., 2007). The reversal potential of $I_{TTX\text{-}I,fast}$ was also consistent with the current being carried by Na^+. Several different intracellular and extracellular solutions were used, each with a different E_{Na}; for the most commonly used SES_{Cs}, the mean fitted E_{Na} was +49.2 ± 2.0 mV (n = 8) for total Na_V current and +49.8 ± 4.7 mV (n = 6) for $I_{TTX\text{-}I,fast}$. The mean within-cell difference between reversal of I_{Nav} and $I_{TTX\text{-}I,fast}$ was −0.98 ± 1.09 mV (n = 5). Therefore, it is likely that the $I_{TTX\text{-}I,fast}$ is carried by Na_V channels and not T-type calcium channels.

PROPORTIONS OF $I_{TTX\text{-}S}$ AND $I_{TTX\text{-}I,FAST}$ CURRENT IN VGNS. $Na_V1.5$ channels are only moderately insensitive to TTX, so doses that almost completely block the larger TTX-S current would be expected to also produce some block of $I_{TTX\text{-}I,fast}$, making a clean separation difficult. However, we can make some estimates based on the dose-response curve for the mixed Na^+ current.

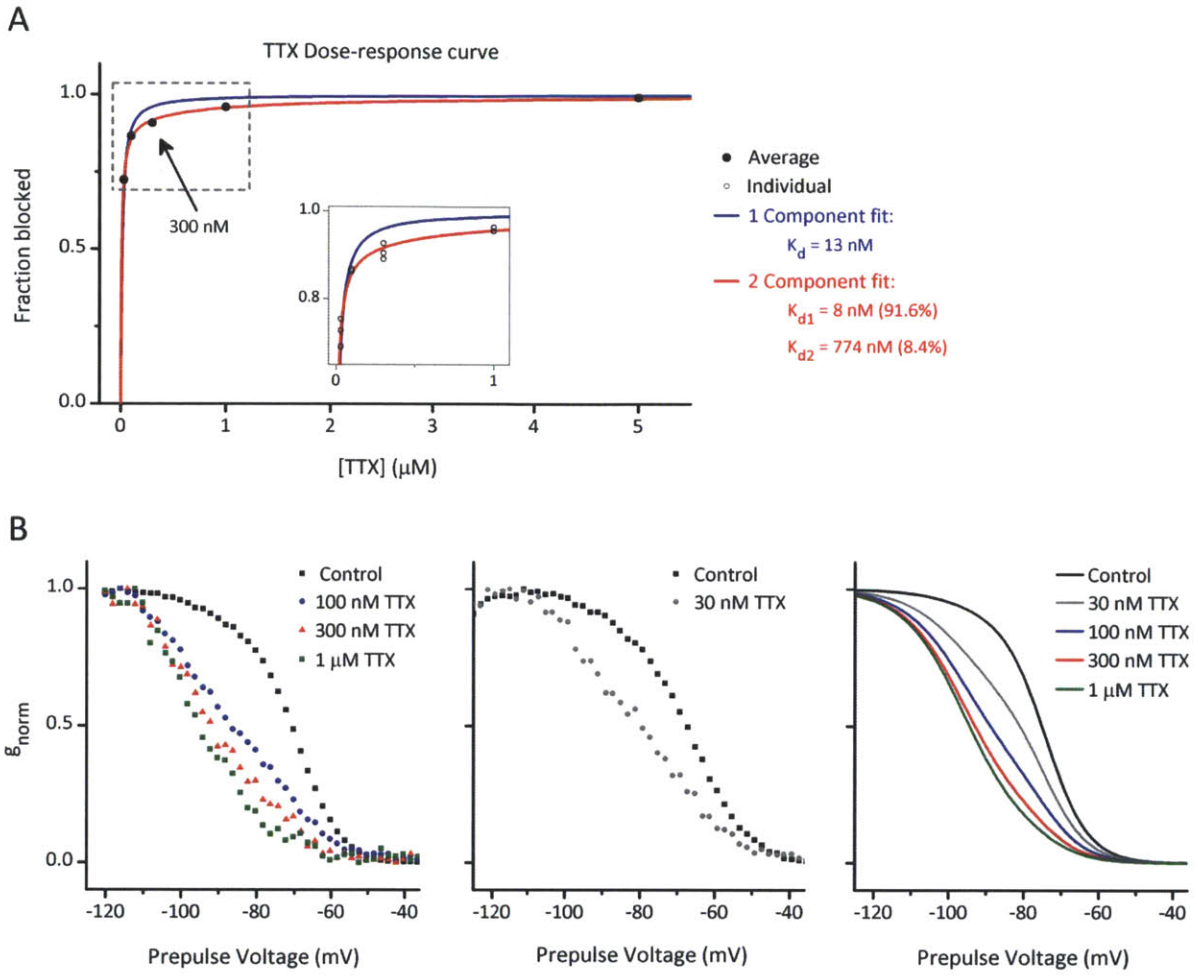

FIGURE 4. The dose-response and inactivation properties of the mixed Na^+ current suggest that $Na_V1.5$ current makes up ~10% of the total Na^+ current. *A*: 11 data points from 5 cells show a small but consistent deviation (see inset) from a single component fit to the Langmuir isotherm (see Methods). A two-component fit finds that 8.4% of the total current has a K_d that is consistent with $Na_V1.5$. *B*: Two cells challenged with various doses of TTX (left and center) show a similar qualitative behavior to a simulation (right) designed with a 10% $I_{TTX\text{-}I,fast}$ component ($V_{1/2inact}$ = −96 mV, s = 8 mV, and $K_{d,TTX}$ = 700 nM) and a 90% TTX-S component ($V_{1/2inact}$ = −74 mV, s = 5.6 mV, and $K_{d,TTX}$ = 5 nM). In the absence of TTX, properties of the 90% component dominate. At moderate doses of TTX (100-300 nM), $V_{1/2inact}$ shifts negatively and slope becomes broad. At high TTX doses (1 μM), the 10% TTX-insensitive component dominates.

It was hard to ensure sufficient stability of one cell to deliver all the drug conditions, so data from cells with $I_{TTX\text{-}I,fast}$ were pooled by normalizing the size of the total current in TTX-free SES_{Cs} to be equal to one. A dose-response curve based on 11 data points from 5 cells is better fit by a two-component than a one-component model (Fig. 4*A*). According to the two-component fit, $I_{TTX\text{-}I,fast}$ comprised on average 8.4% of the total current and had an IC_{50} of 774 nM; $I_{TTX\text{-}S}$ constituted the remainder with an IC_{50} of 8 nM. Although the deviation from a single-

component fit is small, it exceeds the variability between the data points (Fig. 4*A*, *inset*). A mixture of 90% TTX-S current and 10% $Na_V1.5$ current with comparable current densities was reported in dissociated adult canine intracardiac ganglion (containing parasympathetic neurons that regulate heart rate as opposed to the cardiac myocytes which are dominated by $Na_V1.5$) (Scornik et al., 2006). Our estimated K_d for $Na_V1.5$ is within the range reported for $Na_V1.5$ (150 nM – 2 μM, as reviewed in Wooltorton et al., 2007).

The absolute size of the $Na_V1.5$-like component ranged from ~200 pA to ~2000 pA. As cells were of different sizes and were recorded using solutions with different E_{Na} values, we present the average conductance normalized by capacitance, which is proportional to the membrane surface area, rather than average current. Following common usage, we refer to this normalized conductance as a conductance density, even though it is not normalized directly to surface area. The mean conductance density was 1.0 ± 0.2 nS/pF (n = 9). The average maximal conductance of 13.0 ± 2.6 nS (n = 9) yields a density of ~50% of that reported for $Na_V1.5$-like current in immature rat utricular hair cells of the same age range (Wooltorton et al., 2007).

EFFECTS OF OVERNIGHT CULTURE. Overnight culture is sometimes used to reduce satellite cell coverage of VGN somata to facilitate patch clamp recording (e.g., in Limón et al., 2005; Kalluri et al., 2010). Data from 14 cells recorded after overnight culture suggested that $I_{TTX\text{-}I,fast}$ was diminished by culturing in our conditions. The effects of various concentrations of TTX (100 nM, 300 nM, 1 μM) produced no evidence for significant $Na_V1.5$-like current in most of the cultured neurons. In 8 of 12 neurons, sodium current in 300 nM TTX was undetectable or too small to be analyzed, while 3 of the 4 remaining neurons showed possible evidence for a diminished $I_{TTX\text{-}I,fast}$. In recordings from acutely isolated VGNs with $I_{TTX\text{-}I,fast}$, application of TTX shifts the voltage dependence in the negative direction presumably because of the preferential block of the less-negatively inactivating $I_{TTX\text{-}S}$ (Fig. 4*B*). The addition of 100 nM TTX produced an average shift of −20.4 ± 1.25 mV (n = 5) in acute cells with $I_{TTX\text{-}I,fast}$. In contrast, the shift in cultured VGNs was at most −3.8 mV and on average −1.8 ± 0.7 mV in 100 nM TTX (n = 4, none of which were considered to have $I_{TTX\text{-}I,fast}$) (Fig. 5*A*), consistent with either an absent or severely reduced $I_{TTX\text{-}I,fast}$, or a change in its inactivation range. For acutely isolated VGN, adding 300 nM TTX shifted $V_{1/2,\ inact}$ by about 25 mV in the negative direction (Fig. 2*C* and 5*C*). In the three cultured cells that potentially had $I_{TTX\text{-}I,fast}$, the current remaining in 300 nM TTX was only 2.7 ± 0.4 % of the total current, compared with 9.6 ± 2.0 % (n = 6) for acutely-recorded cells with $Na_V1.5$-like current (Fig. 5*B*), and the shift was only about −10 mV (Fig. 5*C*), suggesting that if $I_{TTX\text{-}I,fast}$ were present, it was much reduced in relative size. It is unlikely that our sample of 14 cells failed to include cells with $I_{TTX\text{-}I,fast}$ by chance. As described in a later section, the prevalence of $Na_V1.5$ in acutely dissociated cells was particularly high at the younger ages, with 78% of P1-4 neurons having significant $I_{TTX\text{-}I,fast}$ (as opposed to 64% of neurons for the entire data set of P1-P8) . If $I_{TTX\text{-}I,fast}$ were present at similar incidence and relative size in cultured neurons as in acutely

dissociated neurons, then the probability of not encountering such a current in all six P1-P4 cultured neurons by chance would have been very low (0.22^6, <1%). Therefore, we did not continue to culture the cells and limited subsequent experiments to the time period within 7 hours of dissociation. The density of total I_{Nav} did not differ significantly between acutely dissociated VGNs (9.3 ± 1.1 nS/pF, n = 19) and cultured VGNs (9.0 ± 1.0 nS/pF, n = 14), nor did the voltage-dependent properties (Table 2). [Interestingly, three cells cultured with 5 ng/ mL BDNF had slightly depolarized voltage dependence ($V_{1/2inact}$ = −69.5 ± 0.7 mV, s = 6.1 ± 0.3 mV, n = 3; $V_{1/2act}$ = −31.8, s = 7.4, n = 2), but more data would be needed to confirm and understand this observation. Only data from acutely recorded cells are pooled in the analysis below.]

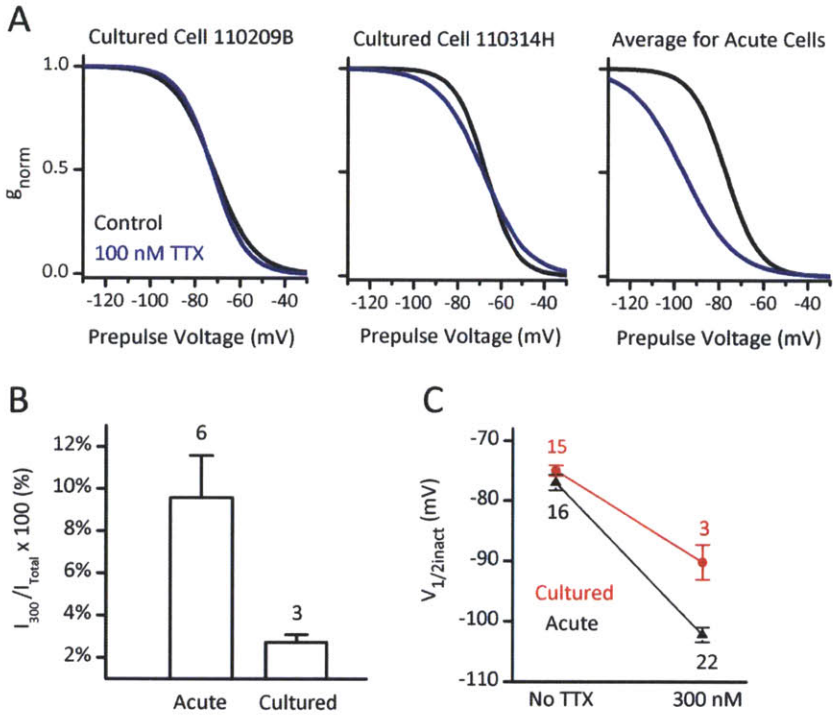

FIGURE 5. Overnight-cultured neurons (n = 14) expressed little or no TTX-insensitive current. In 11/14 cultured VGN, there was no current remaining in 300 nM TTX or so little current that it could not be analyzed quantitatively. This was corroborated by the lack of shift in $V_{1/2inact}$ in 100 nM TTX in 4 out of 4 cultured cells, of which two examples are shown in (*A, left, middle*). This lack of shift is in stark contrast to the large shift that is typically seen in 100 nM TTX for acute cells (*A, right,* average of n = 5). *B-C*: In 3 of the 14 cells, the current remaining in 300 nM TTX was suggestive of $Na_V1.5$-like current. However, the size of this current relative to the total Na^+ current was significantly reduced compared to data from cells recorded from acutely. The largest % remaining for cultured cells (3.3%) was less than the smallest % remaining for acute cells (3.7%). The size of the shift in $V_{1/2inact}$ at 300 nM TTX was also smaller for the 3 acute cells (*C*), pointing to a smaller $Na_V1.5$-like component. $Na_V1.8$-like current was not seen in any of the cultured cells.

CHANGES WITH POSTNATAL AGE. In the rat DRG, $Na_V1.5$ is present in ~80% of neurons at E15 but declines to ~20% by P0 and to ~3% by adulthood (Renganathan et al., 2002). $Na_V1.5$ is also present in developing skeletal muscle and is upregulated after injury (Kallen et al., 1990; Yang et al., 1991). Therefore, it was important to examine the prevalence of $I_{TTX\text{-}I,fast}$, which is likely carried by $Na_V1.5$ channels, as a function of age. Unfortunately, VGNs become harder to record from with increasing age, in part because satellite cells cling more tightly to more mature neuronal somata. That coverage can be reduced by culturing overnight, but we had reason to believe that culturing diminished $I_{TTX\text{-}I,fast}$ and limited ourselves to acutely dissociated cells (above). Given these limitations, we did not extend our data to adulthood, but instead looked at a second group of recordings at P6-8. In this age group, $I_{TTX\text{-}I,fast}$ was observed in 11/32 (32%) of vestibular ganglion neurons. We did not focus on P5 since we wanted an age group that was maximally different from P1-4, so a small number of cells are included at this age. We also had a limited number of cells at P8, which seemed to have too much satellite cell coverage to provide a good yield. The overall trend is one of decreasing incidence with age (Fig. 6).

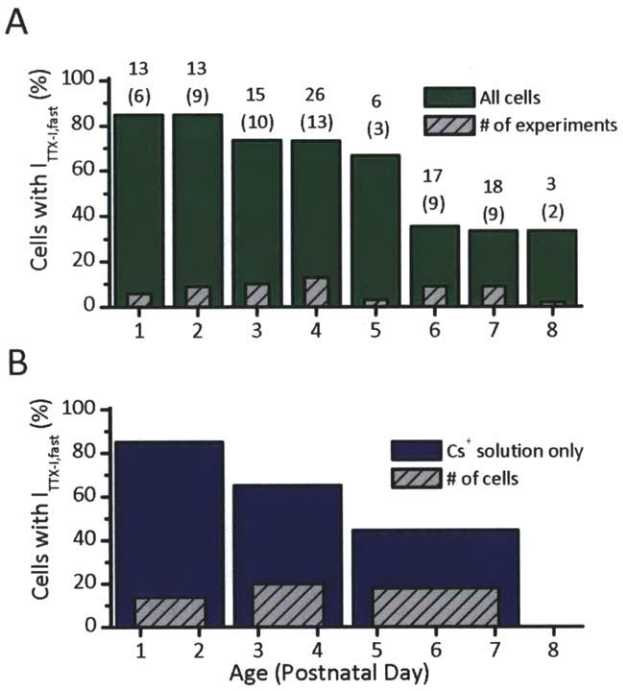

FIGURE 6. The prevalence of $I_{TTX\text{-}I,fast}$ ($Na_V1.5$-like current) shows a decreasing trend with postnatal age. *A*: We plot the percentage of cells with detectable $I_{TTX\text{-}I,fast}$ against age and report above each column the number of cells and number of experiments (*in parentheses*, also plotted in *striped gray*). Typically, $I_{TTX\text{-}I,fast}$ was identified as rapidly-inactivating and negatively-inactivating current in 300 nM TTX, but was in some cases identified based on cadmium sensitivity or a significant negative shift in the voltage dependence and broadening of the inactivation curve at 100 nM or 200 nM TTX. *B*: Internal solutions used for older cells was often K^+-based (for use in current clamp), so for a more matched comparison, we selected a subset of the cells in *A* that were recorded with the most popular Cs^+-based solution used for younger cells. These were pooled into broader age categories because of smaller sample size, and the same general decreasing trend with age is observed.

For most of the P6-P8 recordings, the pipette solutions and analysis method were designed to allow for current clamp recording of physiological firing patterns and contained K^+ instead of Cs^+ (see Methods: Firing Patterns). To check whether the difference in recording solutions between P1–P4 cells and P6–P8 cells caused a change in our ability to detect $Na_V1.5$, we also compared a subset of cells recorded with identical solutions. For cells recorded with SES_{Cs} and SIS_{Cs}, 5/9 (55%) cells recorded at P5-P7 had $I_{TTX\text{-}I,fast}$, compared with 13/20 (65%) cells recorded at P3-P4 and 12/14 (85%) cells recorded at P1-P2. The trend suggested by this smaller dataset agrees reasonably well with the overall pattern of decreasing incidence with age, suggesting that the use of the solutions intended for current-clamp did not much affect our ability to detect $I_{TTX\text{-}I,fast}$. Although the decreasing trend observed in Renganathan et al. (2002) is similar to what we observe, the developmental time course must be different. For instance, <20% of their P1 small DRG neurons express $Na_V1.5$-like TTX-I current, while over 80% of VGN seem to express $I_{TTX\text{-}I,fast}$ at P1 (similar to E15 DRG), and it is still expressed by a large fraction of cells at the end of the first postnatal week.

VERY NEGATIVE INACTIVATION RANGE OF $Na_V1.5$-LIKE CURRENT. The very negative inactivation voltage range raises interesting questions for function since these values imply that most of the current would be inactivated at resting membrane potential. We wished to rule out several potential artifactual effects of our recording conditions on the voltage dependence. TTX block of $Na_V1.5$ is known to exhibit pronounced use dependence caused by higher affinity binding of TTX to the channel after it has opened (Patton and Goldin, 1991; Satin et al., 1992a). This use-dependent TTX block can be seen in a protocol where the cell was held at −90 mV and stepped briefly to +10 mV every half-second (Fig. 7). In the presence of TTX, but not in control records, each subsequent voltage pulse evoked a smaller current until it saturated at 65-80% of the original amplitude.

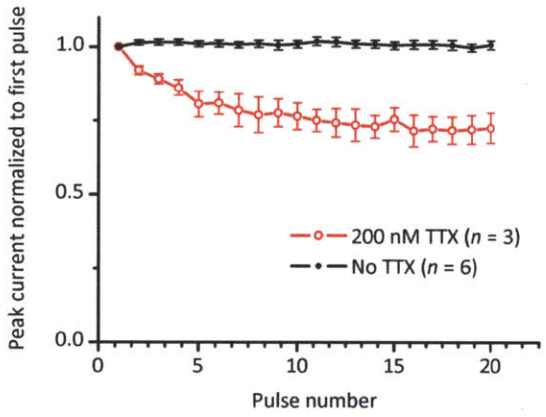

FIGURE 7. Na_V channels showed use-dependent block by TTX. In the presence, but not in the absence, of TTX, the responses to series of brief pulses (7 ms) delivered at a moderate rate (2 Hz) from a negative holding potential (−90 to −100 mV) show a decrease in amplitude over successive pulses. This is thought to distinguish TTX-I from TTX-S currents in cardiac and skeletal muscles, with TTX-I current experiencing more pronounced use-dependent block(Cohen et al., 1981; Noda et al., 1989), a property which can be abolished by targeted mutagenesis of particular residues on $Na_V1.5$ (Satin et al., 1992b). However, pronounced use-dependence has been reported for the TTX-S $Na_V1.2$ subunit expressed in *xenopus* oocyte at 30 nM TTX (Patton and Goldin, 1991). We saw very minimal use-dependent block at 4 nM TTX (near the half-blocking concentration for the TTX-S component) in one cell, but did see significant use-dependent block at 30 nM TTX in another cell.

Since our inactivation protocol involved a series of voltage steps delivered always in the same order, we wanted to verify that use-dependent block was not distorting the measurements. When we repeatedly delivered the first step of the protocol at the normal delivery rate, the amplitude of the current did not diminish, suggesting our short negative voltage prepulse did not create use-dependent TTX block. Preceding the protocol with 8 repeats of the first step, which would have brought any use-dependent block close to steady-state, did not result in significantly different $V_{1/2,\ inact}$ values (Fig. 8). Therefore, the negative voltage range of inactivation was not an artifact created by use-dependent block.

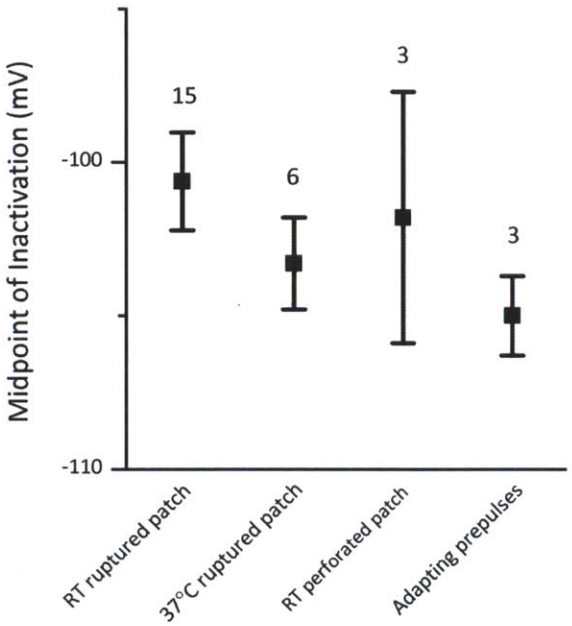

FIGURE 8. The very negative half-inactivation of $Na_V1.5$-like current was robust across a variety of conditions. RT = room temperature. Perforated patch was achieved with Amphotericin-B. Adapting prepulses: the voltage-dependence protocol was preceded by 10 pulses resembling the first sweep at 1 s start-to-start interval to rule out distortion caused by repeated pulse delivery. For instance, if use-dependent TTX block were being induced by our protocol, it might make successive pulses smaller and shift the apparent $V_{1/2inact}$ negatively. The 10 preceding pulses would be expected to then cause near steady-state block, and restore the $V_{1/2inact}$ in the positive direction. This is not observed (in fact, if anything, the values seem more negative), and is corroborated by lack of reduction in amplitude over the course of the 10 prepulses (*not shown*), suggesting that our voltage-dependence protocol does not induce use-dependent TTX block. None of the inactivation midpoints were statistically significantly different (at p=0.05) from the value in standard ruptured-patch condition ($p = 0.34$ for body temperature, $p = 0.78$ for perforated patch, $p = 0.26$ for prepulses).

We also tested whether the $V_{1/2inact}$ values were similar in two recording conditions that were more physiological. In two studies, increasing temperature from room to 37°C shifted the inactivation range +8 mV (for Nav1.5-like current in outer hair cells Oliver et al., 1997) and +19 mV (in myoballs cultured from neonatal rat skeletal muscle Ruppersberg et al., 1987). For our cells (Fig. 8), $V_{1/2inact}$ at 37°C was not significantly different from room temperature recordings. Another influence on $V_{1/2inact}$ could be loss of internal signaling molecules or enzymes that regulate voltage dependence; for example, a hyperpolarizing shift of $Na_V1.5$ has been reported during ruptured-patch whole-cell recordings (e.g., Penniman et al.). In a small sample of VGNs recorded with the perforated-patch method, which prevents changes in intracellular Ca^{2+} concentration or loss of large molecules from the cell, we saw no significant difference in $V_{1/2inact}$ (Fig. 8).

Some vestibular ganglion neurons express a slow TTX-insensitive I_{Na} that resembles $Na_V1.8$

PROPERTIES OF $I_{TTX\text{-}I,SLOW}$. In a different subset of neurons, we saw evidence for another Na_V current in 300 nM TTX which had properties resembling $Na_V1.8$. This current had even lower sensitivity to TTX than the $Na_V1.5$-like current, and will be referred to as $I_{TTX\text{-}I,slow}$. $I_{TTX\text{-}I,slow}$ was seen throughout the entire period of acute recordings (from just under 2 hours to 7 hours) and could be seen on the same day as cells with $Na_V1.5$.

The $Na_V1.8$ channel (also referred to as SNS or PN3) was cloned and identified in the dorsal root ganglion (Akopian et al., 1996), and has also been reported in other sensory ganglia. Because of its strong expression in small C-type nociceptive neurons and lack of expression in the brain, heart, and other tissues (Akopian et al., 1999), it has become an attractive therapeutic target for analgesic drugs. Compared to TTX-S channels, the most distinguishing properties of $Na_V1.8$ are its depolarized activation and inactivation range ($V_{1/2act}$ around −15 mV, $V_{1/2inact}$ around −30 mV), faster recovery from fast inactivation, and slower activation and inactivation time course. The first two properties are thought to contribute to tonic firing during sustained depolarizations (which inactivate TTX-S channels); the slower time course contributes to broader spikes with an inflection or hump during the repolarization phase of the action potential (reviewed in Rush et al., 2007).

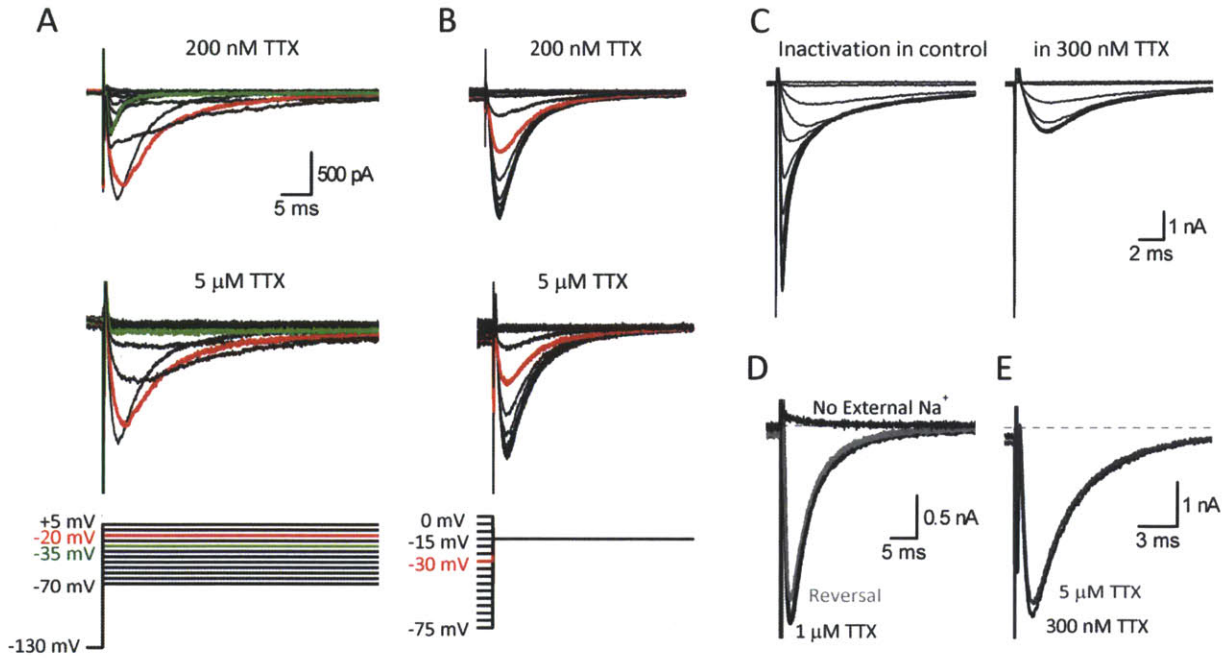

FIGURE 9. Some cells expressed a slow, TTX-insensitive component of Na^+ current that resembled $Na_V1.8$ current. *A-B*: TTX-insensitive current was slower and had more positive voltage-dependence than TTX-S current. In 200 nM TTX, a small amount of fast sodium current remained (*A*, *green trace*) that was more negatively activating (this current did not have properties resembling $Na_V1.5$). *B:* Midpoint of inactivation of $I_{TTX\text{-}I,slow}$ was around −30 mV (*B*). *C*: TTX-sensitive current could almost be completely separated from TTX-insensitive current based on voltage-dependence and kinetics during inactivation protocols (prestep from −120 to −15 mV for 80 ms, in 10 mV increments, test step to −15 mV). *D*: $I_{TTX\text{-}I,slow}$ current was completely and reversibly eliminated by replacement of external Na^+ by $NMDG^+$ (step from −130 to −5 mV). *E*: $I_{TTX\text{-}I,slow}$ was minimally blocked by 5 μM TTX (step from -130 mV to -5 mV). Dashed line indicates 0 nA.

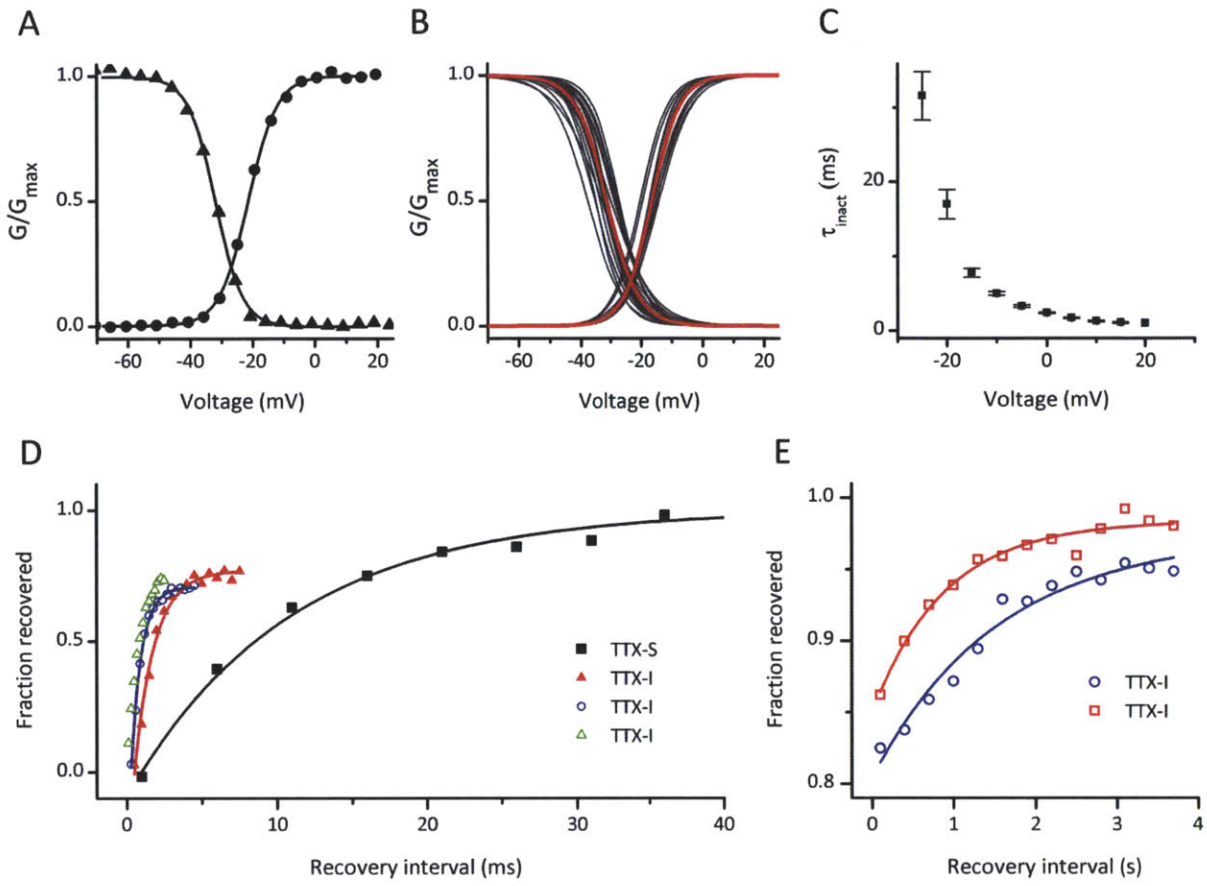

FIGURE 10. $I_{TTX\text{-}I,slow}$ displayed voltage dependence, inactivation time course, and repriming properties characteristic of $Na_V1.8$ current. *A*: Activation and inactivation of cell shown in Fig. 9*A-B*. $V_{1/2inact}$ = −30.9 mV, s = 4.6 mV, I_{max} = −1479.5; $V_{1/2act}$ = −15.0 mV, s = 5.7 mV, g_{max} = 24.4 nS. *B*: Activation and inactivation fits for individual cells (*thin dark gray lines*) and for the average fits (*thick red lines*). Values are given in Table 2. *C*: Time constants of fast inactivation were slow near the midpoint of inactivation (~−30 mV), but approached ~1 s at the highest voltages. (At +20 mV, only 2 measurements qualified (peak inward current at least fifteen times larger than outward current, arbitrarily chosen to minimize distortion of inactivation kinetics due to simultaneous activation of outward current); both points are plotted although they cannot be resolved. Number of cells included for the other voltages: n = 4 (15 mV), n = 5 (10 mV), n = 10 (5 mV), n = 11 (0 mV), n = 11 (−5 mV), n = 12 (−10 mV), n = 11 (−15 mV), n = 11 (−20 mV), n = 7 (−25 mV)) *D-E*: $Na_V1.8$-like current recovered more rapidly from fast inactivation but more slowly from slow inactivation. Inactivation was invoked by 25 ms steps to 0 mV and recovery occurred at −90 mV. Fast recovery for $Na_V1.8$-like current was about ten times faster than for TTX-S current (3 cells shown in *D*), but was incomplete. Slow recovery occurred on the timescale of seconds (2 cells shown in *E*).

In ~28% of acutely dissociated VGN, an obvious inward current remained in 300 nM TTX with relatively slow kinetics, referred to as $I_{TTX\text{-}I,slow}$. The presence of this current could be detected from recordings at 300 nM TTX, and often even from the total Na_V current in the absence of TTX; all such cells are counted for my report of prevalence. However, for analyses of kinetics, we only included recordings with sufficient TTX to block almost all signs of fast Na_V current

(typically 1 μM or 5 μM, but sometimes 300 nM TTX), and traces for which peak inward current was at least fifteen times larger than any remnant unblocked outward current. The slow current had slower time course of activation and inactivation than TTX-S or $Na_V1.5$ current (Fig. 9 and 10*C*; Table 2). The t_{peak} at 0 mV for $I_{TTX\text{-}I,slow}$ averaged 1.4 ms (Table 2), more than four-fold slower than for $I_{TTX\text{-}S}$ and about three-fold slower than for $I_{TTX\text{-}I,fast}$. The difference was more dramatic at −15 mV, with t_{peak} being almost eight-fold slower for $I_{TTX\text{-}I,slow}$ than for $I_{TTX\text{-}S}$ (Table 2). Inactivation of $I_{TTX\text{-}I,slow}$ was well fit by a single exponential and proceeded with a time constant of 2.4 ms at 0 mV, about ten-fold greater than inactivation time constants for $I_{TTX\text{-}S}$ and $I_{TTX\text{-}I,fast}$ (see Table 2 and Fig. 10*C* for τ_{inact} as a function of voltage). Of the known Na_V subunits, the values for $I_{TTX\text{-}I,slow}$ are best matched by $Na_V1.8$: reported t_{peak} is ~2 ms around 0 mV (Elliott and Elliott, 1993; Scholz et al., 1998); reported inactivation time constants range from 3 to 6 ms at 0 mV (Renganathan et al., 2002) (see Table 3). While these values were several-fold slower than for TTX-S or $Na_V1.5$ current, they were much faster than for T-type calcium channels (Table 3).

The voltage dependence of $I_{TTX\text{-}I,slow}$ was also strikingly different from that of both $I_{TTX\text{-}I,fast}$ and $I_{TTX\text{-}S}$ (Fig. 10*A*–*B*). The inactivation midpoint for $I_{TTX\text{-}I,slow}$ was −31 mV, ~40 mV more positive than that of $I_{TTX\text{-}S}$. The activation midpoint was −16 mV, ~25 mV more positive than that of $I_{TTX\text{-}S}$. These values are in excellent agreement with reported values for $Na_V1.8$ current but are much too positive for T-type Ca_V channels (Table 3).

$I_{TTX\text{-}I,slow}$ was carried by Na^+ because substitution of external Na^+ with $NMDG^+$ completely and reversibly eliminated the inward current (eliminated in 13/13 cells; reversed in 7/7 cells, Fig. 9*D*). The reversal potential of $I_{TTX\text{-}I,slow}$ in standard CsCl external was 50.5 ± 1.8 mV (n = 9), compared with 48.8 ± 1.6 mV (n = 10) for the large, fast Na_V current (vehicle condition for cells without $I_{TTX\text{-}I,slow}$, or $I_{TTX\text{-}S}$ obtained by subtraction for cells with $I_{TTX\text{-}I,slow}$) recorded with identical internal and external solutions. As described above, the slow TTX-I current is also not likely to be carried by a known Ca_V channel because its voltage dependence is too depolarized and its time course is too fast (Table 3.). Furthermore, although seals are formed in a bath solution with Ca^{2+}, all drug and control vehicle solutions for voltage-clamp recordings were nominally calcium free (often trace calcium is estimated at 10 μM), making the generation of a >1 nA inward Ca^{2+} current unlikely. The absence of extracellular Ca^{2+} raises the possibility that surface-charge screening effects (Frankenhaeuser and Hodgkin, 1957) are different from standard Ca^{2+} externals. However, we added an equal concentration of additional extracellular Mg^{2+}, which is almost as effective as Ca^{2+} (Hille et al., 1975) and in any case the predicted direction of voltage shift (hyperpolarizing) could not account for a +35 mV depolarizing shift of T-type Ca_V channel voltage dependence. The most likely interpretation is that the slow TTX-I current is carried by TTX-I Na_V channels.

Reported IC_{50} values for block of $Na_V1.8$ channels by TTX range from 60 to >100 μM (Akopian et al., 1996; Sangameswaran et al., 1996; Rabert et al., 1998) [and $Na_V1.9$, the other known highly TTX-insensitive subunit, has extrapolated IC_{50} values of 39 μM (Cummins et al., 1999) and 200 μM (Rugiero et al., 2003).] $I_{TTX\text{-}I,slow}$ was highly resistant to TTX, as it could also easily be seen in 5 μM TTX, a concentration that blocked most of the $Na_V1.5$-like current. Increasing the TTX concentration from 200 nM to 5 μM produced very little additional block of $I_{TTX\text{-}I,slow}$, although it eliminated the tiny remnant fast Na_V current still present at 200 nM TTX (Fig. 9*A–B, E*). The remnant fast Na_V current in 200 or 300 nM TTX was so small it was difficult to isolate and analyze. In only two cells were we able to see the approximate voltage-dependence of a residual fast Na_V current in 300 nM TTX by direct subtraction of 5 μM TTX; its $V_{1/2inact}$ was ~ −70 to −80 mV and therefore did not resemble $I_{TTX\text{-}I,fast}$. In several other cells, there was either no sign of a fast current in 300 nM TTX or the voltage dependence of the fast current inferred by temporal and voltage range separation of unsubtracted traces suggested that an $I_{TTX\text{-}I,fast}$ component was unlikely. This result suggests that at least many, if not all, cells with $I_{TTX\text{-}I,slow}$ current did not express $I_{TTX\text{-}I,fast}$. We can more confidently state that we never saw a slowly inactivating Na_V current in any of the cells where we saw $I_{TTX\text{-}I,fast}$. These observations suggest that $Na_V1.8$ and $Na_V1.5$ subunits may be expressed in largely non-overlapping subpopulations of neurons, however, more data would be needed to strengthen this conclusion.

Recovery from fast inactivation at voltages near resting potential (or more negative) is faster for $Na_V1.8$ currents than for TTX-S currents by an order of magnitude (Elliott and Elliott, 1993). This is consistent with the general observation that time constants for macroscopic transitions of channel states typically become faster away from the midpoint of the inactivation range. Indeed, at −90 mV, fast recovery from inactivation was about ten times faster for $I_{TTX\text{-}I,slow}$ (0.99 ± 0.20 ms, n = 3) than for TTX-S current (10.9 ms, n = 1) (Fig. 10*D*). The values for $I_{TTX\text{-}I,slow}$ are consistent with observed values for TTX-I current in the DRG of ~1 ms at −100 mV (Cummins and Waxman, 1997) and 3.8 ms at −67 mV (Elliott and Elliott, 1993). The time course of repriming for TTX-S current (in cells without ITTX-I,slow) resembles that seen for TTX-S current in large DRG neurons, which is about four-fold faster than that for small DRG neurons (Everill et al., 2001).

Na_V channels can enter into distinct fast (millisecond or submillisecond) and slow (up to seconds) inactivated states, likely involving different conformations of the channels (reviewed in Ulbricht, 2005). Compared to other Na_V subunits, $Na_V1.8$ is known for its relatively rapid entry into a slow inactivated state (the time course is nevertheless much slower than that for fast inactivation), but relatively slow recovery from this state. Slow inactivation of $Na_V1.8$ channels can occur even for short depolarizations from resting potential, contributing to adaptation of responses to physiological stimuli (Blair and Bean, 2003). Variations in the observed values for this property could reflect differences in protocol, but sometimes there are

true variations across cells. For instance, among DRG nociceptive neurons, $Na_V1.8$ current enters into slow inactivation with a time constant of ~140 ms in one neuronal type and a time constant of ~550 ms in another type (Choi et al., 2007). In our VGN recordings, $I_{TTX\text{-}I,slow}$ clearly showed an accumulating slow inactivation during delivery of standard protocols (35-ms test pulses to −15 mV, with 1.5 s start-to-start time for sweeps). In fact, the start-to-start time would have had to be extended to 5 s (Fig. 11*A*) in order to prevent a decrement in the size of the $I_{TTX\text{-}I,slow}$ from sweep to sweep (we could not use such a slow protocol for most recordings involving multiple pharmacological conditions). In recovery from inactivation protocols, only ~75% of the recovery occurred with the fast time constant. With a longer recovery protocol, we also observe a slow component of recovery from inactivation even to 25 ms steps to 0 mV (Fig. 11*B*). It accounted for ~15% of the recovery even to this short step and had a very slow recovery time constant of 1060 ± 196 ms (n = 4).

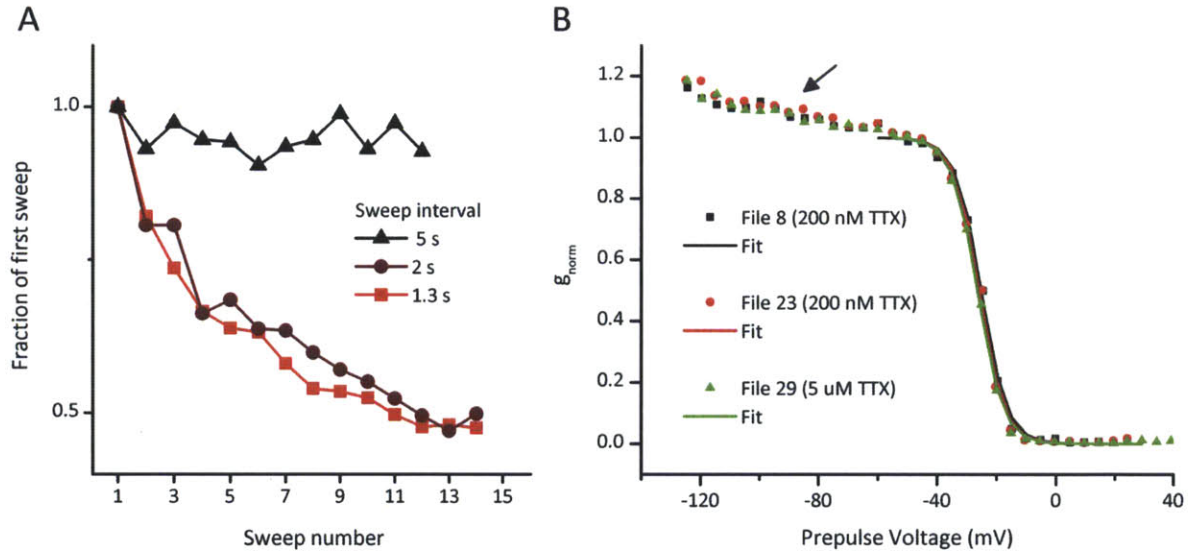

FIGURE 11. Slow inactivation over the course of protocol delivery caused a slight underestimate of the size of $I_{TTX\text{-}I,slow}$. *A*: During a "recovery from inactivation" protocol, responses to the same voltage step decreased during a set of sweeps for start-to-start sweep intervals of 1.3 s and 2 s, but not 5 s (one cell shown). For the shorter start-to-start intervals, a large steady-state decrement was seen, likely due to accumulation of slow inactivation. *B*: This may have accounted for ~20% decrease in maximum conductance in inactivation curves (*gray arrow*) as voltage increased from −120 to −60 mV, quite negative to the fast inactivation region ("inactivation" protocol delivered at 1.5 s start-to-start sweep interval), likely leading to a 10-20% underestimation of the g_{max}. Three files from the same cell, taken at different times after rupture, all consistently show this phenomenon. Y-axis is normalized to fits, which were generated from data points around the $V_{1/2inact}$.

The slow TTX-insensitive current might alternatively be attributed to the $Na_V1.9$ subunit, which was also observed in our PCR analysis. $Na_V1.9$ current (also referred to as NaN) has been described as having much slower kinetics and more negative voltage-dependence than $Na_V1.8$

current (Cummins et al., 1999; Dib-Hajj et al., 1999). These properties would suggest that $Na_V1.9$ should be easily distinguishable from $Na_V1.8$ based on their time course and voltage-dependence. However, it was later discovered that when recordings are performed with Cl^- instead of F^- in the internal solution, the voltage dependence of $Na_V1.9$ (but not $Na_V1.8$) is greatly affected, such that the properties of the two channels are more similar and harder to distinguish than in F^-–based recordings (Rugiero et al., 2003; Coste et al., 2004; Maruyama et al., 2004). For instance, the reported half-activation of $Na_V1.9$ is typically more negative than −50 mV with CsF but is −30 to −40 mV with CsCl. The effect of F^- in the internal solution could arise from its chelation of aluminum and activation of G proteins, among other possibilities. As our recordings were performed without F^- in the internal solution, we wanted to more carefully rule out $Na_V1.9$ as a major contributor of slow TTX-I current in these cells. Even when recorded without F^- in the pipette, $Na_V1.9$ has a more negative activation range than $Na_V1.8$ by about 15 mV (Table 3). $I_{TTX\text{-}I,slow}$ in our VGNs had a $V_{1/2act}$ of ~−16 mV, in complete agreement with the values for $Na_V1.8$ channels and not Nav1.9 channels.

The time course of $I_{TTX\text{-}I,\ slow}$ is more consistent with $Na_V1.8$ than $Na_V1.9$ current. $Na_V1.9$ current is often described as having much slower inactivation than $Na_V1.8$ current in both F^- and Cl^-, but the difference can appear more subtle when compared at the same absolute voltages. Inactivation time constants are a bell-shaped function of voltage, with the slowest time constants typically centered near the half-inactivation voltage. $Na_V1.9$ channels are greatly activated near the half-inactivation voltage where the inactivation time constant would be slowest. $Na_V1.8$ is minimally activated at the half-inactivation voltage, so the slowest inactivation time constants cannot be visualized or measured. This might in part account for why the slowest observable inactivation time constants of $Na_V1.9$ are much slower than those of $Na_V1.8$. However, when the activation and inactivation time constants of $Na_V1.8$ and $Na_V1.9$ are compared at the same absolute voltages in the range where both currents are fully activated, the differences may be much smaller (Renganathan et al., 2002). Even so, the inactivation time constants of $I_{TTX\text{-}I,slow}$ at +5 mV (1.7 ± 0.1 ms, n = 10) and +10 mV (1.3 ± 0.1 ms, n = 5) better matched the reported time constant for $Na_V1.8$ (1.4 ± 0.2 ms) than for $Na_V1.9$ (3.1 ± 0.4 ms) (Renganathan et al., 2002, at +15 mV command voltage, uncorrected for ~9 mV JP).

Based on the voltage-dependence and time course of inactivation, we believe that the $I_{TTX\text{-}I,slow}$ we observe in VGNs is predominantly $Na_V1.8$ and not $Na_V1.9$. Could $I_{TTX\text{-}I,slow}$ consist of multiple components, with a dominant $Na_V1.8$ component and a minority $Na_V1.9$ component? This is difficult to rule out, but if a significant amount of $Na_V1.9$ current were mixed in with $Na_V1.8$ current, we would expect to see deviations from a simple I-V relationship, such as multiple inflections due to the somewhat different voltage-dependence of the two currents (e.g., seen in Coste et al., 2004). In none of seven cells did we see an inflection indicative of a significant second current in the I-V curve and activation curve. Our activation curves are also

well fit by a single Boltzmann sigmoid, also suggesting that a single homogeneous current dominates $I_{TTX\text{-}I,slow}$.

In two VGN, Cd^{2+} (600 μM) blocked $I_{TTX\text{-}I,slow}$ at −20 mV by 69% and 83% by, giving an extrapolated K_d of ~190 μM. A variety of values are found in the literature, probably because block depends on Na^+ flow (is much greater for inward than for outward Na^+ current) and has a modest voltage-dependence (Kuo et al., 2002). We expect calculations that are based on more positive voltages and outward currents to give a higher estimate for the K_d of block by Cd^{2+}. Our extrapolated K_d value is consistent with at least two studies: K_d ~300 μM for inward current at 0 mV (Leffler et al., 2005) and K_d ~200 μM in the presence of inward Na+ current but nine times lower affinity in the presence of outward Na+ current (Kuo et al., 2002).

It is rather difficult to distinguish TTX-I I_{Na} from calcium currents pharmacologically since they can be blocked by many calcium channel blockers, such as Cd^{2+}, mibefradil (a common T-type Ca_V channel blocker), and nitrendipine (a dihydropyridine L-type Ca_V channel blocker) (Yatani and Brown, 1985; McNulty and Hanck, 2004; Coste et al., 2007). Low doses of amiloride spare $Na_V1.8$ and $Na_V1.9$ while blocking $Ca_V3.2$ channels, but some T-type Ca^{2+} currents are also relatively insensitive to this drug (Coste et al., 2007). The TTX-I currents require higher concentrations of Ni^{2+} to block, but the difference is only several-fold when compared with Ni^{2+}-resistant T-type Ca^{2+} currents (Monteil et al., 2000; Coste et al., 2007).

Based on the voltage-dependent properties and time course, we find the current we observe to be inconsistent with a T-type Ca current and consistent with $Na_V1.8$ current. An inactivating, low-voltage activated I_{Ca} (likely carried by T-type Ca_V channels) has been described in neonatal mouse VGNs of the largest diameters; it begins to activate near −60 mV and half-inactivates in the range of −60 to −75 mV, and has slower kinetics near peak than the current we observe (Desmadryl et al., 1997; Chambard et al., 1999; Limón et al., 2005). Lastly, the current is recorded in the absence of external Ca^{2+} and is eliminated by $NMDG^+$ substitution for Na^+, arguing against a Ca_V channel.

SIZE OF $I_{TTX\text{-}I,SLOW}$. The size of $I_{TTX\text{-}I,slow}$ was fairly stable throughout recordings (Fig. 12). The average conductance density of the TTX-insensitive current was 1.47 ± 0.25 nS/pF (n = 7). Since $I_{TTX\text{-}I,slow}$ activation was not calculated for cells where the TTX-I current was small relative to the imperfectly blocked outward current, the conductance average may be biased towards cells with larger currents. Most studies in the literature prefer to report peak current and current density, so we calculated those values for comparison. The current density of $Na_V1.8$-like current varied considerably from cell to cell. Again, we limited our dataset to neurons where almost all fast Na_V current (both TTX-S and TTX-I) had been blocked. For six neurons recorded in Cs^+-based solutions, the peak current density ranged from −55 to −116 pA/pF, with an average

of −81.9 ± 10.4 pA/pF. For four neurons recorded in K^+-based solutions, peak current density ranged from −59 to −154 pA/pF, with an average of −104.7 ± 19.8 pA/pF.

The presence of slow use-dependent inactivation created a decrement in the current size from sweep to sweep. As our standard protocol for activation and inactivation stepped up gradually from a very negative voltage (to allow for detection of $Na_V1.5$ current), a 10–20% decrement was often seen in the activation and inactivation curves for $Na_V1.8$ negative to the sigmoidal region near the voltage midpoints (Fig. 11*B*). The curves were fit around the voltage midpoints, and may therefore underestimate the size of the non-inactivated current by ~10%.

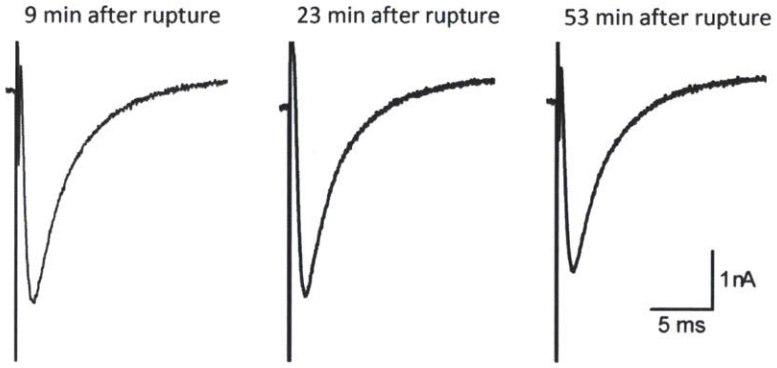

FIGURE 12. Recordings of $I_{TTX\text{-}I,slow}$ were stable with time in whole-cell recording. Current size showed only minimal changes over the course of an hour. Currents were evoked by steps from −125 to −5 mV

To quantify the relative size of $I_{TTX\text{-}I,slow}$ to the total Na_V current, we calculated the ratio of the peak $I_{TTX\text{-}S}$ to the peak $I_{TTX\text{-}I,slow}$. We chose to calculate this ratio rather than a fraction because the peaks of the two currents occurred at different times and did not summate. In some cell (*n* = 5), we had the data required to segregate the two currents pharmacologically: $I_{TTX\text{-}I,slow}$ was isolated with TTX and $I_{TTX\text{-}S}$ was obtained by subtraction. In other cells (*n* = 5), the two currents could be separated based on biophysical differences, a method that was less exact but allowed us to extend the dataset (see Methods). For cells with pharmacological segregation, the ratio of peak $I_{TTX\text{-}S}$ to peak $I_{TTX\text{-}I,slow}$ was as follows (dose used for TTX-I current isolation in parentheses): 2.4 (5 μM TTX); 2.2 (1 μM TTX); 3.5, 4.4 and 6.8 (300 nM TTX). For cells where we used biophysical separation, we obtained additional approximate ratios of 1.8, 2.1, 3.4, 4.3, and 4.8. Therefore, considerable variability in the relative sizes of the currents may exist, as is the case for nociceptors of the DRG. Overall, the peak TTX-S current was typically at least twice as large as the TTX-I current, and 3.6 ± 0.5 times as large on average (*n* = 10).

Although $I_{TTX\text{-}I,slow}$ was a minority of the total current (24% on average, but as high as 36%), it was a much larger fraction of the total compared with $I_{TTX\text{-}I,fast}$ (~10%). The peak $I_{TTX\text{-}I,slow}$ conductance (1.47 ± 0.25 nS/pF) was only about 1.5-fold larger than the peak $I_{TTX\text{-}I,fast}$ conductance (given above), yet $I_{TTX\text{-}I,slow}$ is a substantially larger fraction of the total. This was because cells with $I_{TTX\text{-}I,slow}$ had 2-fold smaller TTX-S currents than the other acutely dissociated cells (Table 2). Furthermore, the influence of $I_{TTX\text{-}I,slow}$ may be larger than these peak current ratios suggest because it lasts longer, thereby accounting for more charge movement for the same peak amplitude. The $I_{TTX\text{-}I,slow}$ could therefore prolong depolarization, affecting other voltage-gated channels (including other Na_V channels) as well as calcium influx.

Not only did cells with $Na_V1.8$ have less TTX-S current, they seemed to have a different kind of TTX-S current with voltage dependence more depolarized by 7 mV (Table 2) ($p = 0.005$ for $V_{1/2inact}$; $p = 0.004$ for $V_{1/2act}$, $p = 0.0007$ for s_{inact}). The larger *s* values (width) of the $I_{TTX\text{-}S}$ *inactivation* curves for the cells with $I_{TTX\text{-}I,slow}$ might reflect multiple components, although the lack of difference in *activation* slope would require such multiple components to have more similar activation ranges. The $I_{TTX\text{-}S}$ in many cells with $I_{TTX\text{-}I,slow}$ displayed significant decrement during the initial sweeps of the protocol well below the fast inactivation range, as if from slow inactivation. A simple metric to quantify this phenomenon is the ratio of the currents for the first versus the 24th sweep of the protocol, which differ only by the duration of their hyperpolarizing pre-step (130 ms *vs.* 50 ms) and how many preceding sweeps had been delivered (see Fig. 1*E*). In theory, this ratio could reflect recovery from fast inactivation, but typical TTX-S Na_V channels would be almost completely recovered even after the shorter 50-ms pre-step at −130 mV, so we believe this ratio reflects the observed decrease in current over the course of successive sweep deliveries. The ratio is 1.28 ± 0.04 (the first sweep is 28% larger) for six VGNS with $I_{TTX\text{-}I,slow}$, but only 1.07 ± 0.04 for fifteen cells lacking $I_{TTX\text{-}I,slow}$ ($p = 0.003$).

CHANGES WITH POSTNATAL AGE. In contrast to the data for $Na_V1.5$-like current, the fraction of neurons with $I_{TTX\text{-}I,slow}$ did not decrease with age from P1-P8 (Fig. 13). The percentage of small DRG neurons expressing $Na_V1.8$ current rose from almost 0% at E17 to ~70% by P0 (2 days later) and to ~80% by 6 weeks (Renganathan et al., 2002). Our prevalence percentages were calculated from all recordable VGN combined rather than a highly-expressing subpopulation (like the small DRG neurons). $I_{TTX\text{-}I,slow}$ incidence (Fig. 13) appears to increase rapidly from none at P0 to 20-50% by P4.

In the sample of ten cells for which the ratio of $I_{TTX\text{-}S}$ to $I_{TTX\text{-}I,slow}$ was estimated, we saw no obvious trends with age in the proportion of the two currents. This differs from the observations of Roy and Narahashi (1992) that small DRG cells express primarily TTX-I current at P3-P4 but expressed more TTX-S current than TTX-I current by P8 (Roy and Narahashi, 1992).

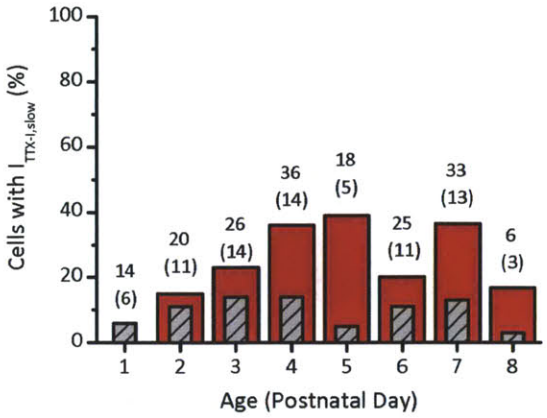

FIGURE 13. $I_{TTX-I,slow}$ rose in prevalence in the first half of the first postnatal week. The total number of cells and number of experiments (*in parentheses*) for which the presence or absence of $I_{TTX-I,slow}$ can be determined is shown above each day. The number of experiments is also plotted for each day (*gray hatched columns, on same scale as percentages*). In those cells with clear $I_{TTX-I,slow}$, it could be clearly seen in the inactivation region of the control Na_V current (see Fig. 9*C*), and could be separated by a sum of two exponentials fit of the response to an activating step to −15 mV (a voltage where $I_{TTX-I,slow}$ inactivation is fairly slow and a single exponential fit of the total I_{Nav} fails). The absence of these features in the control Na_V current was interpreted as an absence of $I_{TTX-I,slow}$.

Neurons with $Na_V1.5$ and $Na_V1.8$ have distinct firing properties and morphology

VOLTAGE RESPONSES TO CURRENT STEPS. To study voltage responses of VGNs with different complements of Na_V currents, I recorded from VGNs in solutions without ion channel blockers (SIS_K and L-15). Recordings were made immediately upon rupture, to reduce possible effects of washout of second messengers on firing patterns. Note that $Na_V1.8$ current size is modulated by GTP and that KCNQ (K_V7) and I_h currents, which are expressed by VGN, can run down during ruptured-patch recordings and alter firing patterns (Kalluri et al., 2010). The most obvious differences in firing were between cells that expressed $I_{TTX-I,slow}$ and cells that lacked $I_{TTX-I,slow}$. Although our methods are correlational and do not allow us to attribute these differences to $I_{TTX-I,slow}$, the differences resemble what has been reported and modeled for $Na_V1.8$ in the literature.

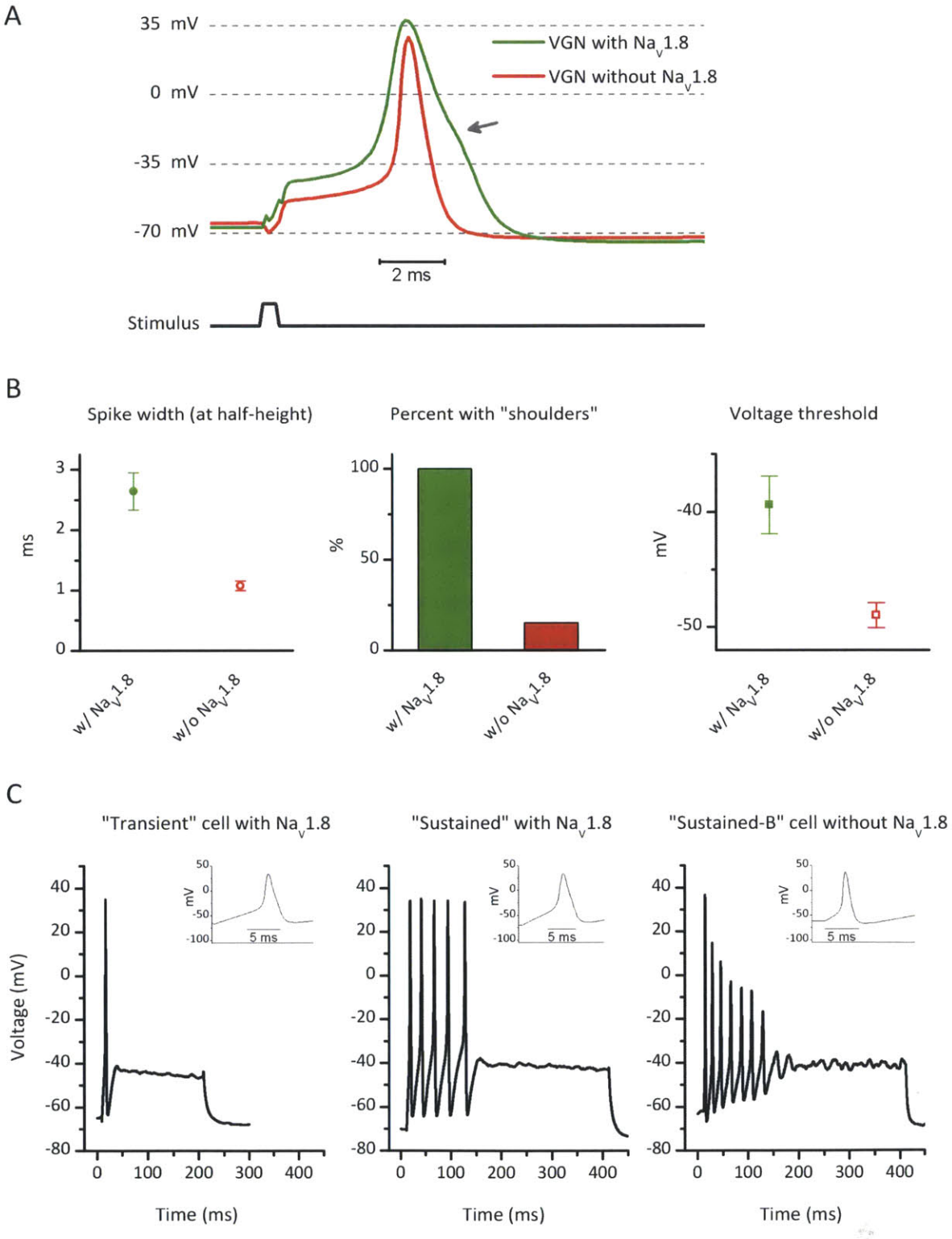
A
35 mV
0 mV
-35 mV
-70 mV
VGN with Na$_V$1.8
VGN without Na$_V$1.8
2 ms
Stimulus
B
Spike width (at half-height)
Percent with "shoulders"
Voltage threshold
ms
%
mV
w/ Na$_V$1.8
w/o Na$_V$1.8
C
"Transient" cell with Na$_V$1.8
"Sustained" with Na$_V$1.8
"Sustained-B" cell without Na$_V$1.8
Voltage (mV)
Time (ms)
5 ms

FIGURE 14. Spike shape and spike pattern differed between cells with $Na_V1.8$ and cells without $Na_V1.8$. Action potentials in cells with $Na_V1.8$ were broader, had more positive thresholds, and showed an inflection during the repolarization (*gray arrow*). A: Two representative examples of responses to 500-μs steps are shown at firing threshold (1150 pA for "sustained" spiking cell with $Na_V1.8$ and 400 pA for "transient" spiking cell without $Na_V1.8$). B: Quantification of the spike shape characteristics of the two groups reveals substantial differences between the groups (see text for average values and significance). C: For traces where cells fired multiple action potentials but ceased firing before the end of the step, cells with $Na_V1.8$ showed minimal or no decrease in spike height, while cells without $Na_V1.8$ showed significant decrease in spike height, presumably due to TTX-S Na_V channel inactivation. Current steps of 160 pA (*left*), 240 pA (*center*), and 130 pA (*right*) were selected to yield similar final voltages. Inset shows a close up of the spike shape.

Action potential properties were assessed using pulses sufficiently brief (500 μs) to reduce the influence of the injected current on the action potential once past threshold. The current amplitude was increased until a spike was evoked, and the properties of the spike were measured at the lowest amplitude that produced a spike. Action potential shape in cells with $I_{TTX\text{-}I,slow}$ showed several consistent features relative to cells without $I_{TTX\text{-}I,slow}$: the voltage threshold (corresponding to a sudden change in the time derivative of voltage, i.e., the start of the upstroke) was less negative (typically above −40 mV), the spikes were wider, and a "shoulder", or inflection, occurred on the repolarization (Fig. 14A).

Voltage threshold of the action potential was quantified as the voltage at which dV/dt reached 4 mV/ms (empirically chosen to be minimal but sufficiently above the noise), and was significantly more depolarized in cells with $I_{TTX\text{-}I,slow}$ by ~10 mV (with: −39.4 ± 2.5 mV, n = 5; without: −49.0 ± 1.1 mV, n = 6, p = 0.0003). This is expected given the reduced size of $I_{TTX\text{-}S}$ and the higher voltages required to activate $I_{TTX\text{-}I,slow}$. These differences in threshold between neurons with and without $I_{TTX\text{-}I,slow}$ are similar to differences between normal and axotomized DRG neurons which express different complements of Na_V channels. Axotomy produces a downregulation of TTX-I currents, a predominance of TTX-S currents, and upregulation of $Na_V1.3$, a subunit with robust ramp currents around resting membrane potential. Together these changes account for why large depolarizations are necessary for action potential generation in normal small DRG neurons (reflecting the depolarized voltage dependence of activation of $I_{TTX\text{-}I,slow}$), but a more hyperpolarized threshold is found in axotomized small DRG neurons, resulting in hyperexcitability after injury (Rush et al., 2007). Note that although voltage thresholds were higher in cells with $I_{TTX\text{-}I,slow}$, current thresholds, which depend on other factors such as input resistance, overlapped for cells with and without $I_{TTX\text{-}I,slow}$ (described in more detail in the following section). The peak instantaneous rate of depolarization on the upstroke of the action potential was twice as fast for cells without $I_{TTX\text{-}I,slow}$, possibly reflecting the reduced TTX-S conductance in cells with $I_{TTX\text{-}I,slow}$ and the slower kinetics of activation for $I_{TTX\text{-}I,slow}$ (with: 99 ± 11 mV/ms, n = 5; without: 207 ± 24 mV/ms, n = 6; p = 0.004).

The slower kinetics and depolarized voltage dependence of inactivation of $I_{TTX\text{-}I,slow}$ might be expected to contribute to broader spikes. At 23-25° C, spike width at half-height was ~2–4 ms (2.64 ± 0.31 ms, n = 5) for cells with $I_{TTX\text{-}I,slow}$ and ~1 ms (1.07 ± 0.08 ms, n = 6) for cells without $I_{TTX\text{-}I,slow}$ (Fig. 14*A*). This is consistent with observations of broader action potentials in DRG and nodose ganglion neurons with $Na_V1.8$ as compared to other neurons (Ritter and Mendell, 1992; Djouhri et al., 2003). However, the absolute width of DRG neurons with $Na_V1.8$ current at room temperature is greater (3.9 ms at 0 mV, and 4.7 ms half-width, respectively for Renganathan et al., 2001; Blair and Bean, 2002), which could be caused by the high input resistance and long time constants of nociceptors, a greater proportion of $Na_V1.8$ current, or participation of Ca_V currents.

Every cell with $I_{TTX\text{-}I,slow}$ had a shoulder (ranging from subtle to very obvious) on the repolarization phase (n = 10; Fig. 14*A*, arrow). In contrast, in 27 cells without $I_{TTX\text{-}I,slow}$, only four had even a hint of a shoulder. Although shoulders are not necessarily caused by $Na_V1.8$ (often associated with Ca^{2+} currents instead), they are consistent with the slower inactivation of $Na_V1.8$ current and have been seen in DRG neurons that have significant TTX-I currents (Ritter and Mendell, 1992; Cardenas et al., 1997). The shoulder in C-type neurons is diminished by removal of external Ca^{2+} (Stansfeld and Wallis, 1985), suggesting a possible correlated expression of $Na_V1.8$ with certain Ca_V currents. However, it has also been shown using the action potential clamp method that in DRG neurons with $Na_V1.8$, ~58% of the current flowing during the shoulder is carried by $Na_V1.8$ (the rest is mostly carried by high voltage-activated calcium current) (Blair and Bean, 2002).

Differences in spike amplitude have been reported for DRG cells, with $Na_V1.8$-expressing cell types having larger spikes (Ritter and Mendell, 1992). A larger overshoot (absolute voltage) has been seen in DRG subtypes with shoulders, such as C fibers (Harper and Lawson, 1985) and overshoot size is correlated with intensity of $Na_V1.8$ staining (Djouhri et al., 2003). The mean peak voltage of the action potential was larger for VGN with $I_{TTX\text{-}I,slow}$ (32.4 ± 1.6 mV, n = 5) than for VGN without $I_{TTX\text{-}I,slow}$ (25.5 ± 2.76 mV, n = 6) but this difference did not reach statistical significance (p = 0.07). (For the difference in means observed (7 mV) and standard deviations (6.85), samples of ~15-20 are required to reach statistical power of 90%.) There was no difference in spike height measured from the peak to the bottom of the afterhyperpolarization (AHP) (with: 105.5 ± 2.1 mV, n = 5; without: 102.9 ± 3.07 mV, n = 6; p = 0.53), at least partly because AHPs were less negative for cells with $I_{TTX\text{-}I,slow}$ (with: −73.0 ± 0.8 mV, n = 5; without: −77.4 ± 1.8 mV, n = 6; p = 0.036) . Given the borderline significance and low statistical power of these comparisons, more data will be needed to determine whether differences in peak voltage of action potentials exist between VGN with and without $I_{TTX\text{-}I,slow}$.

In a model of DRG neurons, adding $Na_V1.8$ current eliminated the dependence of current threshold on membrane potential (Choi and Waxman, 2011). Experimentally, DRG neurons from $Na_V1.8$-null mice are more sensitive to membrane depolarization than neurons from wildtype mice (Renganathan et al., 2001), and a mutation that depolarizes resting potential renders sympathetic neurons, which do not express TTX-I currents, less excitable, while making somatosensory neurons that do express TTX-I currents more excitable (Rush et al., 2006).

The significant overlap of activation and inactivation suggests that $I_{TTX\text{-}I,slow}$ could produce a non-inactivating "persistent" current, but the voltage dependence suggests very little of it would be active at resting potential. Consistent with this, we did not observe spontaneous firing in any of the cells with $I_{TTX\text{-}I,slow}$. Resting membrane potential was −63.9 ± 2.49 mV (n = 5) for cells with $I_{TTX\text{-}I,slow}$ and −67.9 ± 0.7 mV (n = 19) for cells without $I_{TTX\text{-}I,slow}$ ($p = 0.19$). In the literature, no difference in resting membrane potential is seen between $Na_V1.8$-null and wild-type DRG neurons (Renganathan et al., 2001) and no correlation is seen between resting membrane potential and intensity of $Na_V1.8$ immunoreactivity (Djouhri et al., 2003).

Vestibular afferents recorded *in vivo* vary greatly in their spike timing regularity. Since this is the best known example of firing property diversity in the vestibular ganglion, we sought to determine whether differences in Na_V channel expression contribute to this diversity. In a previous study, isolated VGNs were categorized based on their responses to current steps and these categories were proposed to correspond to firing pattern regularity categories seen *in vivo* (Kalluri et al., 2010). Using the current step response as a proxy for firing pattern regularity, we examined whether the presence of $I_{TTX\text{-}I,fast}$ and $I_{TTX\text{-}I,slow}$ was correlated with particular categories of current step responses. First, we confirmed that the same firing pattern categories are present in our data. Kalluri et al. (2010) also found that the categories correlated with cell size and many other properties. In general, we observed the same categories and correlations seen in the Kalluri et al. (2010) study (Fig. 15). "Transient" spiking neurons firing a single action potential in response to a positive current steps had significantly more steady-state outward current in response to a 400 ms voltage step at −60 mV (representing low-voltage-activated K^+ current, K_{LV}) (140.1 ± 33.41 pA, n = 8) and higher firing thresholds for 400-ms current steps (56.6 ± 10.56 pA, n = 11), presumably because of lower input resistance at rest (Kalluri et al., 2010). Among neurons that produced multiple spikes in response to current steps, "sustained-A" neurons that fired sustained trains of action potentials at threshold had little steady-state outward current at −60 mV (12.5 ± 5.84 pA, n = 12), and very low current thresholds (8.6 ± 1.38 pA, n = 16; likely an overestimate because sometimes the lowest step of the protocol triggered spiking). Intermediate "sustained-B" and "sustained resonator" spiking patterns were observed in the remaining cells, with intermediate amounts of current at −60 mV (57.8 ± 18.9 pA, n = 15) and intermediate current thresholds (21.8 ± 2.25 pA, n = 19), and may represent actual subpopulations or developmentally immature transient spikers. The

membrane time constant at rest (which depends on membrane capacitance and therefore cell size as well as input resistance) shows a more complicated relationship to the categories. "Transient" neurons tend to be larger but also to have lower input resistances because of their K_{LV} currents, effects which cancel each other out such that mean time constants are not different between transient and sustained spikers, but are faster for transient spikers than sustained spikers of the same size (Kalluri et al., 2010). In our data set, mean membrane time constants around rest were 16.5 ± 3.71 ms (n = 5) for transient spikers, 24.8 ± 3.13 (n = 9) for sustained-B and sustained resonators, and 32.7 ± 3.32 ms (n = 6) for sustained-A. This may be because our transient spikers (22.4 ± 0.89 µm, n = 11; 17.3 ± 2.8 pF, n = 10) were only slightly larger on average than sustained-A (21.1 ± 0.35 µm, n = 16; 13.1 ± 0.49 pF, n = 16) and sustained-B and sustained-resonators (21.4 ± 0.32 µm, n = 18; 14.5 ± 0.50 pF, n = 18). The lack of significant size difference between groups is consistent with data for the <P8 age range from (Kalluri et al., 2010); Kalluri et al. showed that in the second postnatal week there is a large increase in the average size of transient-spiking neurons, with no change in the average size of sustained spikers. In contrast to Kalluri et al. (2010), we did not observe a statistically significant difference in resting membrane potential between the categories for ruptured patch recordings (Transient: −70.6 ± 1.5 mV, n = 10; Sustained-A: −70.4 ± 0.9 mV, n = 15; and Sustained-B: −68.7 ± 1.5 mV, n = 19). For recordings using the same method (perforated-patch) and internal solutions as Kalluri et al. (2010), resting membrane potential was almost 10 mV less negative than in ruptured patch (−61.8 ± 2.6 mV, n = 6), and there appeared to be a difference between categories despite the small sample. This discrepancy between perforated and ruptured patch may be due to effects of dialysis in ruptured patch mode, or alternatively, the lack of internal Na^+ in the perforated patch solution, which may affect the Na^+/K^+–ATPase and cause depolarization of the resting potential (e.g., see Methods of Blair and Bean, 2002).

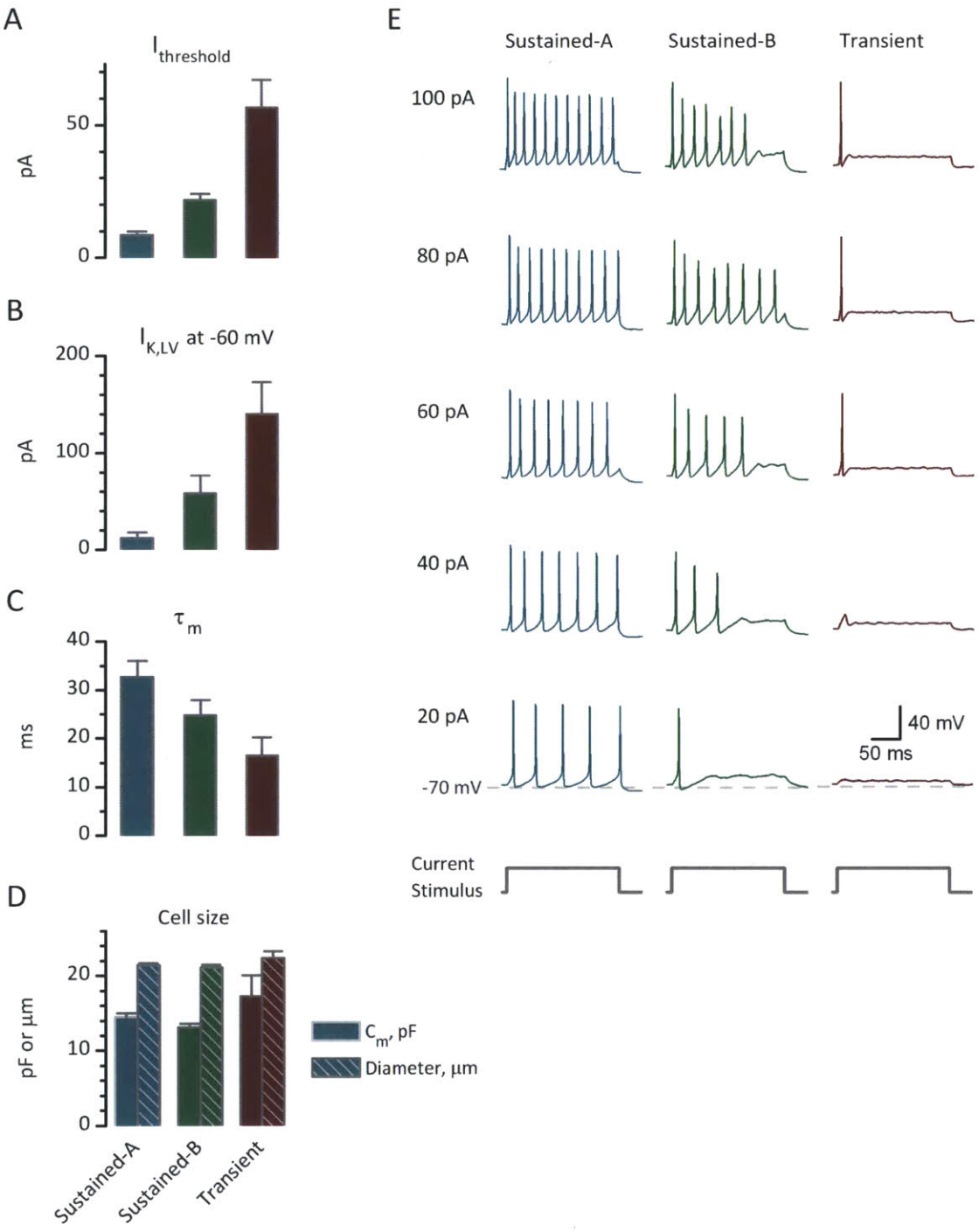

FIGURE 15. Differences between VGN with different firing patterns in response to current steps. Transient VGN had larger current thresholds for spiking than sustained neurons (both A type and B type) (*A*), consistent with their expression of more $I_{K,LV}$ (*B*) and therefore lower R_{in}. *C–D*: The difference in $I_{K,LV}$ is likely to have been responsible for the difference in membrane time constants (τ_m), because membrane capacitance (C_m) did not differ greatly between groups. *E*: Examples of the firing pattern classes over a range of current injection levels. These results are consistent with previous reports from overnight-cultured VGN in the first postnatal week (Kalluri et al. 2010).

$I_{TTX\text{-}I,slow}$-expressing neurons most resembled the intermediate category, with intermediate amounts of outward current at –60 mV (33.6 ± 6.58 pA, n = 9) and intermediate current thresholds (30.0 ± 4.08 pA, n = 4). Mean membrane time constant was 24.1 ± 5.10 ms (n = 5). However, compared to cells without $I_{TTX\text{-}I,slow}$ in the intermediate category ("sustained-B" and "sustained resonators"), we see consistent differences. Cells with $I_{TTX\text{-}I,slow}$ were never able to fire throughout the entire 400-ms current step at any current injection (unlike "sustained-B" neurons). Furthermore, when comparing responses to current steps where both "sustained-B" neurons (without $I_{TTX\text{-}I,slow}$) and $I_{TTX\text{-}I,slow}$-expressing neurons failed to spike for the full 400-ms duration of the step, one notices a striking difference. Spikes in neurons without $I_{TTX\text{-}I,slow}$ decreased in height whereas spikes in neurons with $I_{TTX\text{-}I,slow}$ remained almost the same height throughout the train of spikes until spiking abruptly stopped (Fig. 14*B*). One possible reason for the abrupt termination of the spikes may be accumulating inactivation of TTX-S currents. In small DRG neurons, TTX-S currents are significant around threshold while TTX-I currents provide the majority of the current for the action potential upstroke (Blair and Bean, 2002), leading to the possibility of changing thresholds without changing spike height. The contribution of TTX-S currents to spike initiation may be more significant than seen in Blair and Bean (2002) because of our higher ratio of TTX-S to TTX-I current.

There are multiple reasons to believe that $I_{TTX\text{-}I,slow}$ -expressing neurons did not make up a major part of the dataset of Kalluri et al. (2010): both transient and sustained neurons in that study showed a sensitivity to resting potential with more positive holding potentials increasing voltage threshold, a pattern typical of non- $I_{TTX\text{-}I,slow}$ cells, and mean spike half-widths were 0.8 ms for transient spikers and 1.6 ms for sustained spikers. However, we cannot rule out the possibility that a small proportion of neurons with $I_{TTX\text{-}I,slow}$ were integrated into the sustained spiking category in that study. If neurons with $I_{TTX\text{-}I,slow}$ were not present in the Kalluri et al. study, one possible explanation for the difference is that our data are collected from acutely dissociated neurons, and the majority of the data in Kalluri et al., (2010) was collected from overnight cultured neurons. In our 16 cultured neurons (larger n than for $I_{TTX\text{-}I,fast}$ because $I_{TTX\text{-}I,slow}$ could be identified in cells with only total I_{Nav} recordings), we did not see $I_{TTX\text{-}I,slow}$, consistent with the possibility that they are downregulated in our minimal culture conditions. Another possible difference is that our data were acquired in ruptured patch mode whereas Kalluri et al. (2010) used the perforated patch method. This could in theory lead to differences since components of the intracellular solution, such as GTP, can influence the size of TTX-I currents. However, current clamp recordings were taken immediately after rupture, making such changes an unlikely reason for these differences.

Because all previously described categories of neurons from the Kalluri et al. (Kalluri et al., 2010) study could be seen in the population of neurons without $I_{TTX\text{-}I,slow}$, neurons that express $I_{TTX\text{-}I,slow}$ could represent a distinct classification. It is interesting that both single and multiple

spiking types can also be found within the $I_{TTX\text{-}I,slow}$-expressing population. However, as described above, the multi-spiking pattern differs for cells with and without $I_{TTX\text{-}I,slow}$ in terms of spike accommodation (changes in spike height during the train). The single-spiking $I_{TTX\text{-}I,slow}$-expressing neurons also differ from other single-spiking neurons in that they did not systematically have a large amount of K_{LV} current as assessed by steady-state current at –60 mV or by visual inspection of the trace kinetics at –60 mV, so a different mechanism may render them unable to fire multiple spikes. While $Na_V1.8$ current is associated with multiple-spiking neurons in other systems, the relationship between firing pattern type and presence of $Na_V1.8$ is complex: neurons that express almost exclusively TTX-S currents fire sustained patterns, while sensory neurons with both TTX-S and $Na_V1.8$ current have heterogeneous firing patterns ranging from a single or a few spikes to sustained patterns (summarized in Schild and Kunze, 1997). This observation is generally consistent with what we see, except for the addition of a class of transient spiking neurons through a K_{LV} channel mechanism. (This mechanism may be essential to reducing the membrane time constants for the high temporal precision required of vestibulo-ocular reflexes and auditory encoding in the inner ear.)

$Na_V1.5$ was present in 4 of 7 sustained-A cells, 3 of 7 sustained-B cells, and 2 of 5 sustained resonators, and 1 of 4 transient spikers.

MORPHOLOGICAL DIFFERENCES. Unlike the situation in the DRG, VGNs that expressed $I_{TTX\text{-}I,slow}$ were not the smallest cells in our sample. There are no cells in the vestibular ganglion that correspond to the DRG small cells, as there are no known nociceptors in the VG, and the great majority of cells are myelinated and or have satellite cell enwrappings (Ballantyne and Engström, 1969). Cells with $I_{TTX\text{-}I,slow}$ were of similar size to cells without $I_{TTX\text{-}I,slow}$ in our sample (with: 21.1 ± 0.4 μm, n = 36; without: 20 ± 0.2 μm, n = 123). Unfortunately, within the first postnatal week, cell size is not the best indicator of cell type as sustained and transient neurons are of similar average size, with the transients becoming significantly larger by the second week (Kalluri et al., 2010). Membrane capacitances of cells with $I_{TTX\text{-}I,slow}$ were almost twice higher than those of cells without $I_{TTX\text{-}I,slow}$. In 11 of 19 cells with $I_{TTX\text{-}I,slow}$ but 0 of 40 cells without $I_{TTX\text{-}I,slow}$, I could see fine radial attachments to the glass coverslip. However, the formation of attachments was not necessary to $I_{TTX\text{-}I,slow}$ expression as many cells had robust $I_{TTX\text{-}I,slow}$ without any visible attachments. Since many other properties of sensory neurons co-vary with sodium channel expression, such as sensitivity to growth factors like NGF and GDNF which promote cell-subtratum adhesion and neurite outgrowth (Schubert and Whitlock, 1977; Miwa et al., 2010), it is possible that neurons with $Na_V1.8$ are more likely to attach to the substrate. Indeed GDNF can promote neurite outgrowth from chick vestibular ganglion neurons around the time of completion of synaptogenesis (Hashino et al., 1999). It is also possible that growing processes accumulate certain types of channels more effectively than the soma which is typically an intermodal space. When $Na_V1.7$ (a major component of the TTX-S current in

peripheral sensory and sympathetic neurons) was first identified, it was noted that in cultured DRG neurons, immunoreactivity for $Na_V1.7$ is seen most strongly in growth cones, with lower levels of staining along neurites, and only internal membrane staining at the somata in a pattern suggestive of the trans-Golgi networks involved in protein transport (Toledo-Aral et al., 1997). Staining for $Na_V1.8$ within DRG somata is also typically "cytoplasmic" (although it may be bound to internal membranes) even for antibodies confirmed by null animals or knock downs, or GFP-tagged protein (e.g., Lai et al., 2002; Schofield et al., 2008), and the subunit contains an endoplasmic reticulum (ER)-retention/retrieval signal that can be overcome by expression of the β3 subunit (Zhang et al., 2008). It is possible, therefore, that neurite membranes are better able to externalize $Na_V1.8$ channels which otherwise would remain trapped within the cell, destined for export to a distant part of the sensory neuron.

Photos of the cells were rated and measured independently in duplicate by two scorers, one of whom was naïve to the experimental aims. The two sets of measurements will be referred to as set 1 and set 2. Cells with $I_{TTX\text{-}I,slow}$ had less satellite cell coverage as compared to cells with $I_{TTX\text{-}I,fast}$ in both measurement sets (Fig 16*A*). The cells with $I_{TTX\text{-}I,slow}$ were on average more oval shaped while cells with $I_{TTX\text{-}I,fast}$ were more round. For instance, in set 1, only 18% of cells with $I_{TTX\text{-}I,slow}$ were rated as "round", as compared to 42% of cells with $I_{TTX\text{-}I,fast}$ (set 2: 21% and 37%, respectively). Since the relative prevalence of these two groups changed with age, we also plot the fraction of "round" cells for binned age groups (Fig 16*B*). Even when comparing the "round" fraction within age categories, cells with $I_{TTX\text{-}I,slow}$ were less likely to be round, particularly in the P4-5 and P6-8 age groups. We measured the ratio of the lengths of the long axis to short axis (maximum width perpendicular to the long axis); a perfectly round cell would have a ratio of one. The values for the two sets of measurements were fairly consistent, with a Pearson correlation coefficient of 0.9. The distributions of ratios suggests that cells with $I_{TTX\text{-}I,fast}$ tended to be round while cells with $I_{TTX\text{-}I,slow}$ tended to be oval to varying degrees (Fig 16*C*). The mean of the ratios for the two groups are statistically significantly different ($p = 0.0009$ for set 1; $p = 0.0035$ for set 2).

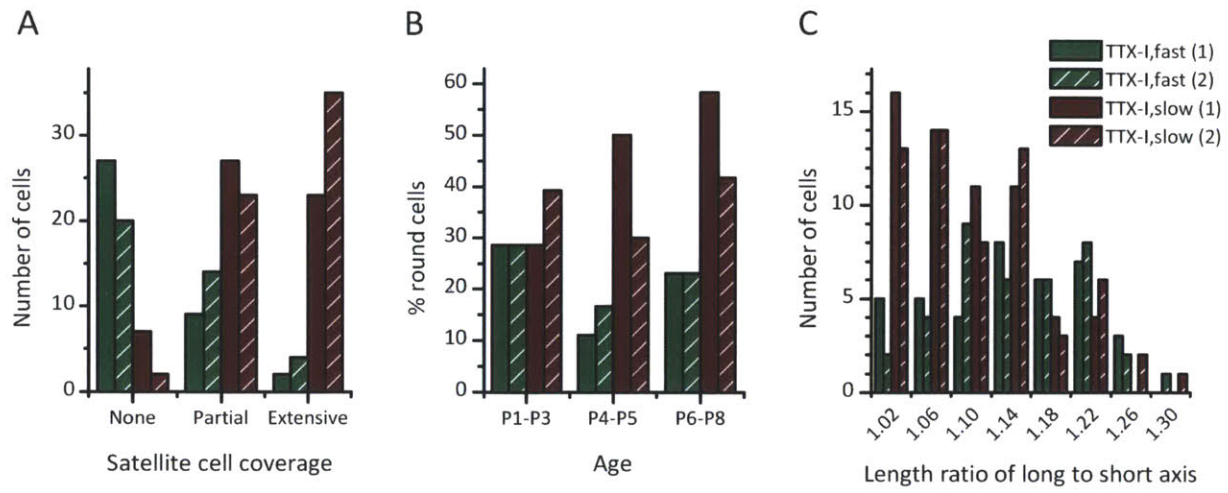

Figure 16. Morphological differences between cells with $I_{TTX\text{-}I,fast}$ and $I_{TTX\text{-}I,slow}$. Neurons with $I_{TTX\text{-}I,slow}$ (the putative $Na_V1.8$ current), were less covered by satellite cells and less likely to be round. Photos of the neurons were rated independently by two scorers resulting in two sets of measurements (shown in solid and hatched bars). *A*: Neurons with $I_{TTX\text{-}I,fast}$ tended to be covered by other cells, whereas neurons with $I_{TTX\text{-}I,slow}$ had less overall coverage. *B*: A larger percentage of neurons with $I_{TTX\text{-}I,fast}$ than of neurons with $I_{TTX\text{-}I,slow}$ were rated as "round" by both scorers. In measurement set 1, the difference develops with age, but this pattern is not seen in measurement set 2. *C*: Both measurement sets found that cells with $I_{TTX\text{-}I,fast}$ tended to have long axis to short axis ratios close to 1, whereas cells with $I_{TTX\text{-}I,slow}$ tended to be slightly elliptical.

$Na_V1.8$ EXPRESSION IN THE VESTIBULAR PERIPHERY**.** A transgenic $Na_V1.8$ reporter mouse, in which neurons that express $Na_V1.8$ also express a red fluorescent protein (tdTomato), was used to reveal the expression pattern of $Na_V1.8$. In the DRG, this mouse expresses Cre recombinase in 93% of small diameter neurons, but only 28% of large diameter neurons (Agarwal et al., 2004). Bright fluorescent signal was detected in many neural fibers in the utricular epithelium, as well as cell bodies within the vestibular ganglion, and could be seen in live tissue microscopy as well as in fixed tissue that was counterstained (Fig. 16, courtesy of Anna Lysakowski and Steven Price, University of Illinois at Chicago). The signal in nerve terminals included complex calyces and dimorphic fibers. Interestingly, signal was also observed in some cochlear neurons and in some sensory, but not motor, neurons of the geniculate ganglion (which contains taste and somatosensory fibers) (communicated by Anna Lysakowski). The fraction of cells expressing tdTomato in the reporter mouse has not been quantified, due to the lack of an adequate counterlabel on this preliminary staining. However, the impression is that a large fraction of the somata express tdTomato, perhaps higher than the ~20% of dissociated VGN that express the current. It has been noted that the fraction of labeled neurons revealed by tdTomato fluorescence may be higher than that seen by other reporter lines, possibly due to high sensitivity to small amounts of Cre recombinase (i.e., low levels of $Na_V1.8$ expression) (Stirling et al., 2005; Gautron et al., 2011). It is also possible that posttranscriptional regulation (such as

regulation of channel translation or channel insertion into membranes) limits our ability to see $Na_V1.8$-like current in many dissociated neurons.

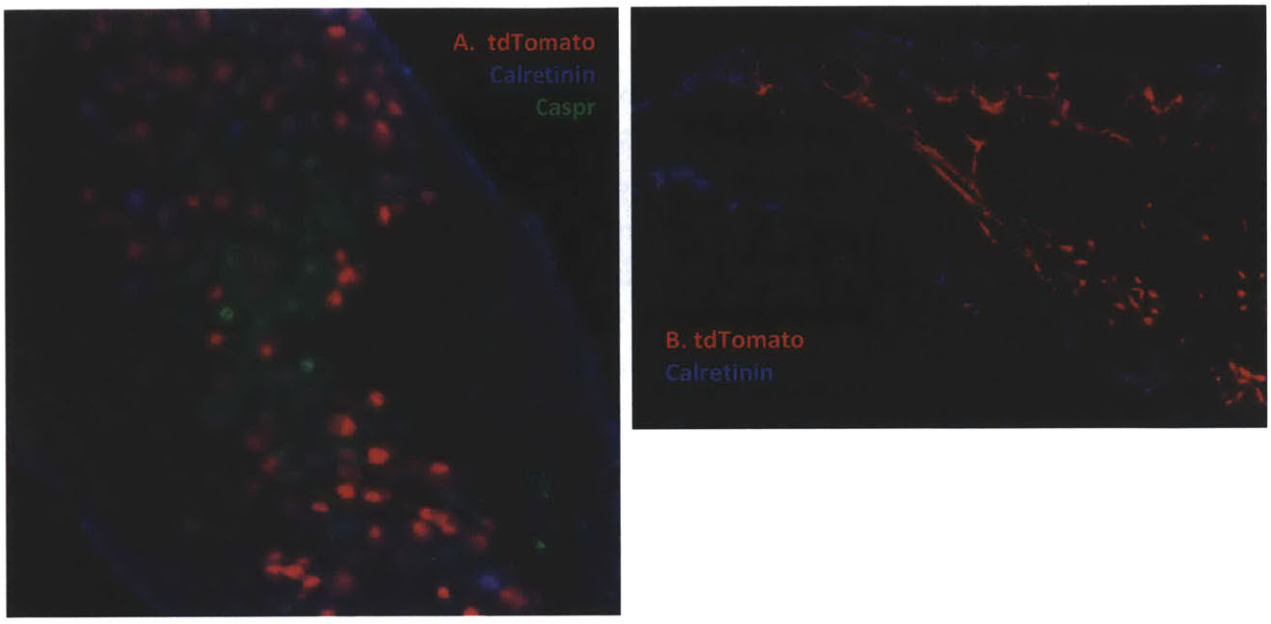

FIGURE 17. In a P12 $Na_V.18$ reporter mouse, red tdTomato signal can be seen in many neurons and neuronal fibers in the vestibular periphery. *A*: Superior vestibular ganglion. Red cells seem to be a bit smaller on average than Caspr-stained (green) cells. Caspr is associated with KCNQ channels expressed by calyces. *B*: Utricular sensory epithelium (cross-section) shows intense staining of calyces around hair cells. Reporter mouse provided by Fu-Cia Yang and Qiufu Ma (Harvard Medical School). Immunostaining done by Steven Price and Anna Lysakowski (University of Illinois, Chicago).

Small persistent currents but no resurgent currents were detected

PERSISTENT AND RESURGENT Na_V CURRENTS. There has been considerable interest in two other unusual forms of Na_V current (persistent and resurgent current) whose unusual properties may contribute to firing. These were not the main focus of this project, but here I report our limited observations relating to these currents. Persistent currents are the steady-state sodium current present in almost all neurons in the region of −65 mV and −40 mV, arguably a consequence of normal Na_V channel gating behavior. They are typically very small (0.5-5% of the transient sodium current), but can still have functional significance in shaping firing frequency and pattern from the subthreshold region where input resistance is high, and can be particularly large in some neurons (reviewed in Bean, 2007). TTX-S persistent currents were assayed by upward and downward ramps of 40 to 50 mV/s between −90 mV to +30 mV before and after application of 300 nM TTX. Persistent currents were very small and often below the resolution of our recording stability (R_s changes, run down of other currents, or changes in seal resistance). For cultured neurons, persistent current ranged from −10 to −12 pA, or 0.2 to 0.3% of the peak transient Na_V current in three cells, and could not be cleanly isolated in three other cells. For acutely dissociated neurons, persistent current was 0.4% (25 pA) of peak I_{Na} in one cell and could not be cleanly isolated in three others. Even with a small fractional size it could still contribute to spontaneous spiking in cells with high input resistances, as observed in many central neurons (Bean, 2007); for example, sustained-A neurons required <10 pA, on average, of sustained current injection to reach firing threshold, and a few of them had apparent spontaneous spiking. TTX-insensitive persistent current is expected to be quite significant given the large overlap in steady-state activation and inactivation of $Na_V1.8$, but was not directly measured in our cells.

TTX-S resurgent current is a transient inward current following a spike that occurs in some neurons through an unusual inactivation and rapid relief of the block upon repolarization. It is correlated with rapid firing and burst firing (Bean, 2007). In none of five acutely dissociated or six cultured cells did we observe such resurgent currents.

DISCUSSION

In acutely dissociated neurons from the superior vestibular ganglion, we obtained evidence for two types of TTX-I Na_V currents ($I_{TTX\text{-}I,fast}$ and $I_{TTX\text{-}I,slow}$) with very different biophysical properties and expression patterns over the first postnatal week. Neurons seemed to express either $I_{TTX\text{-}I,fast}$ and $I_{TTX\text{-}I,slow}$, and the TTX-I current coexisted with large TTX-S currents.

$I_{TTX\text{-}I,fast}$ is widely expressed in early postnatal vestibular ganglion neurons

$Na_V1.5$ IS A CANDIDATE SUBUNIT UNDERLYING $I_{TTX\text{-}I,FAST}$. The profile of $I_{TTX\text{-}I,fast}$, including its time course, voltage dependence, degree of insensitivity to TTX, and sensitivity to Cd^{2+}, is consistent only with the profile of $Na_V1.5$ current. $Na_V1.5$ is unique among known sodium channel subunits for its negative voltage-dependence, with $V_{1/2inact}$ values ranging from −80 to −110 mV (Hanck and Sheets, 1992; Wang et al., 1996; Zhang et al., 1999; Biswas et al., 2009; Huang et al., 2011). In contrast, $V_{1/2inact}$ values of TTX-S channels range from −44 to −78 mV in when expressed in mammalian cells or cell lines (reviewed in Wooltorton et al., 2008). The $V_{1/2inact}$ of $I_{TTX\text{-}I,fast}$ (−102.8 ± 1.5 mV) is within the range reported for $Na_V1.5$ current. $I_{TTX\text{-}I,fast}$ is less sensitive to TTX than $I_{TTX\text{-}S}$ (as evidenced by its predominance at 300 nM TTX), but appears to be mostly blocked at 10 μM TTX. We estimated its K_d for TTX block to be on the order of hundreds of nanomolar, about two orders of magnitude higher than that expected for TTX-S channels (Goldin, 1999), yet lower than the values (60 to >100 μM) found for $Na_V1.8$ channels (Akopian et al., 1996; Sangameswaran et al., 1996; Rabert et al., 1998). Our estimated K_d for $Na_V1.5$ is at the lower end of the range generally reported for $Na_V1.5$ (150 nM–2 μM, as reviewed in Wooltorton et al., 2008). The lowest value of 150 nM was found for an $Na_V1.5$-like current in the medial entorhinal cortex (part of the limbic regions), whereas cardiac, denervated muscle, and heterologous expression studies tend to find values of 1–3 μM (Pappone, 1980; Doyle et al., 1985; Gonoi et al., 1985; Cribbs et al., 1990; Chen et al., 1992; Satin et al., 1992b). Our slightly lower value could be related to the absence of extracellular Ca^{2+} which competes with TTX at its binding site (Weigele and Barchi, 1978; Doyle et al., 1993). However, our K_d matches well with those obtained for $Na_V1.5$-like currents in neonatal outer hair cells (474 nM, Oliver et al., 1997), mouse utricular hair cells (348 nM, Rüsch and Eatock, 1997), and rat utricular hair cells (440 nM, Wooltorton et al., 2007), all of which are recorded in physiological external Ca^{2+}. The higher TTX sensitivity of $Na_V1.5$-like current seen in the inner ear (and limbic brain) relative to other sites may reflect a particular splice variant or modulation by accessory subunits. For instance, it has been found that the exon 6a variant encodes $Na_V1.5$ in brain tissue while the exon 6 variant encodes it in non-brain tissue (Wang et al., 2008).

VOLTAGE-DEPENDENCE OF $I_{TTX\text{-}I,FAST}$. The very negative inactivation range of $Na_V1.5$ poses a puzzle for understanding its function, since it would be predicted to be mostly inactivated at typical resting potentials. Although it is possible that enzyme treatment affects the inactivation range

of $Na_V1.5$, similarly negative values have been observed in some preparations not treated with dissociation enzymes: −104 mV in hair cells recorded *in situ* in the utricular macula (Rüsch and Eatock, 1997) and −99.6 mV for human $Na_V1.5$ channels expressed in transformed HEK cells (Wang et al., 1996). In other studies, somewhat more positive values have been obtained, such as −88 mV for embryonic vestibular hair cells (Géléoc et al., 2004), −91 mV for neonatal vestibular hair cells (Wooltorton et al., 2007), or −92 mV in transfected HEK293 cells (Zhang et al., 1999). The inactivation ranges in hair cells dissociated with crude papain appear to be more negative than in the semi-intact epithelium (Wooltorton et al., 2007; Wooltorton et al., 2008). Therefore, enzyme treatments might cause the inactivation range to appear even more negative. It is unclear whether trypsin and collagenase (the enzymes we used), have any such effects on $Na_V1.5$. The voltage dependence of $Na_V1.5$ inactivation can also be modulated by other factors, such as membrane stretch (Beyder et al., 2010), which may occur during the patch clamp procedure; by Ca^{2+} via its calmodulin binding site and/or CaMKII phosphorylation site (Biswas et al., 2009); by protein kinase C (Qu et al., 1994); or by expression of various β-subunit variants (e.g., Watanabe et al., 2008). Our estimates of voltage dependence may be biased in the hyperpolarizing direction by the use of low (trace) extracellular Ca^{2+}; although Mg^{2+} was raised in compensation, it is a less effective screener of surface charge (Hille et al., 1975). Additional unphysiological features of our Na_V channel isolation recording solutions (such as the presence of TEA) could also have effects on channel biophysics.

The unknown isoform of $Na_V1.5$ that is expressed in VGN may have a more negative inactivation range than heart $Na_V1.5$ channels. It has been shown that the $Na_V1.5a$ isoform is the predominant form found in DRG neurons and that this isoform has more negative voltage dependence of inactivation than the full length $Na_V1.5$ when expressed in a DRG neuroblastoma cell line (midpoint of inactivation -88 versus -83 mV, Kerr et al., 2007). Future experiments should attempt to identify the isoform expressed in the vestibular ganglion and vestibular hair cells.

The other important factor for considering the functional implication of the negative inactivation range is the physiological resting membrane potential, which cannot be determined from ruptured-patch recordings, in which the intracellular and extracellular concentrations of ions are set by the experimenter. Even the use of cell-attached patch methods used sometimes to "noninvasively" measure resting potential (Verheugen et al., 1999) do not resolve the problem of unknown extracellular salt concentrations, unless used *in vivo*. The resting membrane potential of the cell depends largely on the expression of Na^+/K^+–ATPase and the equilibrium potential for K^+ (E_K) which determines the most negative voltage the cell could reach by having open K^+ conductances. Peculiarities of inner ear K^+ transport could result in an atypical extracellular K^+ concentration. To my knowledge, values are not available for developing vestibular epithelium. However, K^+ concentration in rat scala tympani perilymph

(from the cochlea) was measured at 3 mM (Anniko and Wroblewski, 1986), lower than the 5.8 mM in the L-15 medium in which current clamp recordings were made. In 2.5 mM K^+, hair cells (which are typically thought to have fairly positively resting potentials because of their open transduction channels) from P7-P10 organ of Corti had resting potentials of approximately −75 mV (Tritsch et al., 2007). Assuming 120 mM intracellular and 3 mM extracellular K^+, the predicted E_K at body temperature would be −98.5 mV. In cardiac ventricular myocytes, where $Na_V1.5$ is largely responsible for the generation of the fast upstroke of the action potential, the resting membrane potential is between −80 and −90 mV, close to E_K, at least in part because of relative large resting K^+ conductances contributed by inward rectifier potassium channels (Schram et al., 2002; Dhamoon and Jalife, 2005). This is likely beneficial because cardiac myocytes are coupled via gap junctions through which excitation propagates, and a low input resistance and low membrane time constant may allow for more synchronous contraction. Mature vestibular neurons, which drive speedy reflexes, may also have large resting K^+ conductances to reduce low-pass filtering of signal onsets. Furthermore, even our "sustained-A" neurons, which typically had GΩ input resistances, had resting potentials between −70 and −78 mV in our recording conditions, suggesting that there may be other determinants of resting potential, such as the electrogenic action of the Na^+/K^+–ATPase (Brodie et al., 1987). Following an action potential, the afterhyperpolarization of the membrane may bring the membrane voltage below resting potential and then increase it back towards resting level. If the physiological $V_{1/2inact}$ of $I_{TTX-,fast}$ were more positive than measured, the AHP could easily approach the $V_{1/2inact}$ and generate substantial $Na_V1.5$ current (e.g., AHP of -84 mV in Blair and Bean, 2002). However, another factor is the time course of recovery from inactivation, which is slow near $V_{1/2inact}$.

In summary, further experiments should examine the voltage dependence of $I_{TTX-I,\ fast}$ in more physiological conditions to better evaluate its potential to influence spiking. Simulations may also help by showing under what conditions $Na_V1.$-5-like currents can play a role.

DOES $NA_V1.5$-LIKE CURRENT PLAY A ROLE IN DEVELOPMENT OR MATURE FUNCTION? The decrease in $I_{TTX-I,fast}$ expression with age raises the question of whether it participates in development and whether it participates in the mature vestibular ganglion. I present several different (but not mutually exclusive) possibilities and the evidence in support of each. Studies in several systems point to a potential role for the $Na_V1.5$ subunit in development. $Na_V1.5$ is transiently expressed in developing DRG and embryonic or denervated skeletal muscle and not found in the vast majority of adult cells (Kallen et al., 1990; Renganathan et al., 2002). Interestingly, vestibular hair cells, which do not fire action potentials in the mature state, transiently express sodium currents in early development, with a subset of the hair cells expressing mostly an $Na_V1.5$-like current (Wooltorton et al., 2007). Géléoc et al. (2004) reported that an $Na_V1.5$-like current present in vestibular hair cells peaked in size around E16 and dropped significantly by P0.

Subsequently, it was clarified that expression of this current depends on hair cell type and zone, and could still be seen in some hair cells at P21 (Wooltorton et al., 2007). Nevertheless, it is thought that most mature hair cells do not express Na_V currents and are graded encoders rather than spiking cells, raising the question of why many hair cells express this current during development. One possibility is to permit spiking of hair cells which might aid in synaptogenesis and organization of upstream neurons. However, spontaneous spiking seems to primarily depend on Ca_V channels in the cochlea (reviewed in Kennedy, 2012), and has not been seen in vestibular hair cells. The very negative inactivation range also poses a problem for spiking, especially as hair cells are thought to rest less negatively than neurons. Hair cells and VGN receive an efferent projection from the brainstem, which synapses on calyces, type II hair cells, and bouton synapses (summarized in Lysakowski and Goldberg, 2008) and is thought to hyperpolarize the hair cells (Glowatzki and Fuchs, 2000; Holt et al., 2006). Thus, efferent activation may bring hair cells closer to the functional range of $Na_V1.5$.

The pattern of $I_{TTX\text{-}I,fast}$ expression in our VGN suggested a decreasing trend with age, but data would have to be extended to older ages in order to determine the prevalence of mature expression and whether it plays a role in mature function. It is possible that $I_{TTX\text{-}I,fast}$ plays an electrical role in development of VGN, particularly around birth when input resistance is high (before upregulation of K_{LV} current) and synaptic inputs may be immature. Perhaps under these conditions the small depolarizing current provided by $I_{TTX\text{-}I,fast}$ from its relatively negative activation range could contribute to excitability. Indeed the window current (steady-state current at the overlap of activation and inactivation) for $I_{TTX\text{-}I,fast}$ is centered over more negative voltages than that of the TTX-S current and is near the resting potential of the neurons. As development proceeds, efferent activation could lead to gaps in hair cell synaptic release, producing brief hyperpolarizations in VGN potential followed by a depolarization, a trajectory that might recruit $I_{TTX\text{-}I,fast}$ to participate in developmental bursting activity, as observed in the cochlear system (reviewed in Kennedy, 2012).

As development proceeds, tonic depolarizing synaptic input would make $I_{TTX\text{-}I,fast}$ both unnecessary and unavailable due to inactivation, making a more positively inactivating and more rapidly repriming channel such as $I_{TTX\text{-}S}$ or $I_{TTX\text{-}I,\ slow}$ more suited to the high rates of spontaneous and driven activity in the vestibular nerve. In the heart, automaticity (the ability to spontaneously initiate depolarization, as in pacemakers of the cardiac sinoatrial node) is observed in ventricular myocytes during early embryonic development, but is no longer present in later development when the K^+ conductance is much larger (Sperelakis and Pappano, 1983). A window conductance of 0.6% of the peak Na_V current was large enough to induce automaticity and was abolished by a shift in inactivation from -77.7 ± 1.0 mV early in development to -91.4 ± 1.7 mV late in development (Sada et al., 1995). Surprisingly, Na_V current in chick and some other non-mammalian hearts appears to be TTX-sensitive (but with

similar properties to mammalian hearts) (Josephson and Sperelakis, 1989; Vornanen et al., 2011), and it is not clear in this case whether the shift in inactivation reflects a change in subunit composition or a change in the properties of one subunit. A similar difference has been noted in hair cells, in that the negatively inactivating current in avian and reptilian hair cells is apparently TTX-sensitive (Wooltorton et al., 2008). Nevertheless, these studies raise some interesting possibilities for a transient period of excitability based on small window currents and for changes in inactivation properties during development.

Alternatively, $Na_V1.5$-like current may play a role independent of its effect on membrane voltage. Voltage-gated ion channels have been documented to have non-conducting functions (Kaczmarek, 2006), and in particular, Na_V channel β subunits are part of the cell-adhesion molecule superfamily and regulate neurite outgrowth and axon pathfinding (Davis et al., 2004; Brackenbury et al., 2008; Brackenbury et al., 2010). $Na_V1.5$ may interact in some not yet understood way with β subunits around the time of outgrowth and synaptogenesis. Even in the heart, where $Na_V1.5$ plays a clear electrophysiological role in adulthood, $Na_V1.5$-null animals have early cardiac malformations and die between E10 and E11 (Papadatos et al., 2002). Knocking out the homologs in zebrafish resulted in morphological defects that did not appear to be explained by altered membrane electrophysiology (Chopra et al., 2010).

Another possibility is that during the course of development $Na_V1.5$ expression changes in its localization within the cell rather than its overall level. $Na_V1.5$ can still be detected in the vestibular ganglion via RT-PCR at P21 (Wooltorton et al., 2007 and unpublished results) (note, however, that the method was not quantitative and expression continued to be detected in the sensory epithelium even though prevalence of the current had decreased by P21). Immunohistochemical results in P21 and adult tissue suggests that the strongest staining is on the inner face of the postsynaptic calyx (Wooltorton et al., 2007; Lysakowski et al., 2011). Therefore $Na_V1.5$ subunits could be expressed but transported away from the cell body to the calyx terminals, where they may continue to play a role in excitability or cell adhesion into adulthood. At the terminal, $Na_V1.5$ subunits may also be modulated by efferent activation as $Na_V1.5$ channels can be subject to a variety of post-translational modifications (phosphorylation, glycosylation, S-nitrosylation, ubiquitination, methylation) and be regulated by a variety of signaling kinases (Rook et al., 2012). As calyces and transport mature, it may become harder to record $I_{TTX\text{-}I,fast}$ from dissociated somata. In one study on isolated vestibular calyx afferents attached to type I hair cells, 81.1 ± 9.4% (n=4) of the current was blocked by 100 nM TTX (Rennie and Streeter, 2006), as compared with the ~95% expected for purely TTX-S currents with a K_d of 5 nM (Eq. 3), and the ~86% predicted by our fit of the mixed Na_V current dose-response curve. The large variability for the four cells in Rennie and Streeter (2006) may indicate even less block for some cells. To more explicitly test this possibility, future studies would need to obtain high quality Na_V current recordings from calyx terminals. Adult expression

of $Na_V1.5$ in neurons may not be unprecedented. Reports of $Na_V1.5$ gene expression in the limbic regions of the brain have detected this expression in both developing and adult rat and human tissue (Hartmann et al., 1999; Donahue et al., 2000). Although one study of $Na_V1.5$ gene expression in the brain finds a decreasing trend in expression level with age in all brain tissues tested, the decrease was gradual and there was still significant expression at P120 (Wang et al., 2009).

It would be interesting to address some of these questions by examining Na_V channel expression during embryonic development, or during generation of new neurons from inner ear neurospheres. One could examine the temporal pattern and dependence on developmental milestones (e.g., synapse formation). Does onset of expression for $Na_V1.5$ precede that for TTX-S channels? What are the inactivation properties of $Na_V1.5$-like current, the resting potential, and the input resistance at various times in development?

FIRING PATTERNS OF NEURONS WITH $I_{TTX\text{-}I,FAST}$. Our dataset displays the same general firing pattern classes seen in Kalluri et al. (2010), and cells without $I_{TTX\text{-}I,slow}$ resemble those previously seen within this classification. "Transient" neurons fired one or two spikes at the onset of a current step and on average had more K_{LV} and higher current thresholds, while "Sustained-A" neurons fired throughout the current step with minimal accommodation in spike height and frequency even at threshold, which was typically 10 pA of current or less. "Sustained-B" and "Sustained-resonators" had intermediate excitability and fired fewer spikes at threshold or fired a spike followed by ringing, respectively. Since the amount of current often scales with the amount of membrane, and since a correlation between cell size and firing pattern is observable by the second postnatal week, it has been proposed that differences in total resting K^+ conductance resulting from cell size differences might underlie differences in excitability (Risner and Holt, 2006). In our P0-P8 cells, the average sizes of neurons in the three categories are not different. Therefore, cell size cannot directly explain differences in the size of I_{KLV} and in the excitability between "Transient" and "Sustained" neurons in our data.

$I_{TTX\text{-}I,fast}$ was observed in all firing categories, and did not seem more prevalent in any particular category. This result was surprising since immunostaining against $Na_V1.5$ channels was most intense on central calyces, which are associated with irregular firing neurons, and which we hypothesized corresponded to "Transient" firing neurons.

At the ages we examined, the peak $I_{TTX\text{-}I,fast}$ was about 10% of the very large peak Na_V current (the rest contributed by $I_{TTX\text{-}S}$). Assuming a single-channel conductance of about 17 pS (Beyder et al. 2010), our average whole-cell conductance represents ~750 sodium channel molecules. Despite its small relative size, $I_{TTX\text{-}I,fast}$ could produce a significant voltage change especially in

cells with high input resistance. Although the full current (up to 2 nA) is not likely to be evoked by physiological voltage trajectories, we note that "sustained-firing" neurons only need ~10 pA of current to reach firing threshold. Because $I_{TTX\text{-}I,fast}$ activates more negatively than TTX-S currents, it may provide a subthreshold boost to promote firing, and even more so following the de-inactivating afterhyperpolarization of a preceding spike.

EFFECTS OF CULTURE ON TTX-INSENSITIVE CURRENTS. In a small sample of cultured neurons, we observed absent or attenuated $I_{TTX\text{-}I,fast}$ currents and no $I_{TTX\text{-}I,slow}$ with no decrease in TTX-S currents. This was particularly surprising for $I_{TTX\text{-}I,fast}$, which is prevalent at the younger ages. A very negative half-inactivation (around −108 mV) has been seen for the Na_V current in acutely isolated adult rat olfactory receptor neurons (ORNs) but not in cultured ORN; Na_V current was also less sensitive to TTX in acutely isolated than cultured ORN (Qu et al., 2000).

For the $Na_V1.8$ channel, there is clear evidence that co-culturing with Schwann cells (SC) or SC-conditioned media, or in the presence of growth factors such as NGF and GDNF upregulates $Na_V1.8$ current (Hinson et al., 1997; Fjell et al., 1999; Cummins et al., 2000), so culturing in the absence of SCs and growth factors might be expected to reduce $Na_V1.8$ expression.

$I_{TTX\text{-}I,slow}$ is expressed in a subset of vestibular ganglion neurons

In about 20–25% of VGNs, we observed a current ($I_{TTX\text{-}I,slow}$) with a relatively slow time course for an Na_V current but too rapid (especially at positive voltages) to be a Ca_V current (Table 3). This current also had a very depolarized voltage dependence and was eliminated in external solutions lacking Na^+. Together these properties are consistent with $I_{TTX\text{-}I,slow}$ being carried by the peripheral-nervous system specific $Na_V1.8$ subunit. $Na_V1.8$ signal can be consistently amplified from vestibular ganglia using RT-PCR (Wooltorton et al., 2007 and unpublished results, see Introduction), and can be detected in many VGN in a fluorescent $Na_V1.8$ reporter mouse (note that this is not a fusion protein and does not reveal localization of $Na_V1.8$ protein, but rather is designed to illuminate the entirety of cells that transcribe $Na_V1.8$).

Although the kinetics of inactivation are in good overall agreement with $Na_V1.8$ channels, the asymptotic τ_{inact} for $I_{TTX\text{-}I,slow}$ in VGN at positive voltages is ~1 ms (+20 mV), somewhat faster than what has been reported for $Na_V1.8$ channels. This difference could be due to the presence of small amounts of activating outward current at +20 mV which would speed up the apparent inactivation. Other factors that may account for this discrepancy include different isoforms of $Na_V1.8$ (Kerr et al., 2004), co-expression with various β subunits (co-expression of β1 subunit speed up Nav1.8 current by 1.6-fold, Vijayaragavan et al., 2001), or different cellular contexts (Choi et al., 2007).

UNEXPECTED EXPRESSION OF $Na_V1.8$ IN A NON-SOMATOSENSORY PERIPHERAL GANGLION. $Na_V1.8$ has been reported in a number of peripheral somatosensory ganglia such as the nodose and petrosal ganglia (Baccaglini and Cooper, 1982; Belmonte and Gallego, 1983; Bossu and Feltz, 1984; Stansfeld and Wallis, 1985; Ikeda and Schofield, 1987; Stea and Nurse, 1992; Cummins, 2002; Gautron et al., 2011), as well as trigeminal ganglia (Hsiung and Puil, 1990; Harriott and Gold, 2009; Vaughn and Gold, 2010), and a few neurons in the geniculate ganglion (Agarwal et al., 2004 and our observations from the same Nav1.8-Cre transgenic line). Previous reports have found $Na_V1.8$ expression to correlate strongly with nociceptive identity in the DRG (Akopian et al., 1999 and many subsequent studies).

Our results raise the intriguing possibility that non-nociceptive neurons may also express $Na_V1.8$. ($Na_V1.8$ immunoreactivity has been reported in a subpopulation of large retinal ganglion neurons but electrophysiological evidence has not been published (O'Brien et al., 2008).) In addition, we observed fluorescence signal in the cochlear ganglion, another ganglion that is not expected to contain somatosensory nociceptors (notably fluorescence did not appear to label longitudinal fibers in the outer hair cell region, which would have corresponded to unmyelinated type II primary cochlear afferents hypothesized by some to signal acoustic pain (e.g., Brown et al., 1988)). Also somewhat surprising is that the vast majority of VGN are myelinated (Ballantyne and Engström, 1969), whereas C-type DRG neurons are unmyelinated, and models of abnormal demyelination show upregulation of $Na_V1.8$ expression (Black et al., 1999; Black et al., 2000). Finally, our cells with $I_{TTX\text{-}I,slow}$ were not particularly small (although this could change in the second postnatal week as neurons continue to get larger).

$Na_V1.8$ is, however, not exclusively expressed in small unmyelinated nociceptors even among somatosensory ganglion cells. In the DRG, $Na_V1.8$ is expressed by many (mostly nociceptive) medium-sized neurons and large neurons, which are myelinated (Sangameswaran et al., 1996; Novakovic et al., 1998; Djouhri et al., 2003; Coste et al., 2007; Ho and O'Leary, 2011), while chemoreceptor afferents of the petrosal ganglion, which are unmyelinated C-type neurons express very little $Na_V1.8$ (Cummins, 2002). Ho and O'Leary showed evidence for a) high expression of $Na_V1.8$ in some large neurons and b) low expression of $Na_V1.8$ in many large neurons (however, the size of their "large" neurons seems similar to "medium-sized" nociceptors in Coste et al., 2007). In Djouhri et al., (2003), weak $Na_V1.8$-like immunoreactivity was also detected in some low-threshold mechanosensitive (i.e., non-nociceptive) neurons. In the nodose ganglion, some studies find that TTX-I currents and $Na_V1.8$ immunoreactivity are not preferentially distributed to nociceptors (Kwong et al., 2008) or that there is no relationship between cell size or response to capsaicin and sodium current properties (Bielefeldt, 2000). Some vagal afferents (whose cell bodies reside in the nodose ganglion) that are labeled in an $Na_V1.8$ reporter mouse can be traced to tension receptors (Gautron et al., 2011).

In Gautron et al. (2011), the percentage of neurons labeled by the Cre-based reporter mouse seemed higher than what is observed electrophysiologically, and our preliminary data with the tdTomato reporter give a similar impression, although the percentage of labeled neurons has not been quantified. This may be explained by either post-translational regulation (e.g., of plasma membrane insertion), or the high sensitivity of the Cre excision system. In the latter case, even neurons that express low levels of $Na_V1.8$ would be labeled.

Rather than dividing neurons into expressing and non-expressing categories, it may be more informative to examine the heterogeneity across subpopulations in terms of amount of TTX-I current expression. The current density of TTX-I current in somatosensory ganglia vary highly from study to study, making comparison of our VGN currents to somatosensory neuron currents difficult. Differences in cell isolation and culture conditions may underlie some of this variability. For example, the size of the TTX-I current can vary two- to several-fold, depending on the GTP concentration in the internal solution (presumably due to G-protein interactions) (Saab et al., 2003), whether F^- is the internal anion (Saab et al., 2003), and whether secreted growth factors such as NGF (Ritter and Mendell, 1992) or GDNF (Cummins et al., 2000) are included in the culture medium. The current density (as well as the relative size of the TTX-I component) also varies between cell types (e.g., Djouhri et al., 2003; Coste et al., 2007). We consider only studies with predicted E_{Na} values in the range of 48 to 67 mV (close to that used in our study). In some reports, the average current density of $I_{TTX\text{-}I,slow}$ in VGN (~80 to100 pA/pF, not including cells without $I_{TTX\text{-}I,slow}$) is smaller than that of $Na_V1.8$-like current in small DRG neurons, even assuming a three-fold F^- correction factor (e.g., Cummins and Waxman, 1997; Cummins et al., 2000; Choi et al., 2007). In another study, $I_{TTX\text{-}I,slow}$ current density is higher than that seen in most large DRG cells, comparable to a subpopulation of moderate expressing cells, but lower than the highest-expressing population (cells cultured with 50 ng/mL NGF, Ho and O'Leary, 2011). In yet other studies, it is comparable to what is seen overall in DRG neurons (e.g., Elliott and Elliott, 1993; Coste et al., 2007). Considering that we could not further subdivide our $I_{TTX\text{-}I,slow}$–expressing neurons into low, moderate, and high-expressing subpopulations based on morphology or other properties (as in DRG studies), and all expressing cells were averaged together, the maximum current density is also of interest. The maximum current density of ~150 pA/pF is considerably less than that seen in some studies (e.g., Rush et al., 2005; Ho and O'Leary, 2011). Because of this large variability, ideally, VGNs and DRG neurons should be enzymed, cultured, and recorded from using the same method for a proper comparison.

The relative size of TTX-S and TTX-I current in somatosensory ganglia is also variable from study to study (see Table 1. of Black et al., 1996). In some studies, TTX-I current appears as the predominant current with little evidence of TTX-S current (e.g., Stea and Nurse, 1992, petrosal ganglion; Gold et al., 1996, DRG; Ho and O'Leary, 2011, DRG) or with TTX-I current being several

fold larger than TTX-S current (Choi et al., 2007). In other studies, the TTX-S current density is similar to (Blair and Bean, 2002) or several-fold larger than the TTX-I current density (Chen et al., 2011). Our cells ranged from having TTX-S current that was about twice as large as TTX-I current to many-fold larger. In no cell was TTX-I current greater than TTX-S current, as is often reported for small DRG neurons. Overall, VGN with $I_{TTX\text{-}I,slow}$ resembled the group of "partially TTX-sensitive cells" described by Ogata and Tatebayashi (1993) in cultured DRG neurons, in which the proportion of total current attributable to the TTX-I component varied from cell to cell. In that study, the size of "TTX-S cells" fell in the range of large histologically light cells, "TTX-I cells" in the small dark range, and the "partially TTX-S cells" covered the size ranges for both large light and small dark cells, and could correspond to Aδ fibers which are intermediate in size. VGN also appear to resemble the group of large neurons in Rizzo (1994), which had either exclusively large fast TTX-S currents, or a mixture of TTX-S and TTX-I currents.

Rather than dividing neurons into expressing and non-expressing categories, it may be more informative to examine the heterogeneity across subpopulations in terms of amount of expression. The relative size of TTX-S and TTX-I current in somatosensory ganglia is variable from study to study (see Table 1. of Black et al., 1996). In some studies, TTX-I current appears as the predominant current with little evidence of TTX-S current (e.g., Gold et al., 1996, DRG, Ho and O'Leary 2011, DRG; Stea and Nurse, 1992, petrosal ganglion) or with TTX-I current being several fold larger than TTX-S current (Choi et al., 2007). In other studies, the TTX-S current density is similar to (Blair and Bean, 2002) or several-fold larger than the TTX-I current density (Chen et al., 2011). The TTX-S to TTX-I ratio may depend on the cell type (Djouri et al., 2003; Coste et al., 2007). Our cells ranged from having TTX-S current that was about twice as large as TTX-I current to many-fold larger. In no cell was TTX-I current greater than TTX-S current, as is often reported for small DRG neurons. Overall, VGN with $I_{TTX\text{-}I,slow}$ resembled the group of "partially TTX-sensitive cells" described by Ogata and Tatebayashi (1993) in cultured DRG neurons, in which the proportion of total current attributable to the TTX-I component varied from cell to cell. In that study, the size of "TTX-S cells" fell in the range of large histologically light cells, "TTX-I cells" in the small dark range, and the "partially TTX-S cells" covered the size ranges for both large light and small dark cells, and could correspond to Aδ fibers which are intermediate in size. VGN also appear to resemble the group of large neurons in Rizzo (1994), which had either exclusively large fast TTX-S currents, or a mixture of TTX-S and TTX-I currents. The absolute current density we see in VGN is more than what is seen in most large DRG cells, but lower than what is seen for a subpopulation of high-expressing large DRG cells that also had much higher copy number for $Na_V1.8$ mRNA (Ho and O'Leary, 2011).

Future experiments should determine whether expression of $I_{TTX\text{-}I,slow}$ in VGN is correlated with capsaicin responsiveness, as in the DRG. Use of reporter mice containing various portions of regulatory regions (e.g., Puhl and Ikeda, 2008) will help to resolve questions regarding

exactly which cell populations express $Na_V1.8$ as well as shed light on how this expression is regulated at the molecular level. The question of what regulates membrane insertion and functional expression of $Na_V1.8$ is also key; for instance, Ho and O'Leary (2011) note that large neurons displayed high levels of $Na_V1.8$ mRNA despite the absence of TTX-I current in 80% of these neurons.

POTENTIAL FUNCTIONAL EFFECTS OF $I_{TTX\text{-}I,slow}$ EXPRESSION. Although peak $I_{TTX\text{-}I,slow}$ amplitude was smaller than peak $I_{TTX\text{-}S}$ amplitude, its larger window of overlap, larger separation between activation and inactivation time course, and overall slower kinetics may mean that it contributes more current and total charge movement during depolarizations. Consequently, cells with $I_{TTX\text{-}I,slow}$ had action potential shapes that differed consistently from those of other cells in terms of their a) positive voltage threshold, b) increased width, and c) inflection on the repolarization phase (Fig. 14). While these differences would be predicted from the properties of $I_{TTX\text{-}I,slow}$, other types of experiments are needed to establish a causal relationship. These could include direct manipulation of this subunit or a combination of action potential clamp with computer simulations. The presence of $I_{TTX\text{-}I,slow}$ and the more positively shifted properties of the TTX-S current in neurons with $I_{TTX\text{-}I,slow}$ may allow the cells to fire at more depolarized potentials than do the VGNs without $I_{TTX\text{-}I,slow}$. Combining TTX-S and TTX-I currents may extend the range of input intensities over which the neuron is able to fire, although the interaction between the two is complex (for instance, broader spikes may result in more inactivation of TTX-S currents and more K_V current activation). The broader action potentials and reduced inactivation at depolarized voltages may make these neurons more suited to encoding tonic rather than transient stimuli. The model of Schild and Kunze (1997) shows that the maximal firing rate is strongly dependent on the ratio of TTX-S to TTX-I current, although experiments would have to be performed at body temperature to get a more physiological estimate of the maximal firing rate. Although the retardation of firing rate by $I_{TTX\text{-}I,slow}$ seems like a hindrance to temporal encoding, it may expand the dynamic range for intensity encoding. The broader action potential could also increase the synaptic strength at the synapse from VGN onto their postsynaptic neurons by increasing presynaptic calcium influx (Sabatini and Regehr, 1997; Boudkkazi et al., 2011). On the other hand, the increased calcium entry per spike may make neurons with $I_{TTX\text{-}I,slow}$ more vulnerable to excitotoxicity.

It would not be surprising if the $Na_V1.8$-like component made up a smaller proportion of the total Na^+ current in vestibular ganglion neurons than in DRG nociceptive neurons. In our KCl-based solutions, the average resting potential of our $I_{TTX\text{-}I,slow}$ -expressing cells was −69 mV, whereas DRG nociceptive neurons have a resting potential around −50 mV (Caffrey et al., 1992; Renganathan et al., 2001), where a much larger fraction of TTX-S channels would be

inactivated. Furthermore, voltage threshold for spiking in our $I_{TTX\text{-}I,slow}$-expressing cells was around –40 mV, and the activation midpoint for $Na_V1.8$ was around –20 mV, yet current thresholds were modest (typically between 10 and 40 pA). Negatively-resting VGN cells most likely rely on TTX-S channels to reach threshold, so would need more TTX-S current than nociceptive neurons that have less negative resting potentials.

An interesting consequence of having $Na_V1.8$ is that neuronal excitability becomes more resistant to changes in the resting membrane potential. Typically, small depolarizations can greatly reduce the excitability of a neuron by inactivating TTX-S channels. In the presence of a sodium channel that shows minimal inactivation below –40 mV ($Na_V1.8$), however, small standing depolarizations may minimally affect excitability or even increase excitability by bringing the neuron closer to voltage threshold.

Replacing TTX-S channels with TTX-I channels that activate at more depolarized voltages may also allow neurons to titrate their sensitivity and thresholds without changing their overall excitability. Thus, in VGN with $I_{TTX\text{-}I,slow}$, voltage threshold is higher, but spike height is unaltered. Alternatively, the TTX-I current may carry the action potential while TTX-S currents determine sensitivity by depolarizing the neuron into the range that triggers TTX-I currents. This notion receives support from modeling work simulating various combinations of TTX-S and TTX-I currents (Schild and Kunze, 1997). In general, models show that diversity in response properties can be generated by varying the ratio of TTX-S to TTX-I current (Schild and Kunze, 1997; Choi and Waxman, 2011).

The slow inactivation of $Na_V1.8$ may lead to adaptation that shapes responses to sustained stimuli (Blair and Bean, 2003). Therefore, neurons with $I_{TTX\text{-}I,slow}$ might have different adaptation properties to vestibular stimuli.

Lastly, $Na_V1.8$ can be modulated by inflammatory substances such as serotonin, prostaglandin E2, and adenosine (Gold et al., 1996; Cardenas et al., 1997) via PKC and PKA (Gold et al., 1998), calmodulin (Choi et al., 2006), or GTP (Saab et al., 2003). The GTP sensitivity may also allow it to respond to other transmitters coupled to G-protein coupled receptors such as CGRP, which is present in efferent synapses. Future studies could explore modulation of $I_{TTX\text{-}I,slow}$ by substances present in the vestibular periphery.

OTHER Na_V CURRENTS. There are many candidates for the TTX-S current(s) expressed in VGN. $Na_V1.1$, $Na_V1.2$, $Na_V1.6$, and $Na_V1.7$ are all observed in DRG neurons (reviewed in Rush et al., 2007; Ho and O'Leary, 2011) and have properties that are generally similar to our TTX-S currents. It is intriguing that the TTX-S current may be different between cells with and without $I_{TTX\text{-}I,slow}$. Different cellular contexts or populations may have different functional ensembles of

Na_V currents. For instance, in the DRG, TTX-S currents in large neurons tend to be rapidly repriming while currents in small nociceptors tend to be slowly repriming, although it is unclear whether subunit differences underlie these differences in TTX-S current properties (reviewed in Rush et al., 2007). Repriming characteristics may be interesting to investigate in future studies since vestibular ganglion neurons fire at very high rates *in vivo*. Another difference between the TTX-S current in cells with and without $I_{TTX\text{-}I,slow}$ was that the size of the TTX-S component was smaller in cells with $I_{TTX\text{-}I,slow}$. Speculatively, this reduction in TTX-S current may be due to homeostatic mechanisms regulating sodium channel expression based on electrical activity, calcium concentrations, or sodium concentrations (Offord and Catterall, 1989; Chiamvimonvat et al., 1995; Dargent and Couraud, 1990). Indeed, TTX-S currents in the $Na_V1.8$ null mouse are about twice as large as that in wildtype animals (Akopian et al., 1999).

It is somewhat surprising that we did not see a significant $Na_V1.9$ component, given its expression in RT-PCR. There are several possible reasons why $Na_V1.9$ current may be more elusive and labile than $Na_V1.8$ current. It is possible that a small component of $Na_V1.9$ exists with properties that make its separation from $Na_V1.8$ impossible. $Na_V1.9$ can artifactually increase in size more than 20-fold during ruptured patch recording (the effect is particularly pronounced for CsF-containing internal solutions), and this effect is eliminated by recording in perforated patch mode or by inclusion of ATP in the internal solution (Maruyama et al., 2004). When looking only at results obtained with ATP or the perforated patch method, $Na_V1.9$ current is fairly small: ~10–40 pA/pF (depending on cell type and E_{Na}, see Table 3). This may be appropriate for a background channel with slow dynamics and large window current, and which may be slightly open at rest. $Na_V1.9$ current diminishes in size with time after dissociation (Maruyama et al., 2004), and its expression may be more restricted across neuronal subtypes than $Na_V1.8$ expression, as judged from single-cell RT-PCR and electrophysiology (Ho and O'Leary 2011) and combined immunoreactivity and *in situ* hybridization (Fukuoka and Noguchi, 2011). Expression of low calculated mRNA copy numbers (~500) in large DRG neurons was not accompanied by isolatable persistent current in Ho and O'Leary (2011), even for the subpopulation of large neurons that had large $Na_V1.8$ currents, suggesting that either such low levels are difficult to detect electrophysiologically or that post-translational control exists (which may underlie the sudden increases in $Na_V1.9$ current observed with unphysiological recording conditions). The $Na_V1.9$ channels also appear to undergo ultra-slow inactivation (time constant of ~50 s), and are therefore sensitive to the holding potential, although our holding potential of −70 mV would be expected to cause only ~20% inactivation (Rugiero et al., 2003). The small size (in the presence of ATP), similarity in properties to $Na_V1.8$ (in CsCl), and restricted expression could explain why many studies of TTX-I currents in small DRG cells fail to report $Na_V1.9$ and find that the properties of the TTX-I current are largely consistent with $Na_V1.8$ (Akopian et al., 1999, TTX-I current absent in $Na_V1.8$ knock out mouse; Blair and Bean, 2002;

Gold et al., 1996; Zhou et al., 2002). We may have failed to see a significant $Na_V1.9$-like current for any of these same reasons.

In summary, the vestibular ganglion, like the DRG, may comprise multiple populations of neurons with different Na_V channel complements that include TTX-insensitive subunits. These Na_V channels can shape response properties to head motions, such as sensitivity, dynamic range, frequency filtering, and adaptation. These ion channels may be subject to various forms of modulation, undergo changes in pathological conditions, or form the basis for selective therapeutic treatments.

REFERENCES

Agarwal N, Offermanns S, Kuner R (2004) Conditional gene deletion in primary nociceptive neurons of trigeminal ganglia and dorsal root ganglia. genesis 38:122-129.

Akopian AN, Sivilotti L, Wood JN (1996) A tetrodotoxin-resistant voltage-gated sodium channel expressed by sensory neurons. Nature 379:257-262.

Akopian AN, Souslova V, England S, Okuse K, Ogata N, Ure J, Smith A, Kerr BJ, McMahon SB, Boyce S, Hill R, Stanfa LC, Dickenson AH, Wood JN (1999) The tetrodotoxin-resistant sodium channel SNS has a specialized function in pain pathways. Nat Neurosci 2:541-548.

Almers W, McCleskey EW (1984) Non-selective conductance in calcium channels of frog muscle: calcium selectivity in a single-file pore. J Physiol 353:585-608.

Anniko M, Wroblewski R (1986) Ionic environment of cochlear hair cells. Hear Res 22:279-293.

Baccaglini PI, Cooper E (1982) Electrophysiological studies of new-born rat nodose neurones in cell culture. J Physiol 324:429-439.

Backx PH, Yue DT, Lawrence JH, Marban E, Tomaselli GF (1992) Molecular localization of an ion-binding site within the pore of mammalian sodium channels. Science (New York, NY) 257:248-251.

Baird RA, Desmadryl G, Fernandez C, Goldberg JM (1988) The Vestibular Nerve of the Chinchilla. II. Relation Between Afferent Response Properties and Peripheral Innervation Patterns in the Semicircular Canals. Journal of Neurophysiology 60:182-203.

Ballantyne J, Engström H (1969) Morphology of the vestibular ganglion cells. The Journal of Laryngology and Otology 83:19-42.

Banks C, McGinness S, Harvey R, Sacks R (2012) Is Allergy Related to Meniere's Disease? Current Allergy and Asthma Reports 12:255-260.

Barry PH (1994) JPCalc, a software package for calculating liquid junction potential corrections in patch-clamp, intracellular, epithelial and bilayer measurements and for correcting junction potential measurements. J Neurosci Methods 51:107-116.

Bean BP (2007) The action potential in mammalian central neurons. Nat Rev Neurosci 8:451-465.

Belmonte C, Gallego R (1983) Membrane properties of cat sensory neurones with chemoreceptor and baroreceptor endings. The Journal of Physiology 342:603-614.

Berlinger NT (2011) Meniere's disease: new concepts, new treatments. Minnesota medicine 94:33-36.

Beyder A, Rae JL, Bernard C, Strege PR, Sachs F, Farrugia G (2010) Mechanosensitivity of Nav1.5, a voltage-sensitive sodium channel. The Journal of Physiology 588:4969-4985.

Bielefeldt K (2000) Differential effects of capsaicin on rat visceral sensory neurons. Neuroscience 101:727-736.

Biswas S, DiSilvestre D, Tian Y, Halperin VL, Tomaselli GF (2009) Calcium-mediated dual-mode regulation of cardiac sodium channel gating. Circulation Research 104:870-878.

Black JA, Liu S, Tanaka M, Cummins TR, Waxman SG (2004) Changes in the expression of tetrodotoxin-sensitive sodium channels within dorsal root ganglia neurons in inflammatory pain. Pain 108:237-247.

Black JA, Dib-Hajj S, Baker D, Newcombe J, Cuzner ML, Waxman SG (2000) Sensory Neuron-Specific Sodium Channel SNS Is Abnormally Expressed in the Brains of Mice with Experimental Allergic Encephalomyelitis and Humans with Multiple Sclerosis. Proceedings of the National Academy of Sciences 97:11598-11602.

Black JA, Dib-Hajj S, McNabola K, Jeste S, Rizzo MA, Kocsis JD, Waxman SG (1996) Spinal sensory neurons express multiple sodium channel α-subunit mRNAs. Molecular Brain Research 43:117-131.

Black JA, Fjell J, Dib-Hajj S, Duncan ID, O'Connor LT, Fried K, Gladwell Z, Tate S, Waxman SG (1999) Abnormal expression of SNS/PN3 sodium channel in cerebellar Purkinje cells following loss of myelin in the taiep rat. Neuroreport 10:913-918.

Blair NT, Bean BP (2002) Roles of Tetrodotoxin (TTX)-Sensitive Na+ Current, TTX-Resistant Na+ Current, and Ca2+ Current in the Action Potentials of Nociceptive Sensory Neurons. The Journal of Neuroscience 22:10277-10290.

Blair NT, Bean BP (2003) Role of Tetrodotoxin-Resistant Na+ Current Slow Inactivation in Adaptation of Action Potential Firing in Small-Diameter Dorsal Root Ganglion Neurons. J Neurosci 23:10338-10350.

Bossu JL, Feltz A (1984) Patch-clamp study of the tetrodotoxin-resistant sodium current in group C sensory neurones. Neurosci Lett 51:241-246.

Boudkkazi S, Fronzaroli-Molinieres L, Debanne D (2011) Presynaptic action potential waveform determines cortical synaptic latency. J Physiol 589:1117-1131.

Brackenbury WJ, Djamgoz MBA, Isom LL (2008) An emerging role for voltage-gated Na+ channels in cellular migration: regulation of central nervous system development and potentiation of invasive cancers. The Neuroscientist: A Review Journal Bringing Neurobiology, Neurology and Psychiatry 14:571-583.

Brackenbury WJ, Calhoun JD, Chen C, Miyazaki H, Nukina N, Oyama F, Ranscht B, Isom LL (2010) Functional Reciprocity Between Na+ Channel Nav1.6 and B1 Subunits in the Coordinated Regulation of Excitability and Neurite Outgrowth. Proceedings of the National Academy of Sciences 107:2283-2288.

Braz JM, Nassar MA, Wood JN, Basbaum AI (2005) Parallel "pain" pathways arise from subpopulations of primary afferent nociceptor. Neuron 47:787-793.

Brodie C, Bak A, Shainberg A, Sampson SR (1987) Role of Na-K ATPase in regulation of resting membrane potential of cultured rat skeletal myotubes. J Cell Physiol 130:191-198.

Brown MC, Berglund AM, Kiang NY, Ryugo DK (1988) Central trajectories of type II spiral ganglion neurons. J Comp Neurol 278:581-590.

Cardenas CG, Del Mar LP, Cooper BY, Scroggs RS (1997) 5HT4 Receptors Couple Positively to Tetrodotoxin-Insensitive Sodium Channels in a Subpopulation of Capsaicin-Sensitive Rat Sensory Neurons. The Journal of Neuroscience 17:7181-7189.

Carleton SC, Carpenter MB (1984) Distribution of primary vestibular fibers in the brainstem and cerebellum of the monkey. Brain Res 294:281-298.

Carpenter MB, Stein BM, Peter P (1972) Primary vestibulocerebellar fibers in the monkey: distribution of fibers arising from distinctive cell groups of the vestibular ganglia. Am J Anat 135:221-249.

Catterall WA, Perez-Reyes E, Snutch TP, Striessnig J Voltage-gated calcium channels. In: IUPHAR database.

Chabbert C, Chambard JM, Valmier J, Sans A, Desmadryl G (1997) Voltage-activated sodium currents in acutely isolated mouse vestibular ganglion neurones. Neuroreport 8:1253-1256.

Chambard JM, Chabbert C, Sans A, Desmadryl G (1999) Developmental Changes in Low and High Voltage-Activated Calcium Currents in Acutely Isolated Mouse Vestibular Neurons. The Journal of Physiology 518:141-149.

Chen LQ, Chahine M, Kallen RG, Barchi RL, Horn R (1992) Chimeric study of sodium channels from rat skeletal and cardiac muscle. FEBS Letters 309:253-257.

Chen X, Pang R-P, Shen K-F, Zimmermann M, Xin W-J, Li Y-Y, Liu X-G (2011) TNF-α enhances the currents of voltage gated sodium channels in uninjured dorsal root ganglion neurons following motor nerve injury. Experimental Neurology 227:279-286.

Chen YH, Dale TJ, Romanos MA, Whitaker WR, Xie XM, Clare JJ (2000) Cloning, distribution and functional analysis of the type III sodium channel from human brain. Eur J Neurosci 12:4281-4289.

Choi J-S, Waxman SG (2011) Physiological interactions between Nav1.7 and Nav1.8 sodium channels: A computer simulation study. Journal of Neurophysiology.

Choi JS, Dib-Hajj SD, Waxman SG (2007) Differential Slow Inactivation and Use-Dependent Inhibition of Nav1.8 Channels Contribute to Distinct Firing Properties in IB4+ and IB4- DRG Neurons. Journal of Neurophysiology 97:1258-1265.

Choi JS, Hudmon A, Waxman SG, Dib-Hajj SD (2006) Calmodulin regulates current density and frequency-dependent inhibition of sodium channel Nav1.8 in DRG neurons. J Neurophysiol 96:97-108.

Chopra SS, Stroud DM, Watanabe H, Bennett JS, Burns CG, Wells KS, Yang T, Zhong TP, Roden DM (2010) Voltage-gated sodium channels are required for heart development in zebrafish. Circ Res 106:1342-1350.

Cohen CJ, Bean BP, Colatsky TJ, Tsien RW (1981) Tetrodotoxin block of sodium channels in rabbit Purkinje fibers. Interactions between toxin binding and channel gating. J Gen Physiol 78:383-411.

Coste B, Crest M, Delmas P (2007) Pharmacological Dissection and Distribution of NaN/Nav1.9, T-type Ca2+ Currents, and Mechanically Activated Cation Currents in Different Populations of DRG Neurons. The Journal of General Physiology 129:57-77.

Coste B, Osorio N, Padilla F, Crest M, Delmas P (2004) Gating and modulation of presumptive NaV1.9 channels in enteric and spinal sensory neurons. Molecular and Cellular Neuroscience 26:123-134.

Cribbs LL, Satin J, Fozzard HA, Rogart RB (1990) Functional expression of the rat heart I Na+ channel isoform Demonstration of properties characteristic of native cardiac Na+ channels. FEBS Letters 275:195-200.

Cummins TR (2002) Characterization and Developmental Changes of Na+ Currents of Petrosal Neurons With Projections to the Carotid Body. Journal of Neurophysiology 88:2993-3002.

Cummins TR, Waxman SG (1997) Downregulation of Tetrodotoxin-Resistant Sodium Currents and Upregulation of a Rapidly Repriming Tetrodotoxin-Sensitive Sodium Current in Small Spinal Sensory Neurons after Nerve Injury. The Journal of Neuroscience 17:3503-3514.

Cummins TR, Howe JR, Waxman SG (1998) Slow Closed-State Inactivation: A Novel Mechanism Underlying Ramp Currents in Cells Expressing the hNE/PN1 Sodium Channel. The Journal of Neuroscience 18:9607-9619.

Cummins TR, Black JA, Dib-Hajj SD, Waxman SG (2000) Glial-Derived Neurotrophic Factor Upregulates Expression of Functional SNS and NaN Sodium Channels and Their Currents in Axotomized Dorsal Root Ganglion Neurons. The Journal of Neuroscience 20:8754-8761.

Cummins TR, Dib-Hajj SD, Black JA, Akopian AN, Wood JN, Waxman SG (1999) A novel persistent tetrodotoxin-resistant sodium current in SNS-null and wild-type small primary sensory neurons. The Journal of Neuroscience: The Official Journal of the Society for Neuroscience 19:RC43-RC43.

Cummins TR, Aglieco F, Renganathan M, Herzog RI, Dib-Hajj SD, Waxman SG (2001) Nav1.3 Sodium Channels: Rapid Repriming and Slow Closed-State Inactivation Display Quantitative Differences After Expression in a Mammalian Cell Line and in Spinal Sensory Neurons. The Journal of Neuroscience 21:5952-5961.

Davis TH, Chen C, Isom LL (2004) Sodium channel beta1 subunits promote neurite outgrowth in cerebellar granule neurons. J Biol Chem 279:51424-51432.

Desmadryl G, Chambard JM, Valmier J, Sans A (1997) Multiple voltage-dependent calcium currents in acutely isolated mouse vestibular neurons. Neuroscience 78:511-522.

Dhamoon AS, Jalife J (2005) The inward rectifier current (IK1) controls cardiac excitability and is involved in arrhythmogenesis. Heart Rhythm 2:316-324.

Díaz D, Bartolo R, Delgadillo DM, Higueldo F, Gomora JC (2005) Contrasting Effects of Cd^{2+} and Co^{2+} on the Blocking/Unblocking of Human Ca_V3 Channels. Journal of Membrane Biology 207:91-105.

Dib-Hajj S, Black JA, Felts P, Waxman SG (1996) Down-Regulation of Transcripts for Na Channel A-SNS in Spinal Sensory Neurons Following Axotomy. Proceedings of the National Academy of Sciences 93:14950-14954.

Dib-Hajj SD, Tyrrell L, Cummins TR, Black JA, Wood PM, Waxman SG (1999) Two tetrodotoxin-resistant sodium channels in human dorsal root ganglion neurons. FEBS Letters 462:117-120.

Dietrich PS, McGivern JG, Delgado SG, Koch BD, Eglen RM, Hunter JC, Sangameswaran L (1998) Functional analysis of a voltage-gated sodium channel and its splice variant from rat dorsal root ganglia. J Neurochem 70:2262-2272.

DiFrancesco D, Ferroni A, Visentin S, Zaza A (1985) Cadmium-Induced Blockade of the Cardiac Fast Na Channels in Calf Purkinje Fibres. Proceedings of the Royal Society of London Series B, Biological Sciences 223:475-484.

Djouhri L, Fang X, Okuse K, Wood JN, Berry CM, Lawson SN (2003) The TTX-Resistant Sodium Channel Nav1.8 (SNS/PN3): Expression and Correlation with Membrane Properties in Rat Nociceptive Primary Afferent Neurons. The Journal of Physiology 550:739-752.

Donahue LM, Coates PW, Lee VH, Ippensen DC, Arze SE, Poduslo SE (2000) The cardiac sodium channel mRNA is expressed in the developing and adult rat and human brain. Brain Research 887:335-343.

Doyle DD, Brill DM, Wasserstrom JA, Karrison T, Page E (1985) Saxitoxin binding and "fast" sodium channel inhibition in sheep heart plasma membrane. Am J Physiol 249:H328-336.

Doyle DD, Guo Y, Lustig SL, Satin J, Rogart RB, Fozzard HA (1993) Divalent cation competition with [3H]saxitoxin binding to tetrodotoxin-resistant and -sensitive sodium channels. A two-site structural model of ion/toxin interaction. The Journal of General Physiology 101:153-182.

Elliott AA, Elliott JR (1993) Characterization of TTX-sensitive and TTX-resistant sodium currents in small cells from adult rat dorsal root ganglia. The Journal of Physiology 463:39-56.

England S, Bevan S, Docherty RJ (1996) PGE2 modulates the tetrodotoxin-resistant sodium current in neonatal rat dorsal root ganglion neurones via the cyclic AMP-protein kinase A cascade. The Journal of Physiology 495:429-440.

Everill B, Cummins TR, Waxman SG, Kocsis JD (2001) Sodium currents of large (Aβ-type) adult cutaneous afferent dorsal root ganglion neurons display rapid recovery from inactivation before and after axotomy. Neuroscience 106:161-169.

Fang X, Djouhri L, McMullan S, Berry C, Waxman SG, Okuse K, Lawson SN (2006) Intense Isolectin-B4 Binding in Rat Dorsal Root Ganglion Neurons Distinguishes C-Fiber Nociceptors with Broad Action Potentials and High Nav1.9 Expression. The Journal of Neuroscience 26:7281-7292.

Fjell J, Cummins TR, Dib-Hajj SD, Fried K, Black JA, Waxman SG (1999) Differential role of GDNF and NGF in the maintenance of two TTX-resistant sodium channels in adult DRG neurons. Molecular Brain Research 67:267-282.

Frankenhaeuser B, Hodgkin AL (1957) The action of calcium on the electrical properties of squid axons. J Physiol 137:218-244.

Frelin C, Cognard C, Vigne P, Lazdunski M (1986) Tetrodotoxin-sensitive and tetrodotoxin-resistant Na+ channels differ in their sensitivity to Cd2+ and Zn2+. European Journal of Pharmacology 122:245-250.

Fukushima Y, Hagiwara S (1985) Currents Carried by Monovalent Cations Through Calcium Channels in Mouse Neoplastic B Lymphocytes. The Journal of Physiology 358:255-284.

Gates P (2005) Hypothesis: could Meniere's disease be a channelopathy? Internal Medicine Journal 35:488-489.

Gautron L, Sakata I, Udit S, Zigman JM, Wood JN, Elmquist JK (2011) Genetic tracing of Nav1.8-expressing vagal afferents in the mouse. The Journal of Comparative Neurology 519:3085-3101.

Géléoc GSG, Risner JR, Holt JR (2004) Developmental Acquisition of Voltage-Dependent Conductances and Sensory Signaling in Hair Cells of the Embryonic Mouse Inner Ear. The Journal of Neuroscience 24:11148-11159.

Glowatzki E, Fuchs PA (2000) Cholinergic Synaptic Inhibition of Inner Hair Cells in the Neonatal Mammalian Cochlea. Science 288:2366-2368.

Gold MS, Levine JD, Correa AM (1998) Modulation of TTX-R INa by PKC and PKA and their role in PGE2-induced sensitization of rat sensory neurons in vitro. J Neurosci 18:10345-10355.

Gold MS, Reichling DB, Shuster MJ, Levine JD (1996) Hyperalgesic Agents Increase a Tetrodotoxin-Resistant Na+ Current in Nociceptors. Proceedings of the National Academy of Sciences 93:1108-1112.

Goldberg JM (1991) The vestibular end organs: morphological and physiological diversity of afferents. Current Opinion in Neurobiology 1:229-235.

Goldin AL (1999) Diversity of Mammalian Voltage-Gated Sodium Channels. Annals of the New York Academy of Sciences 868:38-50.

Gonoi T, Sherman SJ, Catterall WA (1985) Voltage clamp analysis of tetrodotoxin-sensitive and -insensitive sodium channels in rat muscle cells developing in vitro. J Neurosci 5:2559-2564.

Greco A, Gallo A, Fusconi M, Marinelli C, Macri GF, de Vincentiis M Meniere's disease might be an autoimmune condition? Autoimmunity Reviews.

Hanck DA, Sheets MF (1992) Extracellular divalent and trivalent cation effects on sodium current kinetics in single canine cardiac Purkinje cells. The Journal of Physiology 454:267-298.

Harper AA, Lawson SN (1985) Electrical Properties of Rat Dorsal Root Ganglion Neurones with Different Peripheral Nerve Conduction Velocities. The Journal of Physiology 359:47-63.

Harriott AM, Gold MS (2009) Electrophysiological properties of dural afferents in the absence and presence of inflammatory mediators. J Neurophysiol 101:3126-3134.

Hartmann HA, Colom LV, Sutherland ML, Noebels JL (1999) Selective localization of cardiac SCN5A sodium channels in limbic regions of rat brain. Nat Neurosci 2:593-595.

Hashino E, Dolnick RY, Cohan CS (1999) Developing vestibular ganglion neurons switch trophic sensitivity from BDNF to GDNF after target innervation. J Neurobiol 38:414-427.

Heinemann SH, Terlau H, Imoto K (1992) Molecular basis for pharmacological differences between brain and cardiac sodium channels. Pflügers Archiv European Journal of Physiology 422:90-92.

Hess P, Tsien RW (1984) Mechanism of ion permeation through calcium channels. Nature 309:453-456.

Hille B, Woodhull AM, Shapiro BI (1975) Negative surface charge near sodium channels of nerve: divalent ions, monovalent ions, and pH. Philos Trans R Soc Lond B Biol Sci 270:301-318.

Hinson AW, Gu XQ, Dib-Hajj S, Black JA, Waxman SG (1997) Schwann cells modulate sodium channel expression in spinal sensory neurons in vitro. Glia 21:339-349.

Ho C, O'Leary ME (2011) Single-cell analysis of sodium channel expression in dorsal root ganglion neurons. Molecular and Cellular Neuroscience 46:159-166.

Holt JC, Lysakowski A, Goldberg JM (2006) Mechanisms of Efferent-Mediated Responses in the Turtle Posterior Crista. J Neurosci 26:13180-13193.

Horn R, Marty A (1988) Muscarinic activation of ionic currents measured by a new whole-cell recording method. The Journal of general physiology 92:145-159.

Hsiung GR, Puil E (1990) Ionic dependencies of tetrodotoxin-resistant action potentials in trigeminal root ganglion neurons. Neuroscience 37:115-125.

Huang H, Priori SG, Napolitano C, O'Leary ME, Chahine M (2011) Y1767C, a novel SCN5A mutation, induces a persistent Na+ current and potentiates ranolazine inhibition of Nav1.5 channels. American Journal of Physiology - Heart and Circulatory Physiology 300:H288 -H299-H288 -H299.

Ikeda SR, Schofield GG (1987) Tetrodotoxin-resistant sodium current of rat nodose neurones: monovalent cation selectivity and divalent cation block. The Journal of Physiology 389:255-270.

Jarvis MF et al. (2007) A-803467, a potent and selective Nav1.8 sodium channel blocker, attenuates neuropathic and inflammatory pain in the rat. Proceedings of the National Academy of Sciences 104:8520-8525.

Josephson IR, Sperelakis N (1989) Tetrodotoxin differentially blocks peak and steady-state sodium channel currents in early embryonic chick ventricular myocytes. Pflugers Arch 414:354-359.

Kaczmarek LK (2006) Non-conducting functions of voltage-gated ion channels. Nat Rev Neurosci 7:761-771.

Kallen RG, Sheng Z-H, Yang J, Chen L, Rogart RB, Barchi RL (1990) Primary structure and expression of a sodium channel characteristic of denervated and immature rat skeletal muscle. Neuron 4:233-242.

Kalluri R, Xue J, Eatock RA (2010) Ion Channels Set Spike Timing Regularity of Mammalian Vestibular Afferent Neurons. Journal of Neurophysiology 104:2034-2051.

Kennedy HJ (2012) New Developments in Understanding the Mechanisms and Function of Spontaneous Electrical Activity in the Developing Mammalian Auditory System. J Assoc Res Otolaryngol.

Kerr NC, Gao Z, Holmes FE, Hobson SA, Hancox JC, Wynick D, James AF (2007) The sodium channel Nav1.5a is the predominant isoform expressed in adult mouse dorsal root ganglia and exhibits distinct inactivation properties from the full-length Nav1.5 channel. Mol Cell Neurosci 35:283-291.

Kerr NCH, Holmes FE, Wynick D (2004) Novel isoforms of the sodium channels Nav1.8 and Nav1.5 are produced by a conserved mechanism in mouse and rat. The Journal of Biological Chemistry 279:24826-24833.

Kevetter GA, Leonard RB (2002) Molecular probes of the vestibular nerve. II. Characterization of neurons in Scarpa's ganglion to determine separate populations within the nerve. Brain Research 928:18-29.

Kuo C-C, Lin T-J, Hsieh C-P (2002) Effect of Na+ Flow on Cd2+ Block of Tetrodotoxin-Resistant Na+ Channels. The Journal of General Physiology 120:159-172.

Kurejová M, Pavlovicová M, Lacinová L (2007) Monovalent currents through the T-type Cav3.1 channels and their block by Mg2+. General Physiology and Biophysics 26:234-239.

Kwong K, Carr MJ, Gibbard A, Savage TJ, Singh K, Jing J, Meeker S, Undem BJ (2008) Voltage-gated sodium channels in nociceptive versus non-nociceptive nodose vagal sensory neurons innervating guinea pig lungs. The Journal of Physiology 586:1321-1336.

Lai J, Gold MS, Kim C-S, Biana D, Ossipov MH, Hunterc JC, Porreca F (2002) Inhibition of neuropathic pain by decreased expression of the tetrodotoxin-resistant sodium channel, NaV1.8. Pain 95:143-152.

Leffler A, Herzog RI, Dib-Hajj SD, Waxman SG, Cummins TR (2005) Pharmacological properties of neuronal TTX-resistant sodium channels and the role of a critical serine pore residue. Pflügers Archiv - European Journal of Physiology 451:454-463.

Levi R, DeFelice LJ (1986) Sodium-conducting channels in cardiac membranes in low calcium. Biophysical Journal 50:5-9.

Li A, Xue J, Peterson EH (2008) Architecture of the Mouse Utricle: Macular Organization and Hair Bundle Heights. J Neurophysiol 99:718-733.

Limón A, Pérez C, Vega R, Soto E (2005) Ca2+-activated K+-current density is correlated with soma size in rat vestibular-afferent neurons in culture. Journal of Neurophysiology 94:3751-3761.

Lysakowski A, Goldberg JM (1997) A regional ultrastructural analysis of the cellular and synaptic architecture in the chinchilla cristae ampullares. The Journal of Comparative Neurology 389:419-443.

Lysakowski A, Goldberg JM (2008) Ultrastructural analysis of the cristae ampullares in the squirrel monkey (Saimiri sciureus). The Journal of Comparative Neurology 511:47-64.

Lysakowski A, Gaboyard-Niay S, Calin-Jageman I, Chatlani S, Price SD, Eatock RA (2011) Molecular Microdomains in a Sensory Terminal, the Vestibular Calyx Ending. The Journal of Neuroscience 31:10101-10114.

Madisen L, Zwingman TA, Sunkin SM, Oh SW, Zariwala HA, Gu H, Ng LL, Palmiter RD, Hawrylycz MJ, Jones AR, Lein ES, Zeng H (2009) A robust and high-throughput Cre reporting and characterization system for the whole mouse brain. Nature Neuroscience 13:133-140.

Maklad A, Kamel S, Wong E, Fritzsch B (2010) Development and organization of polarity-specific segregation of primary vestibular afferent fibers in mice. Cell and Tissue Research 340:303-321.

Maruyama H, Yamamoto M, Matsutomi T, Zheng T, Nakata Y, Wood JN, Ogata N (2004) Electrophysiological characterization of the tetrodotoxin-resistant Na+ channel, Nav1.9, in mouse dorsal root ganglion neurons. Pflügers Archiv - European Journal of Physiology 449:76-87.

McNulty MM, Hanck DA (2004) State-dependent mibefradil block of Na+ channels. Molecular Pharmacology 66:1652-1661.

Miwa K, Lee JK, Takagishi Y, Opthof T, Fu X, Kodama I (2010) Glial cell line-derived neurotrophic factor (GDNF) enhances sympathetic neurite growth in rat hearts at early developmental stages. Biomed Res 31:353-361.

Monteil A, Chemin J, Bourinet E, Mennessier G, Lory P, Nargeot J (2000) Molecular and Functional Properties of the Human α1G Subunit That Forms T-Type Calcium Channels. Journal of Biological Chemistry 275:6090-6100.

Moran O, Picollo A, Conti F (2003) Tonic and phasic guanidinium toxin-block of skeletal muscle Na channels expressed in Mammalian cells. Biophys J 84:2999-3006.

Noda M, Suzuki H, Numa S, Stuhmer W (1989) A single point mutation confers tetrodotoxin and saxitoxin insensitivity on the sodium channel II. FEBS Lett 259:213-216.

Noda M, Ikeda T, Suzuki H, Takeshima H, Takahashi T, Kuno M, Numa S (1986) Expression of functional sodium channels from cloned cDNA. Nature 322:826-828.

Novakovic SD, Tzoumaka E, McGivern JG, Haraguchi M, Sangameswaran L, Gogas KR, Eglen RM, Hunter JC (1998) Distribution of the Tetrodotoxin-Resistant Sodium Channel PN3 in Rat Sensory Neurons in Normal and Neuropathic Conditions. The Journal of Neuroscience 18:2174-2187.

O'Brien BJ, Caldwell JH, Ehring GR, Bumsted O'Brien KM, Luo S, Levinson SR (2008) Tetrodotoxin-resistant voltage-gated sodium channels Nav1.8 and Nav1.9 are expressed in the retina. The Journal of Comparative Neurology 508:940-951.

O'Leary ME (1998) Characterization of the isoform-specific differences in the gating of neuronal and muscle sodium channels. Can J Physiol Pharmacol 76:1041-1050.

Ogata N, Tatebayashi H (1993) Kinetic Analysis of Two Types of Na+ Channels in Rat Dorsal Root Ganglia. The Journal of Physiology 466:9-37.

Oliver D, Plinkert P, Zenner HP, Ruppersberg JP (1997) Sodium current expression during postnatal development of rat outer hair cells. Pflügers Archiv European Journal of Physiology 434:772-778.

Papadatos GA, Wallerstein PM, Head CE, Ratcliff R, Brady PA, Benndorf K, Saumarez RC, Trezise AE, Huang CL, Vandenberg JI, Colledge WH, Grace AA (2002) Slowed conduction and ventricular tachycardia after targeted disruption of the cardiac sodium channel gene Scn5a. Proc Natl Acad Sci U S A 99:6210-6215.

Pappone PA (1980) Voltage-clamp experiments in normal and denervated mammalian skeletal muscle fibres. J Physiol 306:377-410.

Patton DE, Goldin AL (1991) A voltage-dependent gating transition induces use-dependent block by tetrodotoxin of rat IIA sodium channels expressed in Xenopus oocytes. Neuron 7:637-647.

Penniman JR, Kim DC, Salata JJ, Imredy JP (2010) Assessing use-dependent inhibition of the cardiac Na± current (INa) in the PatchXpress automated patch clamp. Journal of Pharmacological and Toxicological Methods 62:107-118.

Puhl HL, 3rd, Ikeda SR (2008) Identification of the sensory neuron specific regulatory region for the mouse gene encoding the voltage-gated sodium channel NaV1.8. J Neurochem 106:1209-1224.

Qu W, Moorhouse AJ, Rajendra S, Barry PH (2000) Very negative potential for half-inactivation of, and effects of anions on, voltage-dependent sodium currents in acutely isolated rat olfactory receptor neurons. The Journal of Membrane Biology 175:123-138.

Qu Y, Rogers J, Tanada T, Scheuer T, Catterall WA (1994) Modulation of cardiac Na+ channels expressed in a mammalian cell line and in ventricular myocytes by protein kinase C. Proc Natl Acad Sci U S A 91:3289-3293.

Rabert DK, Koch BD, Ilnicka M, Obernolte RA, Naylor SL, Herman RC, Eglen RM, Hunter JC, Sangameswaran L (1998) A tetrodotoxin-resistant voltage-gated sodium channel from human dorsal root ganglia, hPN3/SCN10A. Pain 78:107-114.

Renganathan M, Cummins TR, Waxman SG (2001) Contribution of Nav1.8 Sodium Channels to Action Potential Electrogenesis in DRG Neurons. Journal of Neurophysiology 86:629-640.

Renganathan M, Dib-Hajj S, Waxman SG (2002) Nav1.5 underlies the [`]third TTX-R sodium current' in rat small DRG neurons. Molecular Brain Research 106:70-82.

Rennie KJ, Streeter MA (2006) Voltage-dependent currents in isolated vestibular afferent calyx terminals. Journal of Neurophysiology 95:26-32.

Risner JR, Holt JR (2006) Heterogeneous Potassium Conductances Contribute to the Diverse Firing Properties of Postnatal Mouse Vestibular Ganglion Neurons. Journal of Neurophysiology 96:2364-2376.

Ritter AM, Mendell LM (1992) Somal Membrane Properties of Physiologically Identified Sensory Neurons in the Rat: Effects of Nerve Growth Factor. Journal of Neurophysiology 68:2033-2041.

Rizzo MA, Kocsis JD, Waxman SG (1994) Slow Sodium Conductances of Dorsal Root Ganglion Neurons: Intraneuronal Homogeneity and Interneuronal Heterogeneity. Journal of Neurophysiology 72:2796-2815.

Rogart RB, Cribbs LL, Muglia LK, Kephart DD, Kaiser MW (1989) Molecular cloning of a putative tetrodotoxin-resistant rat heart Na+ channel isoform. Proc Natl Acad Sci U S A 86:8170-8174.

Rook MB, Evers MM, Vos MA, Bierhuizen MF (2012) Biology of cardiac sodium channel Nav1.5 expression. Cardiovasc Res 93:12-23.

Roy ML, Narahashi T (1992) Differential properties of tetrodotoxin-sensitive and tetrodotoxin- resistant sodium channels in rat dorsal root ganglion neurons. The Journal of Neuroscience 12:2104-2111.

Rugiero F, Mistry M, Sage D, Black JA, Waxman SG, Crest M, Clerc N, Delmas P, Gola M (2003) Selective Expression of a Persistent Tetrodotoxin-Resistant Na+ Current and NaV1.9 Subunit in Myenteric Sensory Neurons. The Journal of Neuroscience 23:2715-2725.

Ruppersberg JP, Schure A, Rüdel R (1987) Inactivation of TTX-sensitive and TTX-insensitive sodium channels of rat myoballs. Neuroscience Letters 78:166-170.

Rusch A, Lysakowski A, Eatock RA (1998) Postnatal Development of Type I and Type II Hair Cells in the Mouse Utricle: Acquisition of Voltage-Gated Conductances and Differentiated Morphology. J Neurosci 18:7487-7501.

Rüsch A, Eatock RA (1997) Sodium currents in hair cells of the mouse utricle. In: Diversity in Auditory Mechanics (Lewis ER, Long GR, Lyon RF, Steele CR, Narins PM, Poinar E, eds), pp 549-555. Singapore: World Scientific Publishing Co. Pte. Ltd.

Rush AM, Cummins TR, Waxman SG (2007) Multiple sodium channels and their roles in electrogenesis within dorsal root ganglion neurons. The Journal of Physiology 579:1-14.

Rush AM, Craner MJ, Kageyama T, Dib-Hajj SD, Waxman SG, Ranscht B (2005) Contactin regulates the current density and axonal expression of tetrodotoxin-resistant but not tetrodotoxin-sensitive sodium channels in DRG neurons. European Journal of Neuroscience 22:39-49.

Rush AM, Dib-Hajj SD, Liu S, Cummins TR, Black JA, Waxman SG (2006) A single sodium channel mutation produces hyper- or hypoexcitability in different types of neurons. Proceedings of the National Academy of Sciences of the United States of America 103:8245-8250.

Saab CY, Cummins TR, Waxman SG (2003) GTP?S increases Nav1.8 current in small-diameter dorsal root ganglia neurons. Experimental Brain Research 152:415-419.

Sabatini BL, Regehr WG (1997) Control of neurotransmitter release by presynaptic waveform at the granule cell to Purkinje cell synapse. J Neurosci 17:3425-3435.

Sada H, Ban T, Fujita T, Ebina Y, Sperelakis N (1995) Developmental change in fast Na channel properties in embryonic chick ventricular heart cells. Canadian Journal of Physiology and Pharmacology 73:1475-1484.

Sangameswaran L, Delgado SG, Fish LM, Koch BD, Jakeman LB, Stewart GR, Sze P, Hunter JC, Eglen RM, Herman RC (1996) Structure and Function of a Novel Voltage-gated, Tetrodotoxin-resistant Sodium Channel Specific to Sensory Neurons. Journal of Biological Chemistry 271:5953-5956.

Sangameswaran L, Fish LM, Koch BD, Rabert DK, Delgado SG, Ilnicka M, Jakeman LB, Novakovic S, Wong K, Sze P, Tzoumaka E, Stewart GR, Herman RC, Chan H, Eglen RM, Hunter JC (1997) A novel tetrodotoxin-sensitive, voltage-gated sodium channel expressed in rat and human dorsal root ganglia. J Biol Chem 272:14805-14809.

Satin J, Kyle J, Chen M, Rogart R, Fozzard H (1992a) The cloned cardiac Na channel α-subunit expressed in Xenopus oocytes show gating and blocking properties of native channels. The Journal of Membrane Biology 130.

Satin J, Kyle JW, Chen M, Bell P, Cribbs LL, Fozzard HA, Rogart RB (1992b) A mutant of TTX-resistant cardiac sodium channels with TTX-sensitive properties. Science (New York, NY) 256:1202-1205.

Schild JH, Kunze DL (1997) Experimental and Modeling Study of Na+ Current Heterogeneity in Rat Nodose Neurons and Its Impact on Neuronal Discharge. Journal of Neurophysiology 78:3198-3209.

Schofield GG, Puhl HL, Ikeda SR (2008) Properties of Wild-Type and Fluorescent Protein-Tagged Mouse Tetrodotoxin-Resistant Sodium Channel (NaV1.8) Heterologously Expressed in Rat Sympathetic Neurons. Journal of Neurophysiology 99:1917-1927.

Scholz A, Appel N, Vogel W (1998) Two types of TTX-resistant and one TTX-sensitive Na+ channel in rat dorsal root ganglion neurons and their blockade by halothane. European Journal of Neuroscience 10:2547-2556.

Schram G, Pourrier M, Melnyk P, Nattel S (2002) Differential Distribution of Cardiac Ion Channel Expression as a Basis for Regional Specialization in Electrical Function. Circulation Research 90:939-950.

Schubert D, Whitlock C (1977) Alteration of cellular adhesion by nerve growth factor. Proc Natl Acad Sci U S A 74:4055-4058.

Scornik FS, Desai M, Brugada R, Guerchicoff A, Pollevick GD, Antzelevitch C, Pérez GJ (2006) Functional expression of "cardiac-type" Nav1.5 sodium channel in canine intracardiac ganglia. Heart rhythm : the official journal of the Heart Rhythm Society 3:842-850.

Sheets MF, Hanck DA (1992) Mechanisms of extracellular divalent and trivalent cation block of the sodium current in canine cardiac Purkinje cells. The Journal of Physiology 454:299-320.

Sheets MF, Hanck DA (1999) Gating of skeletal and cardiac muscle sodium channels in mammalian cells. The Journal of Physiology 514:425-436.

Sleeper AA, Cummins TR, Dib-Hajj SD, Hormuzdiar W, Tyrrell L, Waxman SG, Black JA (2000) Changes in expression of two tetrodotoxin-resistant sodium channels and their currents in dorsal root ganglion neurons after sciatic nerve injury but not rhizotomy. J Neurosci 20:7279-7289.

Smith RD, Goldin AL (1998) Functional analysis of the rat I sodium channel in xenopus oocytes. J Neurosci 18:811-820.

Sperelakis N, Pappano AJ (1983) Physiology and pharmacology of developing heart cells. Pharmacol Ther 22:1-39.

Stansfeld CE, Wallis DI (1985) Properties of visceral primary afferent neurons in the nodose ganglion of the rabbit. J Neurophysiol 54:245-260.

Stea A, Nurse CA (1992) Whole-cell currents in two subpopulations of cultured rat petrosal neurons with different tetrodotoxin sensitivities. Neuroscience 47:727-736.

Stirling LC, Forlani G, Baker MD, Wood JN, Matthews EA, Dickenson AH, Nassar MA (2005) Nociceptor-specific gene deletion using heterozygous NaV1.8-Cre recombinase mice. Pain 113:27-36.

Tanaka M, Cummins TR, Ishikawa K, Dib-Hajj SD, Black JA, Waxman SG (1998) SNS Na+ channel expression increases in dorsal root ganglion neurons in the carrageenan inflammatory pain model. Neuroreport 9:967-972.

Toledo-Aral JJ, Moss BL, He ZJ, Koszowski AG, Whisenand T, Levinson SR, Wolf JJ, Silos-Santiago I, Halegoua S, Mandel G (1997) Identification of PN1, a predominant voltage-dependent sodium channel expressed principally in peripheral neurons. Proc Natl Acad Sci U S A 94:1527-1532.

Tritsch NX, Yi E, Gale JE, Glowatzki E, Bergles DE (2007) The origin of spontaneous activity in the developing auditory system. Nature 450:50-55.

Ulbricht W (2005) Sodium Channel Inactivation: Molecular Determinants and Modulation. Physiological Reviews 85:1271-1301.

Vaughn AH, Gold MS (2010) Ionic mechanisms underlying inflammatory mediator-induced sensitization of dural afferents. J Neurosci 30:7878-7888.

Verheugen JAH, Fricker D, Miles R (1999) Noninvasive Measurements of the Membrane Potential and GABAergic Action in Hippocampal Interneurons. The Journal of Neuroscience 19:2546-2555.

Vijayaragavan K, O'Leary ME, Chahine M (2001) Gating properties of Na(v)1.7 and Na(v)1.8 peripheral nerve sodium channels. The Journal of Neuroscience: The Official Journal of the Society for Neuroscience 21:7909-7918.

Vornanen M, Hassinen M, Haverinen J (2011) Tetrodotoxin sensitivity of the vertebrate cardiac Na+ current. Mar Drugs 9:2409-2422.

Wang DW, George Jr AL, Bennett PB (1996) Comparison of heterologously expressed human cardiac and skeletal muscle sodium channels. Biophysical Journal 70:238-245.

Wang J, Ou S-W, Wang Y-J, Kameyama M, Kameyama A, Zong Z-H (2009) Analysis of four novel variants of Nav1.5/SCN5A cloned from the brain. Neuroscience Research 64:339-347.

Wang J, Ou S-W, Wang Y-J, Zong Z-H, Lin L, Kameyama M, Kameyama A (2008) New variants of Nav1.5/SCN5A encode Na+ channels in the brain. Journal of Neurogenetics 22:57-75.

Watanabe H, Koopmann TT, Le Scouarnec S, Yang T, Ingram CR, Schott J-J, Demolombe S, Probst V, Anselme F, Escande D, Wiesfeld ACP, Pfeufer A, Kääb S, Wichmann HE, Hasdemir C, Aizawa Y, Wilde AAM, Roden DM, Bezzina CR (2008) Sodium channel β1 subunit mutations associated with Brugada syndrome and cardiac conduction disease in humans. Journal of Clinical Investigation.

Weigele JB, Barchi RL (1978) Saxitoxin binding to the mammalian sodium channel. Competition by monovalent and divalent cations. FEBS Lett 95:49-53.

Wooltorton JRA, Hurley KM, Bao H, Eatock RA (2008) Voltage-dependent sodium currents in hair cells of the inner ear. In: Topics in Integrative Neuroscience: From Cells to Cognition (Pomerantz JR, ed), pp 385-413. New York: Cambridge University Press.

Wooltorton JRA, Gaboyard S, Hurley KM, Price SD, Garcia JL, Zhong M, Lysakowski A, Eatock RA (2007) Developmental changes in two voltage-dependent sodium currents in utricular hair cells. Journal of Neurophysiology 97:1684-1704.

Wu L, Nishiyama K, Hollyfield JG, Wang Q (2002) Localization of Nav1.5 sodium channel protein in the mouse brain. Neuroreport 13:2547-2551.

Yamamoto Y, Fukuta H, Suzuki H (1993) Blockade of sodium channels by divalent cations in rat gastric smooth muscle. Jpn J Physiol 43:785-796.

Yang JSJ, Sladky JT, Kallen RG, Barchi RL (1991) TTX-sensitive and TTX-insensitive sodium channel mRNA transcripts are independently regulated in adult skeletal muscle after denervation. Neuron 7:421-427.

Yatani A, Brown AM (1985) The calcium channel blocker nitrendipine blocks sodium channels in neonatal rat cardiac myocytes. Circ Res 56:868-875.

Yu FH, Catterall WA (2003) Overview of the voltage-gated sodium channel family. Genome Biology 4:207-207.

Zeng D, Kyle JW, Martin RL, Ambler KS, Hanck DA (1996) Cardiac sodium channels expressed in a peripheral neurotumor-derived cell line, RT4-B8. The American Journal of Physiology 270:C1522-1531-C1522-1531.

Zhang Y, Hartmann HA, Satin J (1999) Glycosylation Influences Voltage-Dependent Gating of Cardiac and Skeletal Muscle Sodium Channels. Journal of Membrane Biology 171:195-207.

Zhang ZN, Li Q, Liu C, Wang HB, Wang Q, Bao L (2008) The voltage-gated Na+ channel Nav1.8 contains an ER-retention/retrieval signal antagonized by the beta3 subunit. J Cell Sci 121:3243-3252.

Zhou Z, Davar G, Strichartz G (2002) Endothelin-1 (ET-1) Selectively Enhances the Activation Gating of Slowly Inactivating Tetrodotoxin-Resistant Sodium Currents in Rat Sensory Neurons: A Mechanism for the Pain-Inducing Actions of ET-1. The Journal of Neuroscience 22:6325-6330.